

Faculdade de Engenharia da Universidade do Porto



Skin neoplasms dynamic thermal assessment

Ana Carolina dos Santos Ribeiro Magalhães

Versão final

Dissertação realizada no âmbito do
Mestrado em Engenharia Biomédica

Orientador: Ricardo Vardasca, PhD
Coorientadores: Prof. Joaquim Gabriel Mendes (FEUP), Dra. Rita Valença Filipe (IPO)

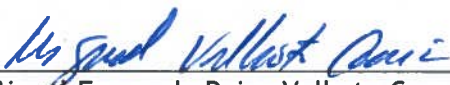
junho 2018

A Dissertação intitulada

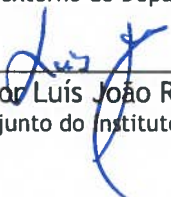
“Skin Neoplasms Dynamic Thermal Assessment”

foi aprovada em provas realizadas em 09-07-2018

o júri


Presidente Prof. Doutor Miguel Fernando Paiva Velhote Correia
Professor Auxiliar do Departamento de Engenharia Eletrotécnica e de Computadores da FEUP
- U.Porto


Doutor Ricardo Ângelo Rosa Vardasca
Investigador externo do Departamento de Engenharia Mecânica - FEUP - U.Porto


Prof. Doutor Luís João Rodrigues das Neves Correia Mourão
Professor Adjunto do Instituto Superior de Engenharia do Porto do Instituto Politécnico do
Porto

O autor declara que a presente dissertação (ou relatório de projeto) é da sua exclusiva autoria e foi escrita sem qualquer apoio externo não explicitamente autorizado. Os resultados, ideias, parágrafos, ou outros extratos tomados de ou inspirados em trabalhos de outros autores, e demais referências bibliográficas usadas, são corretamente citados.


Autor - Ana Carolina dos Santos Ribeiro Magalhães

Faculdade de Engenharia da Universidade do Porto

© Carolina Magalhães, 2018

Abstract

The incidence rates of skin cancer lesions have increased worldwide over the last years, due to excessive exposure to UV radiation. The current diagnostic methods depend greatly on physicians' experience, resulting in distinct diagnosis for the same skin lesion. Consequently, new diagnostic techniques have been developed, in order to reduce the uncertainty of this analysis. Infrared Thermal Imaging (IRT) is an innocuous method that enables the detection of skin physiological alterations, through temperature changes. The implementation of image analysis and processing algorithms to thermograms, allied with artificial intelligence classifiers, make this imaging modality a potential optimal tool for skin cancer diagnosis. Thus, being the central topic of this dissertation.

This research work was focused on the assessment of skin neoplasms with medical infrared thermal imaging. An acquisition protocol for static and dynamic application of this technique in a clinical scenario was developed, as well as different strategies for image analysis and processing. Machine learning algorithms for classification purposes were explored, with different learners and input vectors.

The results show that the distinction between different skin neoplasm types is doable, using medical infrared imaging, specially in the task of melanoma and nevi differentiation. These results get better when thermal information retrieved from images acquired dynamically is used, achieving an accuracy of 84.2% and a specificity of 91.3% with a learner based on support vector machines.

Resumo

A taxa de incidência de lesões cancerígenas da pele tem aumentado nos últimos anos, a nível mundial, devido à exposição excessiva a radiação UV. Os métodos de diagnóstico atuais dependem da experiência do clínico, sendo que análises díspares podem ser encontradas para a mesma lesão. Desta forma, novas técnicas de diagnóstico têm sido exploradas, com o objetivo de reduzir a incerteza do processo. A termografia médica é um método de imagiologia inócuo que permite a detecção de alterações fisiológicas a nível cutâneo, através de diferenças de temperatura. A aplicação de algoritmos de análise e processamento de imagem aos termogramas, aliada a estratégias de classificação com métodos de inteligência artificial, potencia o uso desta técnica como uma ferramenta auxiliar ao diagnóstico de cancro de pele. Assim, este será o tópico central desta dissertação.

Este trabalho de investigação focou-se na avaliação térmica de neoplasias da pele. Elaborou-se um protocolo de aquisição adequado para um cenário clínico e desenvolveram-se algoritmos de análise e processamento de imagens com base nos termogramas adquiridos com a aplicação estática e dinâmica deste método de imagiologia. A implementação de machine learning para tarefas de classificação foi também explorada com diferentes classificadores e vetores de input.

Os resultados obtidos demonstram que a distinção de diferentes tipos de neoplasias de pele é possível, utilizando termografia médica infravermelha, principalmente quando o objetivo principal é a diferenciação de melanomas e nevos melanocíticos. As métricas de classificação melhoram quando esta distinção é realizada com base em informação extraída de imagens obtidas dinamicamente, atingindo valores de exatidão de 84.2% e especificidade de 91.3% com um algoritmo baseado em *support vector machines*.

Acknowledgments

To my family and friends for all the patience, encouragement and support during this stage of my academic life.

To my supervisor Ricardo Vardasca for the guidance and always pushing me to go further with my work.

To my co-supervisors Prof. Joaquim Gabriel and Dra. Rita Valença-Filipe for all the help and passed knowledge.

To Dra. Matilde Ribeiro and Dr. Marco Rebelo for allowing and facilitating the accomplishment of this study at IPO-Porto.

To all the patients that accepted to collaborate in this project.

To the doctors, nurses and operational assistants of Unidade de Cirurgia Ambulatório of Clínica da Pele (IPO-Porto), for welcoming me in their work environment with open arms and making me feel like I was part of the family.

Index

1 Introduction	1
1.1 - Motivation	2
1.2 - Aim	3
1.3 - Contribution	3
1.4 - Dissertation outline	3
2 Skin oncological conditions	5
2.1 - Skin constitution	5
2.2 - Thermophysiology	7
2.3 - Skin neoplasms: formation and angiogenesis.....	9
2.3.1 - Malignant skin neoplasms	10
2.3.2 - Benign skin neoplasms	11
2.4 - Skin cancer statistics: incidence and associated costs	12
2.5 - Diagnostic methods.....	13
2.6 - Treatment methods	14
2.7 - Summary	15
3 Infrared thermal imaging	17
3.1 - Principles	17
3.2 - Applications in medicine: skin neoplasms.....	18
3.3 - Literature Review	19
3.2.1 - Methodology	19
3.2.2 - Results	20
3.2.3 - Study's population	24
3.2.4 - Trends and future challenges	25
4 Machine learning classifiers	27
4.1 - Literature review: AI and imaging	27
4.1.1 - Methodology	27
4.1.2 - Results	29
4.1.3 - Trends and future challenges	34
4.2 - Literature review: AI and thermal imaging	35

4.3 - Summary	36
5 Materials and methods	37
5.1 - Equipment	37
5.2 - Focus group	38
5.3 - Capture protocol	39
5.4 - Data analysis	39
5.4.1 - Infrared thermal image analysis	39
5.4.2 - Statistical treatment	42
5.4.3 - Machine learning classification	44
6 Results	49
6.1 - Sample characterization	49
6.2 - Steady-state image analysis	51
6.3 - Dynamic image analysis	56
6.4 - Statistical analysis	62
6.5 - Machine learning classifiers	62
7 Discussion	77
7.1 - Steady-state image analysis	77
7.2 - Dynamic image analysis	78
7.3 - Statistical treatment	79
7.4 - Machine learning classifiers	79
8 Conclusion	81
8.1 - Future work	81
References	83

List of figures

Figure 2.1 - Scheme of human skin: A - Layers and its main structures; B - Capillary loop.	6
Figure 2.2 - Skin layers and vascular structures encountered.	7
Figure 2.3 - Thermoregulation of skin temperature: A-Vasoconstriction, B-Vasodilation.	7
Figure 2.4 - Malignant skin lesions: A - Superficial spreading melanoma; B - Basal cell carcinoma; C - Squamous cell carcinoma; D - Merkel cell carcinoma.....	11
Figure 2.5 - Benign skin lesions: A - Melanocytic nevi; B - Dysplastic nevi; C - Actinic keratosis; D - Seborrheic keratosis, E - Strawberry nevus; F - Lipoma.	12
Figure 3.1 - PRISMA flow diagram.	20
Figure 5.1 - Equipment for image acquisition: A - Thermal imaging camera: FLIR E60sc; B - Aluminium medal.	37
Figure 5.2 - Stages involved in the acquisition protocol.	39
Figure 5.3 - Infrared thermal image analysis scheme of static and dynamic acquired images. ..	40
Figure 5.4 - A - Selected skin tumour area; B - Scheme of temperature diagonals and its multiplication; C - Vertical and horizontal temperature vectors.	41
Figure 5.5 - Scheme of image partition and scanning performed by the MATLAB algorithm.	42
Figure 5.6 - Confusion matrix model.	45
Figure 6.1 Skin neoplasm incidence according to body region.	49
Figure 6.2 - Frequency of patients' characteristics in study's sample.	50
Figure 6.3 - Static thermal profile characteristic of SCC, BCC and melanoma lesions.	51
Figure 6.4 - Static thermal profile characteristic of AK, Nevi, SK, Cyst and Other lesions.	52
Figure 6.5 - Static thermal profile characteristic of melanoma and melanocytic lesions.	52
Figure 6.6 - Static thermal profile characteristic of SCC and AK lesions.	53
Figure 6.7 - Static thermal profile characteristic of benign, malignant and non-neoplastic lesions.	53
Figure 6.8 - Average lesion temperature and standard deviation for SCC, BCC and melanoma lesions.	54
Figure 6.9 - Average lesion temperature and standard deviation for SCC, BCC and melanoma lesions.	54

List of tables

Table 2.1 - Nerve fibres classification and respective conduction velocities.	8
Table 2.2 - Incidence and mortality rate of melanoma and other skin malignant neoplasms in Portugal per 100 000 malignant tumours.	12
Table 4.1 - Recent publications regarding the use of machine learning classifiers for medical diagnosis using IRT imaging.	36
Table 5.1 - Properties of thermal imaging camera FLIR E60sc.	38
Table 5.2 - Exclusion and inclusion criteria defined for the research study.	38
Table 5.3 - Steady-state parameters collected from Image X and Y.....	41
Table 5.4 - Dynamic variables collected from Image X and Y.	42
Table 5.5 - Labels assigned to each category.	43
Table 5.6 - Possible feature combination for input vector, according to image acquisition process.....	45
Table 5.7 - Number of hidden layers selected for each classification test, according to image acquisition process.	46
Table 5.8 - Number of nearest neighbours (k) considered for each classification task, according to image acquisition process.....	47
Table 6.1 - Mean and standard deviation value for patients' age, height, weight and BMI.	51
Table 6.2 - Results of U-Mann Whitney and Kruskal-Wallis test: variables influenced by patients' factors.	62
Table 6.3 - Accuracy values for different classification tasks with SMO, iBk and Multilayer perceptron classifiers with S1, S2, ..., S40 and SM constituting the input vector.	63
Table 6.4 - Sensitivity values for different classification tasks with SMO, iBk and Multilayer perceptron classifiers with S1, S2, ..., S40 and SM constituting the input vector.	64
Table 6.5 - Specificity values for different classification tasks with SMO, iBk and Multilayer perceptron classifiers with S1, S2, ..., S40 and SM constituting the input vector.	65
Table 6.6 - Accuracy values for different classification tasks with SMO, iBk and Multilayer perceptron classifiers with S1, S2, ..., S40 and SSTD constituting the input vector.....	66
Table 6.7 - Sensitivity values for different classification tasks with SMO, iBk and Multilayer perceptron classifiers with S1, S2, ..., S40 and SSTD constituting the input vector.....	67
Table 6.8 - Specificity values for different classification tasks with SMO, iBk and Multilayer perceptron classifiers with S1, S2, ..., S40 and SSTD constituting the input vector.....	68

Table 6.9 - Accuracy values for different classification tasks with SMO, iBk and Multilayer perceptron classifiers with DX, DO, ..., D5 and DMX, DM0, ..., DM5 constituting the input vector.	69
Table 6.10 - Sensitivity values for different classification tasks with SMO, iBk and Multilayer perceptron classifiers with DX, DO, ..., D5 and DMX, DM0, ..., DM5 constituting the input vector.	70
Table 6.11 - Specificity values for different classification tasks with SMO, iBk and Multilayer perceptron classifiers with DX, DO, ..., D5 and DMX, DM0, ..., DM5 constituting the input vector.	71
Table 6.12 - Accuracy values for different classification tasks with SMO, iBk and Multilayer perceptron classifiers with DX, DO, ..., D5 and DSTDX, DSTD0, ..., DSTD5 constituting the input vector.	72
Table 6.13 - Sensitivity values for different classification tasks with SMO, iBk and Multilayer perceptron classifiers with DX, DO, ..., D5 and DSTDX, DSTD0, ..., DSTD5 constituting the input vector.	73
Table 6.14 - Specificity values for different classification tasks with SMO, iBk and Multilayer perceptron classifiers with DX, DO, ..., D5 and DSTDX, DSTD0, ..., DSTD5 constituting the input vector.	74
Table 6.15 - Best overall classification results.	75

Abbreviations, Acronyms and Symbols

List of abbreviations and acronyms

ABCDE	Asymmetry, Border irregularity, Colour, Diameter, Evolution
ACC	Accuracy
AdaBoost	Adaptative Boosting
AI	Artificial Intelligence
AK	Actinic Keratosis
ANN	Artificial Neural Networks
AVA	Arteriovenous anastomosis
BCC	Basal cell carcinoma
BMI	Body Mass Index
BoF	Bagging of Features
CAD	Computer-Aided Diagnosis
CL II	Clark level II
CL III	Clark level III
CL IV	Clark level IV
CLSM	Confocal Laser Scanning Microscopy
D	Maximum temperature difference
DTI	Dynamic thermal imaging
ES I	Early stage
FGF	Fibroblast growth factors
FN	False Negative
FP	False Positive
GA	Genetic Algorithms
HH	Hyperthermic halo
IPO-Porto	Instituto Português de Oncologia do Porto Francisco Gentil, E.P.E.
IBk	Instance Based for k-Neighbour classifier
IR	Infrared
IRT	Infrared Thermal Imaging
k-NN	k-Nearest Neighbours
LDA	Linear Discriminant Analysis

LDI	Laser Doppler Imaging
LIT	Lock-in Thermal Imaging
MMS	Mohs micrographic surgery
MSC	Melanoma skin cancer
NETD	Noise Equivalent Temperature Difference
Nevi	Melanocytic Nevi
NMSC	Non-melanoma skin cancer
NO	Nitric oxide
Non-neoplastic	Skin neoplasm scar tissue
OCT	Optical Coherence Tomography
Other	Other benign neoplasia
PDT	Photodynamic therapy
PWC	Pairwise coupling
RCM	Reflectance Confocal Microscopu
RF	Random Forest
ROC	Receiver Operating Characteristic
ROI	Region of interest
SA-SVM	Self-Advised Support Vector Machines
SCC	Squamous cell carcinoma
SK	Seborrheic Keratosis
SMO	Sequential Minimal Optimization classifier
SMOTE	Synthetic Minority Oversampling Technique
SN	Sensitivity
SP	Specificity
SVM	Support Vector Machines
T _c	Core temperature
TN	True Negative
TP	True Positive
TRT	Thermal recovery time
T _s	Shell temperature
TT	Telethermography
UV	Ultraviolet
VEGF	Vascular endothelial growth factors

List of symbols

C	Convection
DM	Average lesion temperature for dynamic analysis
DSTD	Standard deviation of lesion temperature for dynamic analysis
E	Evaporation

J	Total irradiated energy
k	Number of neighbours
K	Conduction
M	Metabolic rate
n	Number of training set instances
p	Probability value
S	Heat storage
Sd1	Lesion temperature diagonal - number 1
Sd2	Lesion temperature diagonal - number 2
Sh	Lesion horizontal temperature profile
SM	Average lesion temperature for static analysis
SSTD	Standard deviation of lesion temperature for static analysis
Sv	Lesion vertical temperature profile
W	Mechanical work
ε	Emissivity
σ	Stefan-Boltzmann constant
T	Absolute temperature
$\overline{x_c}$	5-connected pixels with highest average temperature
$\overline{x_h}$	5-connected pixels with lowest average temperature

Chapter 1

Introduction

The incidence rates of melanoma (MSC) and non-melanoma skin cancer (NMSC) have increased over the last decades [1], affecting more than 2 million individuals worldwide [2]. Only in 2012, European countries registered an incidence rate for MSC of 11.1 per 100 000 population, having Portugal contributed with an 8.2 [3], excluding NMSC. Even though, detailed statistics concerning the occurrence of non-melanoma is rare, it is of knowledge that its number exceeds largely the one of MSC and, for this reason, increased attention has been given to this type [1].

When skin fails to adapt to aggressive environmental changes, a defect occurs in the maintenance of physiological balance. The external stimuli can result in dermal and/or epidermal lesions, like skin neoplasms, and an abnormal process is triggered in the most exposed organ of the human body [4].

Skin neoplasms are formed when damaged skin cells multiply in a rapid and uncontrolled manner, as oppose to dying and being replaced by healthy ones, due to faulty apoptotic and regulatory mechanisms. This continuous abnormal growth of tissue leads to the formation of a mass on site, that displays no function for the host organism [5]. Its classification as benign or malignant lesions resides in particular features. The first tumour type includes, e. g., nevi and seborrheic keratosis, and is characterized by low growth rates, being unable to spread to adjacent tissues. Malignant tumours grow at high rates and frequently metastasize, invading other body locations. This latter neoplasm type may further be divided into melanoma (MSC) and non-melanoma skin cancer (NMSC), such as basal cell carcinoma (BCC) and squamous cell carcinoma (SCC), according to its origin [6], [7].

Throughout the years, authors have appointed several factors and risky behaviours as possible causes for skin neoplasms to arise, especially the malignant ones. Exposure to arsenic [8], immunodeficiency [9], phenotypic characteristics [10], high number of nevi, family background of MSC or previous record of NMSC [11] have been linked to this pathological process. However, excessive exposure to ultraviolet (UV) radiation and history of sunburns during childhood are, most definitely, the primary causes for skin cancer development, justifying its common appearance in bare regions of the body, such as head, face, arms and dorsum of the hands [12].

One of the main challenges for skin cancer is its detection, since most malignant tumours are treatable if detected at an early stage [13]. Currently, visual inspection is the primary method for skin cancer diagnosis and is typically performed by a physician, taking into account the ABCDE clinical rule (Asymmetry, Border, Colour, Diameter, Evolution). This examination presents varying precision rates, since it highly depends on the experience of the health care professional [14]. In addition, early detection is complex and often non-existent, decreasing the chances of a successful treatment, when dealing with non-benign tumours [15]. If a lesion is suspected to be malignant, surgical excision is performed, followed by an histopathological study to establish an accurate diagnosis [16]. In order to improve skin cancer detection, reducing the mortality rates associated with this disease, and avoiding discomfort and unnecessary scar tissue provoked by the current time-consuming procedures, new diagnostic methods have been explored, such as dermoscopy, laser Doppler imaging and infrared thermal imaging (IRT) [14], [15].

IRT takes advantage of the ability of the outer layer of the skin to emit IR radiation, to aid in medical diagnosis. The electromagnetic waves, in the range of 1 to 14 μm , emitted by this coat due to the underlying vasculature, are detected by infrared cameras, producing images according to the skin's emissivity of natural infrared radiation, i. e., thermograms [17], [18]. The recorded temperature values can be analysed, with different image processing tools, and used to detect normal or abnormal physiological processes[17], as those that take place in skin lesions. This non-invasive and non-ionizing[19] method has been applied, in different studies, in static experiments, i. e., without any thermal stimulus prior to the image acquisition process, or dynamically, with the application of a thermal stress to the lesion site before the thermogram formation. The second methodology has shown better results in skin cancer detection, particularly in the diagnosis of early stage melanoma [20].

Still, understanding the information supplied by thermograms can be a challenging task for the physician. Thus, the introduction of artificial intelligence (AI) computational methods in this task can be of value, to supply a second opinion. The use of AI for decision support systems in medicine has been present for over 50 years. Machine learning algorithms represent a key branch of this area, specially when dealing with medical decisions, due to its ability to learn before drawing a conclusion [21]. In the case of skin cancer diagnosis, the set of variables retrieved during image analysis and processing can be used as inputs for a classifier, that delivers an output result, assigning each lesion to a given group [21]. High accuracy and efficiency rates are one of the main advantages of the application of these algorithms in medical diagnosis, since the developed learners can capture and integrate information a way that the human brain cannot, in a fraction of the time.

1.1 - Motivation

The increasing rates of skin cancer and associated numbers of death are a current problem in global population. Since its detection and diagnosis are the primary mean to reduce its impact,

new methodologies, like IRT, are needed to overcome some of the weaknesses of the current diagnosis processes and provide future assessment of treatment efficiency.

1.2 - Aim

In this dissertation, IRT will be used dynamically, with the aim of characterizing the thermal signature of different skin lesion types, diagnosed in patients of IPO-Porto. Machine learning classifier will be used for classification purposes, using thermal information retrieved from image analysis and processing.

At the end, it is expected the differentiation of malignant and benign lesions, the distinction between distinct types of skin neoplasms and the correlation of such with the statistical data related to the studied population.

1.3 - Contribution

The results of this research project can be applied further along, in a clinical scenario, supplying complementary information to health care professionals, in the area of dermatology and plastic and reconstructive surgery. The outcomes can aid in the early diagnosis of skin lesions and subsequent distinction, lessening biopsy procedures, or in the prevention of recurrences, working as a screening tool. In any event, improving healthcare for patients and reducing costs associated with the pathology.

The knowledge acquired throughout this dissertation contributed for the publication of 4 scientific articles, included in Appendix I.

1.4 - Dissertation outline

The presented work is divided in eight chapters. The current, - Introduction -, explaining the problem, motivation, aim and contribution of this work. In chapter II, an overview of the skin's constitution and associated thermoregulatory mechanisms is encountered, followed by a collection of sections dedicate to skin cancer formation, types and related statistics. The diagnosis and treatment techniques currently on the market are also regarded. In the next chapter, an introduction to medical thermography is performed and a literature review is included to define the current state of the application of IRT in the detection/monitoring of skin neoplasms and understand its faults. A bibliographic research is also found in chapter IV but focused on the application of artificial intelligence classifiers in skin cancer detection with different imaging modalities. Chapter V includes a detailed description of the materials and methodology of this project, particularly the developed static and dynamic image analysis strategy and implemented classifiers. The comparison between the images acquired using static and dynamic thermography are addressed in Chapter VI, followed by the discussion of such in VII. Lastly, Chapter VIII, the conclusion, contains the primary achievements and the suggested future improvements.

Chapter 2

Skin oncological conditions

In this chapter, a brief description of the skin's constitution is presented, as well as the process involved in the thermoregulation of the human body. Following, the formation of skin neoplasms and the anatomic and physiological alterations involved are addressed, risk factors and potential triggers. A distinction between malignant and benign lesions is regarded with a more detailed description of the different neoplasms encompassed by each type. The main treatments and diagnosis techniques currently utilized are also appointed.

2.1 - Skin constitution

The skin of an adult weights between 3 to 5 kg, and coats, approximately, an area of 2 m², varying in thickness from 1.5 to 4.0 mm, depending of the body region that is covered [4], [22]. Being the biggest and most exposed organ of the human body, it is responsible for interacting with the external environment, transmitting outside stimuli to the interior [23]. Its constituents accomplish the specific functions for which the skin is responsible.

The skin is composed by two main layers: epidermis and dermis - Figure 2.1A (adapted from [24]).

The first and topmost coat - epidermis - is defined as a stratified squamous epithelium and is commonly divided into four sheets of cells: stratum basale or stratum germinativum, stratum spinosum, stratum granulosum and stratum corneum; which perform barrier functions [25]. The cellular content of this layer includes, in its majority, keratinocytes (85-95%), that play a key role in Vitamin D synthesis [4]. Additionally, Langerhans's cells and melanocytes, are also found in this layer, providing protection against antigens or microbes and UV radiation, respectively, as well as Merkel cells that possess a sensory function. No blood vessels are encountered in the epidermis [25].

The underlying sheet of connective tissue - dermis - presents lymphocytes, mononuclear phagocytes, Langerhans's cells and mast cells in its cellular composition [25]. In addition, it presents a high number of fibroblasts, that are responsible for the production of collagen and

elastin fibres, granting structural support and resistance to mechanical stress [26]. Other structures, such as hair follicles, sweat glands, sebaceous glands, apocrine glands, nerves and lymphatic vessels can also be encountered in this layer [26].

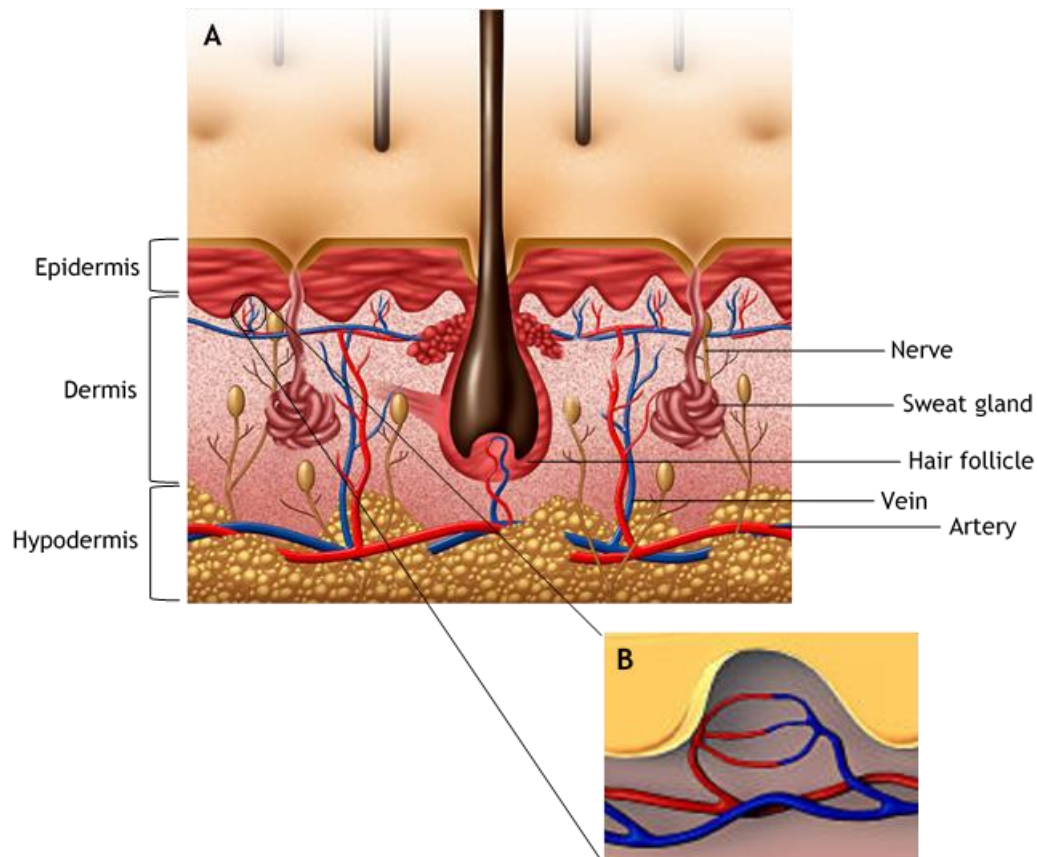


Figure 2.1 - Scheme of human skin: A - Layers and its main structures; B - Capillary loop.

In contrast to epidermis, dermis is highly vascularized, presenting a vascular structure organized, mostly, in two horizontal levels. On the lowest part of the dermis lies the deeper plexus, nurturing hair follicles and sweat glands with its arterioles, while on the upper part, the arterioles and venules that compose the superficial plexus, give rise to capillary loops [4] - Figure 2.1B (adapted from [27]).

Some authors [26] consider, yet, a third coat, the hypodermis or subcutaneous tissue, which is basically composed by the fat that lies beneath the dermis. This skin layer presents an important venous plexus whose blood flow is regulated by arteriovenous anastomosis (AVA), i. e., thick-walled vessels that connect arteries to veins [28], [29] - Figure 2.2 (adapted from [29]). Together with the dermis vascular network, these structures play an essential role in the regulation of body temperature, fulfilling one of the most important functions of the skin - thermoregulation [30].

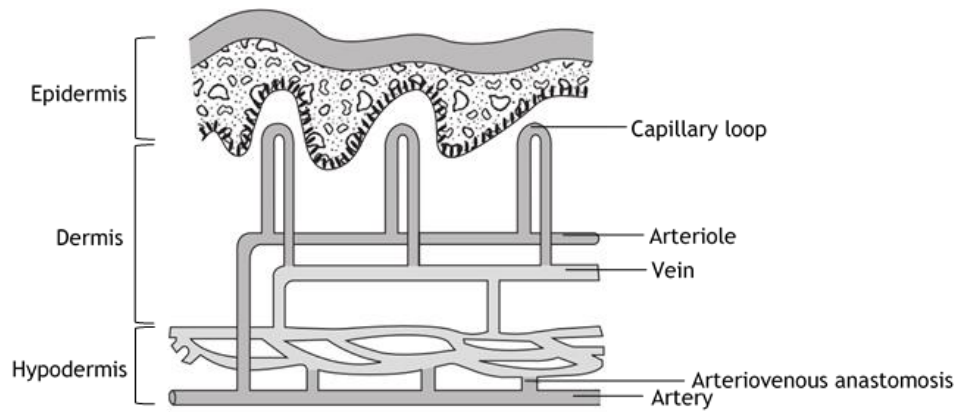


Figure 2.2 - Skin layers and vascular structures encountered.

2.2 - Thermophysiology

The maintenance of body temperature is vital for the proper functioning of the human organism, since a small deviation of 3.5 °C, from the core temperature (T_c) of 37 degrees Celsius, can lead to physiological complications and even death [31]. This thermal equilibrium is maintained or achieved by the thermoregulatory system, through heat loss and heat generation, after the detection of a temperature alteration by thermoreceptors [18], [32].

The T_c is completely regulated by the hypothalamus and maintains its value thoroughly constant, whereas the shell temperature (T_s), i.e., the temperature of skin, subcutaneous tissue and muscle tissue, is regulated, primarily, by skin's microvasculature and thermal changes in the surrounding environment, and oscillates in a wider range of temperature values [31]. Under a normal physiological status, T_s is lower than T_c [28].

When in a cold environment, the cold receptors located in the skin transmit information to the hypothalamus, through the sympathetic nerve system [29]. Following, a motor response, that includes vasoconstriction of the AVA in the periphery is send lowering blood flow in the dermis. As a consequence, a decrease in T_s is verified, as an effort to resemble the environmental conditions, decreasing, therefore, heat losses [32] - Figure 2.3A (adapted from [33]). In contrast, when in a hotter atmosphere, vasodilation is encouraged to increase blood circulation in the periphery and raise skin temperature. Thus, heat losses increase with the mentioned purpose [29] - Figure 2.3B (adapted from [33]).

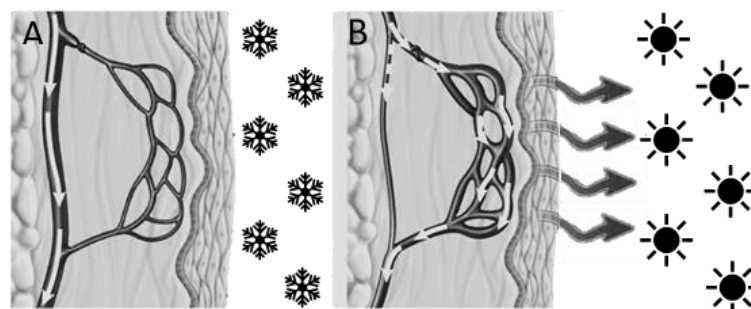


Figure 2.3 - Thermoregulation of skin temperature: A-Vasoconstriction, B-Vasodilation.

These thermoreceptors vary in their constitution and number, making the time-response of thermal stimulus different, depending on the temperature range. While cold receptors are composed by myelinated A δ fibres, hot sensors present unmyelinated C fibres. This histological difference affects the response times of both nerve types, making the transduction of information through action potentials much faster in A δ fibres [34] - Table 2.1 [35]. Its location also varies, with cold sensors situated at, approximately, 0.15 to 0.17 mm from the skin surface and hot ones at a depth of 0.3-0.6 mm [29]. These facts, combined with the excess of cold sensors in relations to warm ones, makes the detection of cold stimulus much faster than the detection of warm ones [34].

It is of interest to point that the activation of different sensors depends on the temperature stimuli. For example, cold receptors will not respond to hot stimuli and the contrary is verified in warm ones. When a temperature below 20°C or above 45°C is reached, the thermal receptors are inactivated and pain sensors - nociceptors - are stimulated [36]. This immediate activation is mediated by A δ fibres [35], explaining the sensation of pain before heat when burning occurs.

Table 2.1 - Nerve fibres classification and respective conduction velocities.

Fibre type	A β	A δ	C
Conduction velocities (m/s)	36-90	5-36	0.2-1

The temperature regulation mechanisms located on the surface of the body can also be applied to control T_c. This process happens at all times when heat generated by metabolic activity is directed, by blood vessels, to the skin, in order to maintain the core temperature value [28]. Thus, as the metabolic rate of tissues increases, its temperature also rises, and an increment of blood flow in the periphery is needed to lower this value [28].

The heat losses that take place on the skin-environment interface are influenced by external factors, occurring by convection, conduction and radiation, and evaporation [17]. The latter is observed when the core temperature is risen, as in physical activities, transferring water in a liquid form to the gaseous state, at the expense of energy that is released in the form of heat [28]. Convection takes place when heat is transported through a moving medium [28], e.g., blood circulation pathways, as the one described previously. In opposition, conduction only occurs with a non-moving medium, mainly with solid objects, since exchanges with gaseous or liquid environments are achieved by convective processes [29]. An example of this physical process is heat conducted between the skin surface and cloth items [29]. Lastly, radiation heat losses consist on the emission of infrared waves by the skin's surface, being the greater contributor for heat transferences during mild thermal situations [30].

All the mentioned contributions for heat transferences can be summarized by the Heat balance equation (1) that describes the generation of heat (M), its transfer to the surrounding environments (E, R, K and C) when in excess after mechanical work (W), and its storage (S) [37] :

$$M - W = E + R + C + K + S \quad (1)$$

being M , W , E , R , C , K and S metabolic rate of the body, mechanical work, evaporation, radiation, convection, conduction and heat storage, respectively.

2.3 - Skin neoplasms: formation and angiogenesis

Like any cell in human body, skin cells are controlled by regulatory mechanisms, in order to assure its replacement, if needed. When this process is defective, by cellular damage or degenerative alterations, apoptosis fails to occur and the deficient cell continues to growth and multiplies in an uncontrolled manner. Ultimately, a skin neoplasm, also referred to as skin tumour, i. e., an accumulation of cells with no biological purpose, can arise at this site [7]. When in the presence of these cell aggregations physiological alterations, that interfere with the normal functioning of the body, can take place.

In the early stages of development, tumour cells do not present nutritional needs or oxygen depletion, due to the sufficient blood perfusion in this area, assured by pre-existent blood vessels [17]. Yet, the vascular flow encountered is boosted thanks to a neuronal messenger: nitric oxide (NO); produced intra and extravascular by the vasculature that nurtures neoplastic cells [17]. Its release causes vasodilation, increasing the perfusion in the lesion site [38]. In the case of skin tumours, that are generally localized in or close to the skin surface, this perfusion changes can prevail over the thermoregulatory system in the area, causing alterations in heat transfers [17]. When the metabolic needs of the neoplasm cell population exceeds oxygen and nutrient supply, new blood vessels are recruited from surrounding arteries and arterioles [17] and tumour induced angiogenesis takes place [39]. The formation of these neovessels is triggered by the tumour's environment, but also by growth factors, such as vascular endothelial growth factors (VEGF) and fibroblast growth factors (FGF) [40]. The neovascularization rate depends on the tumour malignancy, being that benign lesions undertake neovascularization less quickly than malignant ones [41] and are mostly related to blood vessels ectasia and hyperaemia [42].

The formation of skin lesions, despite their malignancy, can be related to numerous factors. Phenotypic characteristics, such as skin and hair colour, weakened immune system and family history of skin neoplasms can influence the person's predisposition for skin tumour development. However, excessive exposure to UV light is considered a primary risk factor [11]. This radiation type can cause DNA defects and mutate genes, being, thus, regularly associated with the arising of all types of skin cancer [12]. Exposure to tar or arsenic is also a hazardous behaviour [43].

Neoplasms can be classified as benign or malignant according to a specific set of characteristics. Benign lesions present low growth rates, taking a considerable amount of time to double its size. This type of tumours is constituted by well differentiated cells that are encapsulated by connective tissue, easing its surgical removal, and are unable to penetrate its surroundings. For this reason, benign neoplasms grow in a localized manner, pushing the

surrounding healthy tissue - expansion growth [6], [7]. In contrast, malignant tumours exhibit poorly differentiated cells with an elevated growth rate, recruiting blood vessels to supply its high metabolic needs. These cells are able to invade adjacent tissue, growing by infiltration, and can often metastasize through the vascular and lymphatic system. For these reasons, if not detected early, malignant lesions can establish secondary tumour sites throughout the body and kill its host [6], [7]. According to its tissue or cell of origin, skin neoplasms can be named and identified [44].

2.3.1 - Malignant skin neoplasms

Malignant skin tumours can be divided in melanoma skin cancer (MSC) and non-melanoma skin cancer (NMSC). The latter, is usually used to refer to basal cell carcinoma (BCC) and squamous cell carcinoma (SCC), even though many other types, e.g., Merkel cell carcinoma, can be included in this group [10].

Melanoma starts developing in melanocytes, growing horizontally - radial growth - or vertically - vertical growth - to invade deeper tissue. The second growth phase is responsible for metastasization, since the damaged cells gain access to blood and lymphatic vessels, as they pass from the epidermis to the dermis [45]. They are mostly classified as lentigo maligna, superficial spreading (Fig. 2.4A, adapted from [45]), acral lentiginous or nodular melanoma [44]. This type of tumour, responsible for most of skin cancer related deaths, is usually flat, presenting high border irregularity and a multicolour appearance that ranges from brown and dark purple tones to skin like colours [44], [46]. Its different variations are normally encountered in light skin subjects, with red or blond hair, as oppose to darker individuals [45], being its appearance connected not only to sunlight exposure and genetic factors, but also to previously existent melanocytic nevi, that can evolve to a malignant form [44].

The most common malignant skin tumour, BCC, arises when basal cells proliferate and invade the dermis - (Fig. 2.4B, adapted [47]). They may be noduloulcerative, cystic, cicatricial, superficial and pigmented. Its appearance might vary from blue to pink nodules, according to its type, being, at times, in an ulcerative state [44]. This cancer type is mainly located on the face of light-skinned subjects and it is mainly connected to UV exposure during childhood years [46].

A faulty proliferation of keratinocytes is responsible for the emergence of squamous cell carcinoma [48] - Fig. 2.4C (adapted from [48]). SCC incidence is often associated with long-term sun exposure, evolving, in most cases, from other skin lesions already present, i.e., actinic keratosis [10]. It usually presents a smooth surface that tends to adopt a verrucous texture that can further evolve and form a crusty horn-like structure [48]. Its variants may include verrucous carcinoma, scrotal, vulvar, lip and penile squamous cell carcinoma [48].

Even though rare, Merkel cell carcinoma is considered to be one of the deadliest skin cancers. A purple or pinkish nodular structure, prone to recurrences, appears on the skin of, normally, elder Caucasian individuals [49]. The trigger of this dermal lesion has not been established, though its common appearance in skin areas exposed to the sun, such as neck and head [46] - Fig. 2.4D (adapted from [49]).

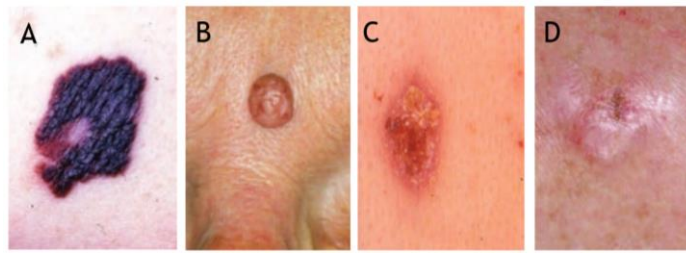


Figure 2.4 - Malignant skin lesions: A - Superficial spreading melanoma; B - Basal cell carcinoma; C - Squamous cell carcinoma; D - Merkel cell carcinoma.

2.3.2 - Benign skin neoplasms

The most common skin lesions encompassed by benign neoplasms are nevi, keratoses, angiomas and lipomas [44], [50].

Benign nevi comprise several types of skin lesions, such as melanocytic and dysplastic nevi. The first tumour, commonly known as mole, finds its source site, like all existing nevi, in melanocytes, i.e., the cells responsible for the skin pigmentation [7] - Fig. 2.5A (adapted from [44]). Usually, these neoplasms present a congenital origin, being already present at birth. However, they can also be acquired, mostly due to family genetics associated with excessive sunlight during infant years, appearing mainly before the age of 20. It normally presents a diameter smaller than 10 mm and colours ranging from black to brown or blue, with a flat or prominent structure [44]. Even though its benignity, some melanocytic nevus can evolve and give rise to malignant lesions [51]. Dysplastic nevus is a particular type of atypical melanocytic nevus, being interpreted as an intermediate stage between its mother lesion and melanoma - Fig. 2.5B (adapted from [51]). Most of these skin tumours present irregular borders and uneven pigmentation [51]. Both types of nevi are frequently encountered in people with fair-skin [44].

As the name implies, keratoses originate in the upper layer of the skin when keratinocytes are damaged. Actinic and seborrheic keratoses are the main examples of this skin tumour class [44]. Actinic lesions are often provoked by excessive exposure to UV radiation, appearing, particularly, in elderly people with clear complexion - Fig. 5C (adapted from [52]). These grey or pink tumours with crusty surfaces are considered pre-malignant lesions, being frequently indicated as precursor neoplasms for the development of SCC [10], [48], [52]. In opposition, seborrheic keratosis tends to remain benign through the course of life, despite its worrying appearance - Fig. 5D (adapted from [44]). It usually presents itself with a warty shape and pigmentation varying from yellow to dark brown [44], [53].

Hemangiomas or angiomas, are tumours composed by an excessive accumulation of blood vessels [45]. Some may arise in early childhood years, i. e., strawberry nevus, presenting itself as a puff-like structure with colours in the red/purple spectrum - Fig. 5E (adapted from [44]). It usually appears on the head and tends to regress almost completely until the age of 10 [44], [45].

Angiomas that have its origin during adulthood - cherry angiomas - do not recede, emerging as multiple papules with a red colour [44], [45]. Its cause have not yet been defined, even though the suspicion of specific hormones and the exposure to certain chemical products are believed to have relevance [50].

The last benign tumour type - lipoma - is composed by an aggregation of fat cells, present in the hypodermis layer, that manifests as a round structure, rubbery to the touch [44] - Fig. 5F (adapted from [44]). Like cherry angiomas its triggers are unknown, being related, at times, with traumas or chromosome 12 reassortment [50]. The removal of this benign tumour only occurs if any pain or discomfort is reported by the patient or if a doubtful diagnosis reached [50].

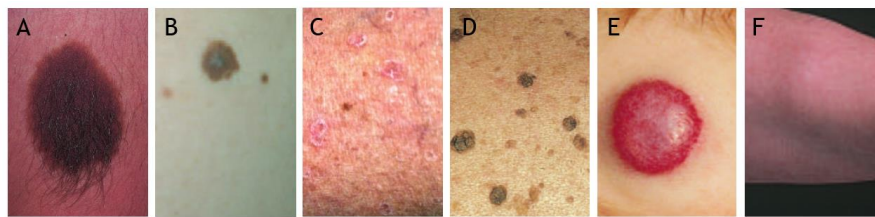


Figure 2.5 - Benign skin lesions: A - Melanocytic nevi; B - Dysplastic nevi; C - Actinic keratosis; D - Seborrheic keratosis, E - Strawberry nevus; F - Lipoma.

2.4 - Skin cancer statistics: incidence and associated costs

The number of skin tumours diagnosed over the last decades has increased considerably, making MSC and NMSC the cancer types with highest incidence in Caucasian individuals [1]. Each year, 2 to 3 million cases of non-melanoma tumours are estimated to occur worldwide, having an incidence rate 15 to 22 times greater than melanoma skin cancer [2]. Despite that, MSC is accountable for over 80% of the number of deaths linked to malignant skin tumours [54]. Only in Europe, an incidence rate of 11.1 per 100 000 was registered in 2012 for MSC, with a mortality rate of 2.3. Countries such as Portugal, with high numbers of sunny hours, are among the most affected, presenting a skin cancer mortality rate of 2.45, according to the WHO, in 2014 [55]. Despite these alarming trends, the mortality rates of malignant skin neoplasms have been stabilizing or rising lower [1], as it is verified in Table 2.2 [56].

Table 2.2 - Incidence and mortality rate of melanoma and other skin malignant neoplasms in Portugal per 100 000 malignant tumours.

Year	Melanoma		Skin - Others	
	Incidence rate	Mortality rate	Incidence rate	Mortality rate
2010	8.9	2.3	1.3	1.5
2008	8.2	2.0	1.2	1.4
2007	7.5	1.8	1.1	1.5

The increase of the incidence rates aforementioned has affected healthcare finances associated with, not only diagnosis, treatment and patient follow-up, but also monetary losses

caused by absence at work due to illness [57]. In 2005, Sweden spend 142.4 million euros due to skin tumours, being the diagnosis of melanoma the number one contributor for this expense. The costs related to NMSC also influenced the final amount, being one of primary cause for such a great expenditure [57]. The “increase incidence - increase cost” factor was documented in the United States, with an increment of 4.5 billion dollars in the space of 5 years for skin cancer treatment, due to a large number of new cases [58]. Apart from these examples, several other countries present a high financial load related to skin neoplasms [59]. A status that could be avoided or diminished with early detection methods associated with preventive measures [60].

2.5 - Diagnostic methods

The detection of skin lesions begins with a visual inspection, frequently based on the ABCDE clinical rule, even though other diagnosis methods, like the 7-check point list or the Menzies method, can also be applied [61]. This search is normally performed by a dermatologist that checks the lesion for Asymmetry, Border irregularity, Colour and Diameter and Evolution. However, self-monitoring systems to evaluate skin lesions are a current reality, having many companies developed smartphones apps for this purpose, like Melanoma detection from Fraunhofer Institute [62]. At any indication of malignancy, a biopsy, i.e., the partial - incisional - or complete removal - excisional - of the lesion, is performed, followed by a set of tests, e.g., a histological study to establish a diagnosis. However, this time-consuming process can be painful and increase patient stress, leaving, at times, unaesthetic and/or unnecessary scars [63]. Despite its disadvantages, this method continues to be the *gold standard* for skin cancer diagnosis.

For this reason, the search for advanced diagnosis techniques, that are innocuous for the patient, is an emerging quest.

Dermoscopy, dermatoscopy or epiluminescence microscopy is a non-invasive technique that has been used by practitioners as a diagnosis tool for pigmented skin lesions, particularly, melanomas. An immersion oil is placed over the tumour and a hand-held microscope, with a magnification of 10x to 100x, allows the visualization of epidermal and upper dermal structures, allowing an in-vivo examination [14], [63]. Some equipment provide image storing, facilitating the posterior comparison of lesions in patient follow-up. Due to its successful results in melanoma diagnosis, with reported specificity of 95% and increased sensibility [64], it is considered the gold standard for non-invasive diagnosis methods, even though its accuracy drops when used by clinicians with none to less experience [65]. For cancerous neoplasms, several evaluations throughout time can be required to determine the malignancy of the tumour, leading to lesion worsening and, subsequently, increased life risk [66]. In addition, some dermatologists still consider this method a bit pricey [67].

Another non-invasive diagnosis technique, explored mainly for melanoma skin cancer screening, is Laser Doppler Imaging (LDI). LDI uses a monochromatic laser beam to irradiate the lesion site. When the tissue is reached, scattering, absorption and spectral broadening of the laser occurs, according to the existent blood flow at that region, reflecting radiation with a different

wavelength. The encountered wavelength differences can be used to calculate flux [14], [68]. Thus, knowing that malignant tumours display high vascular networks, LDI has been used to distinguish melanomas from benign lesions. However, this is a costly technique and it has been showed that its application can result in a high number of false-negatives [69].

Another harmless imaging technique that has been introduced in the diagnosis of skin cancer is Optical Coherence Tomography (OCT). Cross sectional images of the damaged tissue are obtained after incidence of a longitudinal infrared beam, allowing the visualization of the macro structures that compose it, as well as its vascular and adnexal components. Nonetheless, the tumour expansion for adjacent tissues is not detectable, since cellular and subcellular features are not visible [70]. Some primary research has shown the use of OCT for basal cell carcinoma and actinic keratosis characterization, but more research is needed to attain the usefulness of this tool in skin cancer detection [71].

2.6 - Treatment methods

The treatment of choice for skin neoplasms depends on the lesion type, size, location and stage, as well as the patient's health condition and age [10]. A vast selection of options is available, with more aggressive techniques, such as surgical excision and Mohs micrographic surgery (MMS), and mild ones, e.g., cryotherapy, photodynamic therapy (PDT) and topical immunotherapy.

When leading with doubtful malignant lesions, excisional surgery of the skin neoplasm, almost certainly, will be the first treatment step. Depending on the lesion extent, a radius of excision is selected, to ensure complete removal, and other methods, such as radio or chemotherapy, can be used as adjuvant treatments, especially when the needed radial borders are impossible to obtain [49]. The discomfort and stress added to the skin tissue loss, that can, in more aggressive tumours, leave an unaesthetic scar, are some of the inconveniences appointed. Benign lesions are often left untouched, being only removed if unsightly or easily injured [44].

MMS can be interpreted as an improved version of a standard excision procedure, being only implemented for the removal of skin cancers. It is more expensive and consumes more time, but the chances of cure are higher [72]. The surgeon removes the lesion with a given margin, examines histologically on-site the removed tissue and, if any residual tumour is detected in the neoplasm borders, an additional portion of skin is removed [72]. In terms of aesthetics, this technique provides the best outcome possible [73].

Yet, these aggressive treatments should be avoided in elder and/or debilitated patients [44]. As an alternative, non-invasive options have also been applied, with less frequency, to skin lesions.

In PDT, a photosensitizer is applied to the lesion site, causing the tumour destruction, after activation with a light source. It can be used for the treatment of basal cell carcinomas and actinic keratoses, allowing the cure of multiple lesions at the same time. Additionally, it eases the treatment of tumours located in areas that are surgically hard to access [72].

Cryotherapy has also been used in BCC, SCC and keratoses treatments, where liquid nitrogen or CO₂ in a snow form, is used to freeze the lesion that eventually falls on its own. However, some precaution is advised to avoid any nerve damage due to over freezing [74].

BCC, SCC and melanoma have also been cured by topical immunotherapy. Depending on the lesion type a contact sensitizer, e.g., imiquimod, is applied. Even though the mechanisms involved in this process are not clear, it is believed that a cellular response against this substance is triggered, entrapping the cancer agent through hapten bounds [75].

Even though the non-invasiveness of these techniques is a plus, the time needed to witness the treatment success can lead to recurrences in some cases, hence the preference for surgical excisions [76].

2.7 - Summary

In short, the detection of skin cancer has yet to evolve in order to overcome the current difficulties that are presented. Since metabolic activity is highly connected to the malignancy of skin lesions, a diagnosis method that focus its results on the vascular response of the tumour site seems to be the best approach. IRT fulfils that need and is, therefore, the focus of the next chapter.

Chapter 3

Infrared thermal imaging

Chapter 3 approaches a brief history of IRT in the medical field, followed by the process involved in the implementation of this diagnostic technique. A review of the application of IRT in skin cancer detection, in recent studies, is presented, with detailed research strategy and main conclusions obtained.

3.1 - Principles

The human skin separates the body core from the surrounding environment. When subjected to an internal or external stimulus its status alters, leading, frequently, to skin temperature variations [77].

This disturbance has been used for several ages as a diagnostic symptom, being first reported in 480 B.C., when Hippocrates placed mud over a patient body and witnessed its change in dryness over time. The skin emission of thermal radiation allowed the differentiation of cold and hot spots, as the drying process occurred [39]. Centuries later, Santorio used a “thermometer”, inspired by Galilei’s “thermoscope”, to measure body temperature [78]. After great advances, this technique was used by Czerny, to obtain a thermogram of the human body, in Frankfurt (1928), being later accessible for medical use in the mid 1950’s [17]. Since then, several research studies have been conducted in order to explore the full potential of this tool in healthcare applications.

IRT uses thermal cameras to record the infrared (IR) radiation that is emitted by the body in the range of 1-14 μm . In other words, natural heat losses that occur in the outer layer of the human skin, due to, mostly, underlying vasculature, are detected and translated to images representative of that radiation - thermograms [17], [18]. The human skin presents an emissivity value of 0.98, being closest to a blackbody, i. e., an object with perfect emissivity, value of 1 [78]. Thus, it is an optimum candidate for thermal evaluation, since the released energy, that is recorded, can be

used to estimate the temperature values of a given body region, through the Stefan-Boltzmann equation (2) [79].

$$J = \varepsilon \times \sigma \times T^4 \quad (2)$$

being J , ε , σ and T , total irradiated energy, emissivity, Stefan-Boltzmann constant and absolute temperature, respectively.

The amount of emitted heat varies according to environmental factors [17]. For this reason, some precautions need to be adopted in order to avoid incorrect thermal measurements. First, room temperature and humidity need to be monitored and kept at, approximately, $21 \pm 1^\circ\text{C}$ and $\leq 50\%$, respectively, for subject acclimatization and measurement execution [80]. Following, any cloth items need to be removed from the lesion site, as these would act as an insulator, as well as hair, if possible. Additionally, make-up, nail polish, lotions or any other products that might camouflage the skin surface should be removed before performing the thermal recordings [77]. If all these aspects are considered, thermal images can be used as a representation of a person physiological state [78].

3.2 - Applications in medicine: skin neoplasms

The application of IRT can be verified in several medical areas. In rheumatology it has been used for the treatment monitoring of inflammatory arthritis, in clinical dermatology for the assessment of burn areas and, most recently, for the evaluation of skin areas affected by malignant neoplasms [19].

As explained in detail in chapter 2, when a physiological abnormality, e.g., the formation of a tumour, occurs, metabolic alterations take place, changing the dynamic of the organism. Most of these changes can be verified by blood flow differences in the lesion site, when compared to a healthy situation, resulting, ultimately, in a disturbance of the thermal equilibrium [19]. In skin neoplasms, this disruption has been reported in several studies, using this alternative tool. Normally, benign neoplasms are portrayed by hypothermic patterns, appearing colder than the surrounding skin tissue. In contrast, malignant tumours are usually represented by elevated temperatures, creating a hyperthermic pattern in the final thermogram, thus, being frequently referred to as “hot spots” [81]. This increase in temperature is attributed to the increment of blood flow, in the lesion site, that is necessary to maintain the elevated growth rate of this type of neoplasms, as well as increased metabolism.

Different thermal methodologies can be adopted, according to the user needs and final goals.

In static or steady-state IRT the image acquisition process occurs without any prior stimulation.

When used dynamically, a chemical, thermal or mechanical stress can be applied on the location of interest, followed by the capture of the images, while skin recovery occurs [82]. The advantage of applying the latter method lies on the fact that, after a disruption of the thermal balance, different temperature outlines representative of beneath structures can arise and be visible in the

obtained thermograms [83]. This allows a more detailed diagnostic information, since physiological alterations that occur in the interior might not be expressed in external temperature differences, as in the case of early stage melanoma. This approach also eases the identification of malignant lesions located in body regions that are characteristically hot, e. g., neck, axilla, temple and Scarpa's triangle [80]. Additionally, the thermal patterns verified in raw thermograms can also be of service for surgeons, helping in the outline of excisional margins [81]. For these reasons, IRT, particularly dynamic, has been the focus of recent studies related to skin neoplasms diagnosis and treatment screening, as described in the following sub-sections.

3.3 - Literature Review

A systematic review was conducted to ascertain the current state of the applications of medical IRT in skin neoplasms diagnosis, as well as to understand the possible challenges that can arise during this process. At the end, some improvements for future studies conducted in this area are established and some points are regarded for the future collection of IRT images.

3.2.1 - Methodology

Search Strategy

The literature research was conducted, using the following combination of keywords, in the bibliographic databases: Scopus, PubMed and ISI Web of Science, respectively: ((TITLE-ABS-KEY (skin cancer) AND TITLE-ABS-KEY (thermography OR (infrared imaging) OR (thermal imaging)))); ((skin cancer [Title/Abstract]) AND (thermography[Title/Abstract] OR (infrared imaging[Title/Abstract]) OR (thermal imaging[Title/Abstract]))); TOPIC: (skin cancer) AND TOPIC: (thermography OR (infrared imaging) OR (thermal imaging)). The terms used for the search were clear and basic, to increase the number of results encountered, and the field selection applied in each reference source was used to guarantee the consistency of the research. The Boolean operator OR was included in the search, since “infrared imaging” and “thermal imaging” are often used as synonyms of “thermography”. Only publications with dates from 01/01/2014 to the date of this research, i. e., 31/03/2017 were included. A duplicate removal was performed at the end.

Screening and eligibility results

The title and abstracts of the encountered publications were, firstly, analysed, including only the articles that referred the use of medical thermography for the evaluation of skin neoplasms.

The first eligibility criterion involved the elimination of articles that reported the use of IRT in skin cancer cells, instead of the neoplasm itself. Additionally, meeting abstracts and revision articles were eliminated, making the second criterion. The third selection parameter consisted in keeping the articles written in English, excluding publications in other languages. Considering

that this review is focused in a single imaging modality, i. e., thermography, some articles based on the use of infrared spectral imaging, encountered due to the terms used in the bibliographic research, were removed, making the fourth eligibility criteria. Finally, publications focused on the description of thermal technology used for the detection of skin cancer, were eliminated from the remaining results.

The final set of articles were then separated into three main classes: clinical studies for diagnosis applications, treatment monitoring in clinical situations and theoretical studies, for a full text review. The entire process was performed taking into account the PRISMA rules for systematic reviews described in [84], [85]. Figure 3.1 (adapted from [85]) summarizing the phases of this revision process.

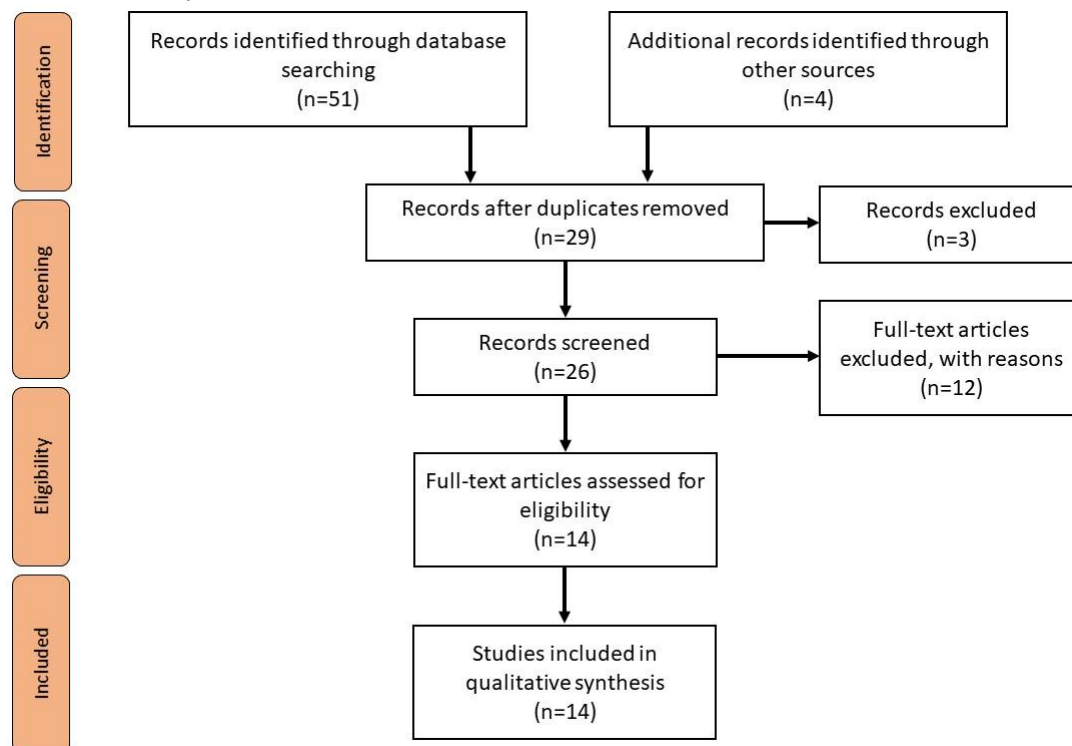


Figure 3.1 - PRISMA flow diagram.

3.2.2 - Results

The conducted bibliographic search resulted in a total of 51 publications, being 10, 9 and 32 encountered in ISI Web of Knowledge, PubMed and Scopus, respectively. Four additional records were identified through Google Scholar, being included in the literature search results. After duplicate removal, 29 articles were kept. The abstract and title screening resulted in the exclusion of 3 articles, since no application of medical thermography to skin neoplasms was studied in the publication. The eligibility criteria previously mentioned lead to the elimination of 12 articles, being the first, second, third and fourth criterion responsible for the exclusion of 1, 3, 3 and 5 publications, respectively. Thus, 14 full-text articles remained for revision, 6 articles describe the use of IRT as a diagnosis support tool in clinical applications, 3 concern the use of thermography

for skin neoplasms treatment screening in clinical studies and 5 are included in the theoretical studies category, for diagnosis purposes.

Diagnosis support method - Clinical studies

Concerning the use of IRT for the detection and identification of skin lesions, a consent is verified in all the articles, indicating that thermography, applied with all its variants, has the possibility to be an effective complementary diagnostic support tool.

The differences in temperature encountered between lesion areas and the surrounding tissue proved to be useful in the distinction between malignant and benign skin neoplasms [86], [87].

Godoy *et al.* [86] used one of the most elaborated and though strategies to acquire dynamic IR images. A plastic square marker, surrounding the lesion site, was used as a spatial reference to allow the subsequent alignment of the collected IRT images.

A visible picture of this ensemble was taken to allow the correct localization of the skin tumour in the thermal images. Following, a longwave infrared camera captured a sequence of IR images for 15 s, for future reference, and the skin neoplasm was subjected to a cold stimulus, using a Ranque-Hilsch vortex, with a 30 second duration. The thermal recovery was then recorded for 2 minutes. The developed algorithm for the processing of the thermal data in MATLAB performed, firstly, the alignment of the collected images, through the Harris corner detector method. Then, the user delimited the lesion site with *imellipse* and, to offset any non-uniform cooling, only pixels inside and outside the neoplasm location with the same initial temperature were selected for thermal analysis. If the temperature difference verified between these two areas was higher than a given threshold, then, the lesion was considered malignant. They achieved a sensitivity and specificity value of 95% and 83%, respectively, after analysing 43 skin cancers and 59 benign skin neoplasms. The described methodology presents very strong points, such as, the pixel selection and the use of a temperature difference - threshold - to distinguish between benign and malignant lesion, regardless of the mathematical sign of that value, as it is commonly verified in similar studies. However, the threshold selection is performed in order to maximize the sensitivity and specificity value based on the population enrolled in that specific study, meaning that different results may be encountered for a different study group if the same threshold is to be used. The use of a plastic marker also needs to be re-evaluated, since its placement in some body areas, and subsequent thermal measurements, might be impossible.

The characterization of distinct types of skin lesions, using IRT, has also been successfully studied, with the goal of providing more information to the practitioner, during the diagnosis process, either by a steady-state [88] or a dynamic [89] process.

A common idea is denoted by Di Carlo *et al.* [89], in respect to the thermal patterns presented by the neoplasms, referring that, in general, malignant lesions are characterized by hyperthermic patterns, while the benign ones, present lower emissivity values. The use of video thermography associated with thermostimulation - +5°C for 20 seconds - allowed the complete

separation between basal cell carcinomas (BCC) and actinic keratosis (AK) lesions, having the first type of skin neoplasm displayed a hypothermic halo and the latter a hyperthermic one [89], conflicting with the previously mentioned assumption. The dermoscopy results, used as a comparison tool, were not as satisfactory with an inconclusive diagnosis of 22% of lesions, showing that IRT might be more promising in the distinction of certain skin lesion types.

The work of Stringasci M. *et al.* [88], with steady-state thermography, reinforced, partly, these findings, having BCC displayed lower emissivity values. When compared to intradermal nevus, this latter displayed lower temperatures than the basal type. The distinction between squamous cell carcinoma (SCC), which showed an hyperthermic pattern, and AK, with temperature values similar to the skin, was also successfully carried out. A contradictory result of what is usually encountered in the literature was reached, having nodular melanoma displayed a hypothermic pattern in relation to the surrounding healthy tissue. According to Stringasci M. *et al.* this outcome could be justified by a thermal absorption caused by the dense pigmentation of this type of lesion. However, since only one lesion of each type was analysed the conclusions drawn are questionable and more patients would be needed to obtain statistically significant findings.

For the last two articles mentioned, none contained any detailed information, concerning the analysis of the IRT images.

IRT proved to be a secure tool to aid in the detection of melanoma [90], [91] with high specificity, even though it presents varying sensitivity values, depending, partly, on the equipment used.

Solivetti *et al.* [90] tested the use of telethermography (TT), associated with thermo-stimulation, for the detection of melanoma in-transit metastasis. A high-frequency ultrasound equipment was used as the gold standard, resulting in 100% sensitivity. In opposition, TT only diagnosed 15 lesions (22%), but with no false-positives, meaning 100% specificity. For bigger nodules, especially if located closer to the skin's surface, the probability of identifying melanoma metastasis as such increased and an even greater augment was verified when TT was combined with a cold stress. It is not safe to say that TT can replace ultrasound in the detection of this type of skin neoplasm, however it could be used as a complementary tool to avoid patient's discomfort and stress with unnecessary biopsies. Additionally, more test subjects would be needed to support the results, since the population size of the study - 52 lesions - was not very significant.

Concluding, in a distinct study [91], dynamic thermal imaging (DTI) was employed to monitor atypical skin neoplasms, indicative of early melanoma lesions. A metal plate was used for the cooling process - 5°C during 20 seconds - and a thermal recovery of 30 seconds was monitored. Hot patterns were detected in 60.78% of lesions. Even though atypical nevi may lead to melanoma development, its presence does not always indicate an abnormal metabolic activity in the lesion site, hence the detection value obtained in this research. All and all, the potential of this tool for precocious diagnosis is demonstrated, but a histological exam of the encountered hyperthermic lesions should have been considered to increase the credibility of the final results.

Treatment monitoring - Clinical studies

Apart from diagnosis, medical IRT has demonstrated its usefulness on the patient follow-up, through the evaluation of skin lesions, such as actinic keratosis [43] and melanoma [92], after treatment.

Laino et al. [43] used active TT to successfully evaluate the reduction of the hyperthermic halo (HH) of AK, after its removal and lesion site treatment with Eryfotona. The lesions were cooled with a balloon, for 20 seconds, filled with an alcohol and water mix at +5°C. Before lesion removal the HH was verified in all the patients, having an average size of 3.46 cm² and fast thermal recovery times (TRTs). Dynamic thermography allowed the visualization of the reduction of both these parameters, after treatment with Eryfotona, having a mean HH of 0.64 cm² and TRTs similar to healthy skin tissue, i. e., longer than 2 minutes. The calculations of HH and TRT were performed by a computer, but detailed information regarding this step is not supplied.

IRT also helped in the monitoring of melanoma tumours, during electrical stimulation therapy via liquid metal printed electronics on mice skin, as seen in [92]. Li J. *et al.* resorted to thermography to monitor the temperature of the skin, covering the tumours, and demonstrate that no significant thermal alterations occurred during the treatment stage.

Additionally, steady-state thermographic measurements have been used to verify the changes that occur in the skin temperature gradient of basal cell carcinomas, during treatment with photodynamic therapy [81]. Cholewka *et al.* stated that the extent of thermal changes, exceeds the place of injury, suggesting that the treatment itself might affect a larger area than expected and, for that, the conclusions drawn need to be well thought-out.

Theoretical studies

Medical IRT has shown its potential, in theoretical studies, for the detection of melanoma, in distinct phases of development. Bonmarin and Le Gal constructed a computational model, that emulated different skin cancer stages, and tested the ability of steady-state and transient-state - lock-in thermal imaging (LIT) - thermography in the detection of such tumours. In LIT the thermal stimulation is periodically performed at a given frequency and the thermal images are processed, by the lock-in principle, commonly used in materials testing, obtaining an amplitude and phase image [54]. The melanoma skin models - stage I, II, III, IV and V - were constructed with varying blood perfusion, due to the Pennes bio-heat equation, and different metabolic activities. As expected the thermal signal of stage I was poorly detected when steady-state was used. In dynamic testing, the phase images, retrieved from the demodulation of the transient skin surface temperature signals, seemed promising for the detection of such precocious lesions. However, the modulation frequency used influences the depth of the skin tissue evaluated, meaning that higher frequencies would be sufficient for the detection of early stage melanoma, while higher values are needed for more penetrating tumours. This decrease of frequency, encompasses an increase of 13 minutes in the time necessary for the evaluation, complicating its use in a medical scenario.

Another mathematical model, developed by Bhowmik *et al.* [93], studied the use of dynamic infrared imaging - +10°C during 60 seconds -, in 4 different melanoma stages, i. e., early stage (ES I), Clark II (CL II), III (CL III) and IV (CL IV), for its detection and establishment of criteria for the early diagnosis. The detection of advanced phases was easily performed, in contrast with the thermal evaluation of ES I, since the heat from the vascular structures of the skin under analysis, override the lesion. The thermographic evaluation of stage I melanoma was achievable only after lesion location, showing the presented model was not fully efficient in this detection.

In a more recent study, the same author [94] proposed the use of frequency modulated thermal wave imaging, for the detection of the abovementioned stages, in a 3-D computational model. After heating, most lesions were detectable. However, as in [93], ES I was camouflaged by blood vessels, as well as CL II, showing that the active thermal imaging method proposed, displays a low efficiency in the detection of ES I and CL II. Its identification was only possible after the merging of the thermograms with the phase images acquired from the thermal signals.

Steady-state IRT was also successfully applied by Agyingi *et al.* [95], to distinguish between benign lesions and melanomas with no vasculature, depending on the metabolic rate and tumour size selected for the theoretical model. However, the presented model was tested in a 2-dimensional space, which is somewhat inaccurate when compared to a real scenario.

Cheng and Herman [96] used DTI, in a 2-D skin surface model, to study the most suited cooling method and parameters for the detection of early stages melanoma. The tested hypothesis included cooling: at a constant temperature, e.g., gel pack, cotton patch previously immersed in cold water and air flow or liquid submersion; with varying temperatures - 4, 12 and 20°C - for a period longer than 30 seconds. The encountered optimal conditions included constant cooling at 20°C for a period of 2 min, that could be adjusted according to the stage of the lesion under evaluation. These thermostimulation parameters differ widely from the ones normally used in thermographic studies, especially the suggested temperature. Even though comfortable for the patient, 20 degrees Celsius does not differ greatly from the normal skin temperature. Thus, it seems inefficient in the creation of the thermal gradient necessary to detect these types of lesions.

3.2.3 - Study's population

Concerning clinical studies for diagnosis purpose [86]-[91], the number of participants varied from 15 [90] to 110 [87], with a minimum of 52 lesions evaluated [90] and a maximum of 135 [89]. Article [88] did not report on the number of patients or tumours included in its research. The age interval was not specified in [86]-[88]. In the remaining articles, 13 and 91 were the younger [87] and older age [89]. The average population age was only indicated by [89] and [91], being 72 and 38 years, respectively.

The studies focused on treatment monitoring [43], [81], [92] presented a minimum of 6 participants [81] and a maximum of 30 [43]. The lesion number was the same as the participant's

one. Only [43] referred the age of the youngest and older patient, 55 and 75, respectively, and correspondent mean age, 64,3 years.

No population data is included for theoretical studies [54], [93]-[96], since the implemented computer models shape the assessed skin neoplasms.

3.2.4 - Trends and future challenges

For clinical studies, the increase of the patient population number is one of the main trends appointed for future work, by some authors [81], [86], [89], [90], in order to confirm the validity of the presented methods and attain extensive statistical analysis. The development of new image acquisition protocols is also of concern, due to the common presence of hair, that affects the thermal measurements, and the need of patient immobility, during the image acquisition process, which can be uncomfortable for the subject under test [86]. Further research, focusing on the development of new diagnosis algorithms, for the analysis and processing of the IRT images, are needed, to improve the final results [88]. It is of value to exploit, in a more detailed way, the physiology of skin neoplasms, to better understand the differences in temperature, between the lesion site and the surrounding healthy skin, during the thermal recovery [86]. Additionally, the definition of rates of specificity and sensitivity of the thermal information, retrieved from the results of the studies, are also of importance [88].

Concerning theoretical approaches, the construction or refinement of 3D skin lesion computational models is necessary, in order to resemble, as much as possible, with a real biological model [95]. Upcoming research, related to the study of different modulation frequencies in LIT is appointed as necessary for the diagnosis of stage I and II melanoma [54]. Moreover, the investigation of different tumour sizes, locations and varying blood vessel sizes could also be of interest, for future work [93], [95].

The dynamic use of IRT appears to be a rising tendency in skin cancer studies [54], [86], [88]-[91], [93], [94], [96], as a means of improving thermal patterns, facilitating the detection and characterization of different skin cancer types. This technique appears to be often allied with a cold stress, which seems appropriate considering the cold thermoreceptors located on the skin. The suggested duration of the stimulus varied between 20 seconds [43], [89], [91] to 2 minutes [96], being 1 minute a possible candidate to shorten the test time and assure, simultaneously, the effective cooling of the leased area. Most reports did not include the duration of the thermal measurements, being 2 minutes the selected time in the ones that do [86], [96].

Thus, taking in account all the remarks abovementioned, an acquisition protocol, for the collection of DTI images, is presented in chapter 5.

Chapter 4

Machine learning classifiers

The use of artificial intelligence (AI) for decision support systems in medicine has become a closer reality in clinical scenarios. Machine learning algorithms represent a key branch of this area, specially when dealing with medical decisions, due to its ability to learn before drawing a conclusion. In the case of skin cancer diagnosis, a secondary opinion can be reached, using a set of input variables, retrieved from image analysis and processing. Thus, aiding in medical decisions with the hopes of improving patient care and reduce costs.

This chapter includes a detailed bibliographic research concerning the use of machine learning classification algorithms for medical diagnosis with different imaging modalities. Recent implementations of AI algorithms using information retrieved from medical infrared images are also mentioned.

4.1 - Literature review: AI and imaging

4.1.1 - Methodology

Search Strategy

The presented bibliographic research was performed in the reference sources ISI Web of Science, PubMed and Scopus, with the following keyword combinations, respectively: TOPIC: (skin cancer) OR TOPIC (skin neoplasm) AND TOPIC: (imaging) AND (classification methods); ((skin cancer[Title/Abstract]) OR (skin neoplasm)) AND (imaging) AND (classification methods [Title/Abstract])); (TITLE-ABS-KEY ("skin cancer") OR TITLE-ABS-KEY ("skin neoplasm") AND TITLE-ABS-KEY (imaging) AND TITLE-ABS-KEY ("classification methods")). The selected fields of search, in each database, were used to assure uniformity in the results encountered and the use of complex and unclear terms was avoided to guarantee a maximum number of results. Since the terms "skin cancer" and "skin neoplasm" are common interchangeable expressions,

the Boolean operator OR was applied. No time restriction was considered. After the database search a duplicate removal was followed.

Screening and eligibility results

A title and abstract screening of the encountered articles was initially performed to consider only those that reported the use of classification methods in skin cancer images.

The first eligibility criterion consisted in the removal of meeting abstracts and revision articles. Secondly, only publications written in English were kept, eliminating articles submitted in other languages. Considering that this review focused on the use of classifiers for skin cancer classification, articles that described the use of classification methods for other purposes were excluded, as well as research studies that classified skin neoplasms with different approaches, e.g., ABCDE rule, making the third and fourth selection rule, respectively. Lastly, publications that did not report values of accuracy, sensitivity, specificity or other classification metrics, were also removed.

The remaining publications were categorized based on the imaging modality used to characterize the skin neoplasm: Dermatoscopy, Microscopy, Spectroscopy, Digital photography, Histopathological images and Others. A full text review was conducted following the PRISMA rules for systematic reviews detailed in [84], [85]. The revision process is described in Figure 4.1 (adapted from [85]).

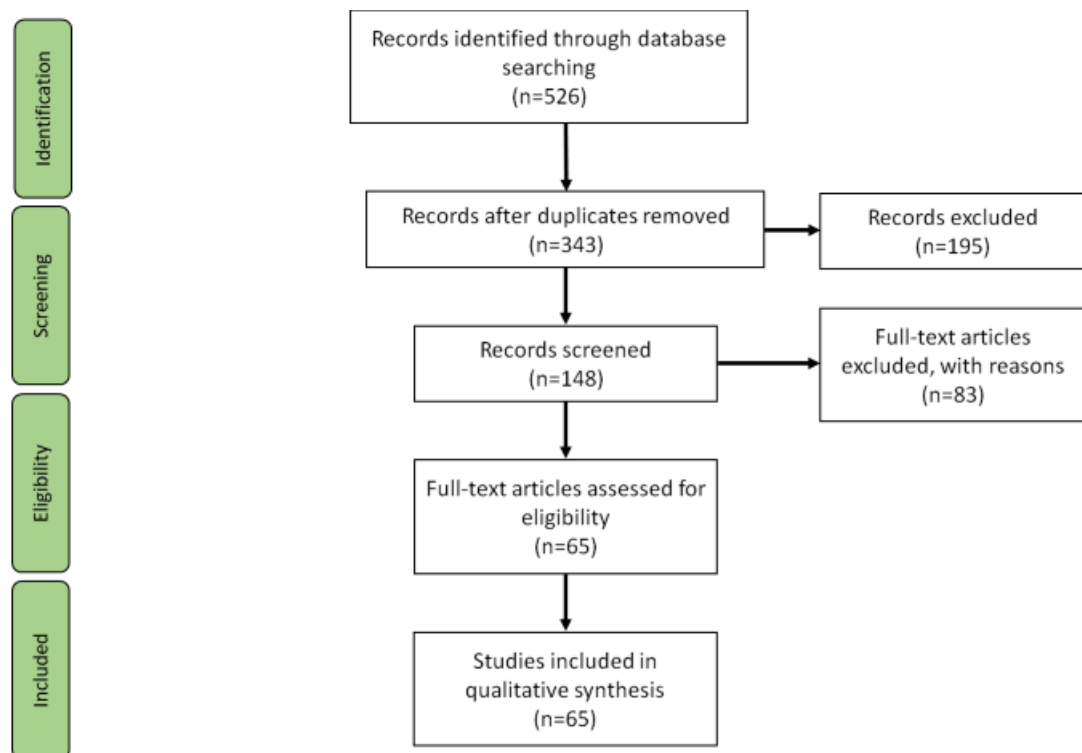


Figure 4.1 - PRISMA flow diagram.

4.1.2 - Results

A total of 526 publications were selected from the database search, with 251, 194 and 81 publications found in ISI Web of Science, PubMed and Scopus, respectively. The duplicate removal lead to the exclusion of 183 articles. The remaining 343 publications were submitted to a title and abstract screening process, that resulted in the elimination of 195 records, since artificial intelligence computational classification methods were not applied to skin cancer images for classification purposes. Following, 83 articles were removed from the final results, due to the eligibility criteria defined, being 19, 7, 33, 15 and 9 eliminated due to the first, second, third, fourth and fifth criterion, respectively. The end results included 65 publications eligible for revision with 34, 6, 7, 12, 3 and 3 articles concerning the use of dermoscopy, microscopy, spectroscopy, digital photography, histopathology, combination of several and other imaging modalities to analyse the neoplasia, respectively.

Dermoscopy

The successful use of artificial intelligence methods for the assessment of skin lesions represented by computerized digital dermatoscopy images, is one of the most documented subjects of this field.

The majority of authors reporting on this topic, demonstrate the usefulness of several classification algorithms in the evaluation of lesion' malignancy, distinguishing benign from malignant melanocytic tumours. Grzesiak-Kopec et al [97] presented 2 different strategies for this purpose, using single classifiers: Naive Bayes, Random Forest and k-Nearest Neighbour (k-NN); and a meta-learning approach with Bootstrap Aggregating and Vote Ensemble Classifier. The k-Nearest Neighbour classifier is one of the easiest to comprehend and execute. In spite of its simplicity, it can compete with other more complex learners, outperforming them in some situations. The classification of a given instance is performed according to the label attributed to its k nearest neighbours, with the possibility of implementing different metric measurements for distance calculation [98]. The research outcomes of the metaheuristics exceeded the ones of single-classifiers, having bagging applied to Random Forest presented the highest sensitivity value (0.851). Pairwise coupling (PWC) of SVM, k-NN and Gaussian maximum likelihood was applied by Rahman et al [99] to different colour and texture features extracted from skin lesion' images. The implementation of fusion by sum of the single classification results exceed the performance of the lone machine learning algorithms, delivering an accuracy (ACC) of 75.69%. Pennisi at al [100] showed the ability of Naive Bayes, Adaptive Boosting (AdaBoost), k-NN and Random Trees machine learning methods in the detection of melanomas among benign lesions, segmented with Delaunay Triangulation. The best results were encountered with AdaBoost, with sensitivity (SN) and specificity (SP) values of 0.935 and 0.871, respectively. With the same purpose, Ruiz et al. [101] uses k-NN, Artificial Neural Networks (ANN) and Bayes learners in a collaborative method, improving the end results. The functioning of Artificial Neural Network (ANN) algorithms is often compared to the workings of the human brain. This comparison is justified by the presence of

neurons in the NN, that compose three different types of layers: input, hidden and output. The neurons communicate through interconnections, exchanging information, until the final output is reached [102], [103]. A number of 7 neighbours and 7 hidden layers, were encountered as the optimal parameters for the k-NN and ANN algorithm, respectively. A part from these, several other authors choose similar approaches, comparing single learners to select the classifier that best performs, depending on the provided data [104], [105].

The implementation of more complex approaches for the purpose of classifying pigmented skin lesions was performed by Masood et al [106], with the development of a Deep belief network, using labelled and unlabelled data, in parallel with a self-advised single vector machine learning algorithm responsible for improving the classification results. This strategy addressed the frequent problem of insufficient training data, delivering classification errors lower than other common classifiers. Schaefer et al [107] presented another method to tackle this data imbalance, using an ensemble of various one-class-classifiers based on support vector data description. The Support Vector Machine (SVM) classifier is a supervised learning algorithm commonly applied in pattern recognition tasks. This method constructs several n-hyperplanes that maximize the separation between two classes. Depending in the type of input data, i. e., liner or non-linear, several kernel functions can be selected to acquire the optimum classification results [103], [108]. The final classification results showed its superiority in comparison to other ensemble classifiers based on SVM, commonly used in this situation. The combination of Multilayer Perceptron (ANN), Naive Bayes, Decision tree, k-NN and SVM classifiers documented by Castillejos-Fernández et al [109] also exceed the performance of the single classifiers in the task of malignancy classification. The relevance of the features selected for input is stressed, as the ensemble accuracy decreased with the increase of feature number. This topic is also highlight by Faal et al [110], after achieving better classification results with an ensemble of k-NN, SVM and Linear-discriminant analysis (LDA) algorithms with different feature inputs for the different classifiers, as oppose to the same shape, colour and textural components. The impact of input vectors was also tested by Rastgoo et al [111] with the implementation of an ensemble learning with Random Forest (RF) and Weighted combination constructed with RF, SVM and LDA, where the combination of several features achieve higher specificity results (94%), instead of the use of a single characteristic. This exact conclusion was reached by the same author [112], but applying single learners, namely, SVM, RF and Gradient boosting. In both articles, RF outperforms the others. Fengying et al [113] build a meta-ensemble model for the classification of melanocytic lesions, composed by 3 different ensembles based on NN, each feed with different inputs, with posterior combination of the outputs. Its overall sensitivity and accuracy exceeded RF, Gentle AdaBoost, SVM, k-NN, Fuzzy NN and systems based on Bagging of Features (BoF) models. Lastly, Abbas et al. [114] manipulated image features representative of lesion' patterns to classify pigmented skin tumours, through the use of majority voting with support vector machine, achieving accuracy, sensitivity and specificity values of 93%, 94% and 84%, respectively.

Apart from ensemble models and meta-learning approaches, the implementation of single learners for melanocytic lesion classification is also fairly common. SVM is the favoured learning model, being used standardly by the majority of authors, that preferred to focus on elaborate feature extraction and selection methods [115]-[118]. Specifically, Jaworek-Korjakowska et al. [119] used this type of learning algorithm to develop a Computer-Aided Diagnosis (CAD) system for the detection of micro malignant melanoma that outdid other literature models, with sensitivity of 90% and specificity of 96%. La Torre et al. [120] tested the performance of support vector machine classifiers with different function kernels, namely, χ^2 , Gaussian and Generalized Gaussian. The latter showed remarkable results, detecting all cancerous lesions. Codella et al. [121] explored the application of SVM to whole and partitioned images, segmented using ensemble approaches, resulting in an area under the receiver operating characteristic (ROC) curve of 0.843.

Support Vector Machine has also been used to deal with class imbalance situations for melanoma classification. Celebi et al. [122] implemented Random under-sampling and Synthetic minority oversampling technique (SMOTE) and concluded that SMOTE is a better approach, since the first option can eliminate valuable data and reduce drastically the number of samples, hardening the learning process. Since SVM can ignore input samples that are not linearly separated during the training step, Masood and Al-Jumaily [123] opted for a Self-Advising SVM (SA-SVM) strategy, to retrieve information from the misclassified data, during this phase. SA-SVM presented higher accuracy, sensitivity and specificity, followed by SVM with radial basis function, quadratic, polynomial, linear and multi-layer perceptron kernel, decreasingly. The classification capacity of SVM with different kernel functions was also explored by Wahba [124], defending the importance of kernel selection, according to the type of features included in the input vector. Since the supplied dataset was non-linearly separable, the quadratic polynomial function kernel delivered the top results. The same kernel was found to be the most adequate by Yuan et al. [125] to prevent the increase of error rate.

Few authors exceed the 1 level distinction with SVM, introducing a second classification step. Suganya [126] developed a model to, firstly, categorize melanocytic and non-melanocytic lesions, followed by the differentiation of melanoma from nevus and BCC from seborrheic keratosis, respectively. Joseph and Panicker [127] divided normal and abnormal skin lesions, further classifying the last into Atypical nevi or melanoma. Both achieved sensitivity, specificity and accuracy values close to or above 90%.

Melanoma detection also proved to be doable with the implementation of back-propagation neural networks (NN) classifiers, although with inferior performance metrics when compared to SVM. Premaladha and Ravichandran achieved an accuracy value of 87%, considering an error lower than $e^{-0.5}$, while Messadi et al. [128] established a maximum error of 0.1, achieving a correct classification rate of 76.76%. The implementation of additional algorithms for the optimization of ANN performance in skin cancer classification is also found. Common methods include the use of Genetic Algorithms (GA) [129] and Particle swarm optimization (PSO) [130].

Additionally, Random Forests learning methods have also been applied to dermatoscopy images for both melanoma [131] and BCC [132], [133] classification. Ferris et al. [131] constructed a model of 1000 decision trees and a threshold for malignant diagnosis of 0.4, with sensitivity results higher than the ones of physicians and specificities lower. Kharazmi et al. [132], [133] explored the use of vascular features for basal cell carcinoma automatic detection with 100 trees. No reference is made to the reasons considered for the selection of tree number.

When compared to the abovementioned classifiers, the implementation of k-NN outside of ensemble models or comparative approaches is more uncommon. For melanoma recognition in dermatoscopy images, Ganster et al. [134] choose a 24-NN strategy, achieving a better overall performance when only two classes (benign and malignant) were considered, as oppose to three (benign, dysplastic and malignant). A neighbourhood of 24 was selected, considering that it ensured the best results, according to the available dataset.

Microscopy

Machine learning algorithms have demonstrated their potential in the detection of melanoma tumours, analysed through microscopy techniques. The use of decision trees appears to be the preferred choice for the classification phase, whether the image collection is performed by confocal laser-scanning microscopy (CLSM) [135]-[137] or reflectance confocal microscopy (RCM) [138]. The reported sensitivity and specificity values of CLSM papers exceed the 90% mark, with values reaching 97% and 96% [136], [137], respectively. The same classification and regression tree (CART) software is implemented by all authors, although no mention of the parameters selected is encountered.

The use of features extracted from fluorescence images, as inputs for machine learning classifiers, has also been approached, with Odeh et al. [139] reporting excellent results, for the k-NN algorithm, in the classification of benign and malignant skin lesions and not so good outcomes in the differentiation of BCC and AK tumours. A Euclidean distance metric was used, and several k were tested (1, 3, 5, 7 and 9). The best results were achieved with k=1, however this can be misleading due to possible overfit of the data. The author accentuates the relevance of feature selection, testing the use of Genetic algorithm and Sequential Scanning selection technique for this purpose. Odeh and Baareh [140] explored further one of the authors previous works and tested other options, namely, ANNs with GA and an Adaptive Neuro-Fuzzy Inference System for the same classification purposes. Nonetheless, k-NN with GA outperformed all the others.

Spectroscopy

Artificial intelligence algorithms have achieved satisfactory results in the identification of the deadliest form of skin cancer, in spectroscopy images. However, these are often worse than the ones attained in dermoscopy and microscopy methods. Li et al. [141] trained and tested the k-NN, ANN and Naïve Bayes classifiers, detailing the parameters choice. While default values

were chosen for the application of the latter algorithm, ANN was used with back-propagation and the number of 6 hidden units was justified by the sum of the number of inputs and outputs divided by 2. To balance noise and result robustness, a number of 3 neighbours was selected for k-NN. SVM was the learner of choice for Liu et al. [142] that verified a particular improvement in classification results, when patient age was added to the input feature vector. Tomatis et al. [143], [144] focused their research on the implementation of neural networks for classification of multispectral images, achieving sensitivity and specificity values higher than 70% on both works.

The use of electrical impedance spectra as input for melanoma detection was successfully tested by Mohr et al. [145] with the SVM classifier, achieving high accuracy. With the same goal Aberg et al. [146] combined the results of 4 different learners (partial least squares discriminant analysis, SVM, ANN and k-NN) to obtain a sensitivity value of 95%.

Lastly, k-NN was used by Maciel et al. [147] to discriminate other skin disorders, e. g., psoriasis from neoplastic lesions, represented in spectral images. Oddly, the increment of k had little to none influence on the great sensitivity and specificity results encountered.

Digital Photography

Classification strategies based on Support vector machine learning are favoured when evaluating features extracted from macroscopic images. Similar to previously mentioned imaging methods, discrimination of melanoma among other lesions is the main objective, and accuracy values from 79% [148] to 97% [149] have been achieved. Takruri et al. [150] constructed a multi-classifier to improve the accuracy of melanoma detection, based on 3 SVM algorithms with Radial Basis Function (RBF) kernel. The top result of 88,9% accuracy was achieved when Probability Averaging Fusion was used to combine the classifiers results, instead of Majority Voting. The RBF kernel was also selected by Oliveira et al. [151], as well as the histogram intersection kernel, due to the non-linearity of the data, to increase algorithm efficiency. Likewise, Spyridonos et al. [152] made the same kernel selection, but for the detection of AK among healthy skin, attaining sensitivity and specificity values in the range of 63.7-80.2% and 65.6-82.3%, respectively.

Has in other papers with different imaging techniques for skin lesion classification, some authors rather focus their work on the development of novel feature extraction and selection strategies to achieve the best possible outcomes [153]-[156]. Jafari et al. [157] choose this approach, extracting different sets of colour features that were used as inputs for an ANN classifier. Neural networks performance in melanoma diagnosis, based on extracted colour features, was also studied by Przystalki et al. [158]. SVMs learners with linear, polynomial, quadratic and sigmoid kernel were used for comparison, with the highest accuracy (97.44%) corresponding to the linear function.

The implementation of nearest neighbour methods in macroscopic images was described only by Cavalcanti and Scharcanski [159]. A k of 1 and the Euclidean distance metric were selected to distinguish benign from malignant lesions. In order to reduce the number of false

negatives obtained by this approach, a set of Bayes classifiers was applied afterwards, leading to an increase in sensitivity of 94.92% to 96.37%.

Histopathological images

The detection of non-melanoma skin cancers and pre-cancerous lesions has successfully been done with the analysis of histopathological images. SVM is the outperforming machine learning algorithm, showing sensitivity and specificity values higher than 90% [160] and 80% [161], respectively. Its use in semi-advised learning models is also encountered, but for melanoma recognition. Like in [106] for dermoscopy images, Masood et al. [162] choose this strategy to address the issue of limited unlabelled data, using SVM to adjust the weight of each sample. The SA-SVM outperformed the standard SVM learner.

Other imaging modalities

Lesion classification strategies based on information retrieved from uncommon imaging modalities, have also been studied by some authors. Parameters from teraheart pulse images of BCC lesions were retrieved and used for its distinction from healthy skin, using SVM algorithms [163]. Kia et al. [164] classified healthy skin, melanoma, BCC and benign lesion' sonograms with multilayer perceptron (ANN), achieving sensitivity of 98% and specificity of 5%. Even though the authors emphasize the importance of high sensitivity, the obtainment of specificity as low is not acceptable, since unnecessary patient stress would be caused, due to the high number of false positives. Hence, the proposed classifier needs improvements. Lastly, Ding et al. [165] used 3D texture features and 2D ABCD parameters for melanoma diagnosis with support vector machine. A multilayer perceptron kernel was selected, reaching accuracy of 87.8%.

4.1.3 - Trends and future challenges

Most publications [109]-[112], [115], [116], [118], [139], [153]-[157] concerning the use of classifiers for skin cancer detection seem to highlight the importance of feature extraction and selection stages to attain the best results. Thus, it is expected further research in this area, focusing on image analysis and processing, in preference of new machine learning strategies.

In fact, there is a loophole in the description of the classification task, since some papers [97], [117], [127], [132], [161] lack any reference to the parameters selected for the implementation of the algorithm of choice. The decision of using platforms that already include pre-written algorithms, i. e., WEKA, MATLAB and LIBSVM, could be the cause, since some authors prefer the implementation of standard models, instead of exploring other parameter options. Nonetheless, papers concerning the development of highly complex classification systems can also be found [106], [123], [162] and its increment should be pursued.

The increase of available labelled data is of concern to improve the training task. However, the majority of studies rely on images available on databases [100], [139] or supplied by

hospitals[111], [134], being dependent of the number of samples that is given. Therefore, strategies to address this issue are of interest for future work and have already been explored by some authors [106], [162].

The use of Support Vector Machine (SVM) algorithms seems to be the prime choice for skin cancer classification, either on basic models [119], [120] or more complex algorithms [107], [150], suggesting upcoming research with this tendency.

Lastly, new publications pertaining to classification models for skin cancer detection, should focus on finding a good balance between specificity and sensitivity values, to avoid faulty diagnosis for healthy and ill patients, respectively.

4.2 - Literature review: AI and thermal imaging

The use of machine learning algorithms for classification purposes using thermal infrared imaging, is a fairly recent topic [103]. Its application towards medical diagnosis has grown, particularly in breast cancer detection [166]-[169], being also applied towards the identification of other medical conditions, e.g, thyroid cancer [170], extreme fatigue [171], rheumatoid arthritis [172], hypertension [173] and psoriasis [174].

Such as in publications [170], [171], [173] concerning other imaging modalities, most authors focus on feature selection and extraction strategies to improve classification results. In IRT these parameters normally include statistical measurements.

Algorithms based on support vector machine, neural networks and k-nearest neighbours seem to be the preferred choice [103], for AI application in IRT images, with accuracy, specificity and sensitivity values competitive with other imaging modalities, has it is verified in Table 4.1.

Table 4.1 - Recent publications regarding the use of machine learning classifiers for medical diagnosis using IRT imaging.

Publication	Objective	Classifier	Best performance
Strąkowska et al. (2018)	Psoriasis screening	SVM, LDA, k-NN (k=3, 7, 9, 11, 13)	k-NN: ACC=96%
Umapathy et al. (2017)	Diagnosis of arthritis rheumatoid	k-means, k-fuzzy means (k=3)	k-means: SN=86.6%, SP=79%
Acharya et al. (2012)	Breast cancer diagnosis	SVM	ACC=88.10%, SN=85.71%, SP=90.48%
Lashkari et al. (2016)	Breast cancer diagnosis	SVM, k-NN, Naïve Bayes, Probability NN, AdaBoost	AdaBoost: ACC>80%
Francis et al. (2017)	Breast cancer diagnosis	SVM (cubic polynomial kernel)	ACC=94.4%, SN=97.2%, SP=91.7%
González et al. (2017)	Thyroid cancer diagnosis	k-NN	ACC=91%
Kandlikar et al. (2017)	Breast cancer diagnosis	ANN, SVM	SVM: ACC=90.9% ANN: ACC=80.95%
Lopez et al. (2017)	Detection of extreme fatigue	Deep convolutional NN	ACC=81.51%
Alpar and Krejcar (2018)	Detection of vasospasms	Fuzzy c-means (c=2)	-
Ramesh and Thiruvengadam (2018)	Diagnosis of hypertension	SVM	ACC=93%, SN=90%, SP=94%

4.3 - Summary

The conducted bibliographic research presented in this chapter allowed a better understanding of the implementation of different classifiers in medical diagnosis. Concerning classification tasks with IRT, the classifiers SVM, k-NN and ANN seem to be the most adequate and will be utilized in the following chapter for this purpose. The selection of some parameters will also be performed based on the knowledge acquired in this literature review.

Chapter 5

Materials and methods

The methodology followed in this study is based on the collection and analysis of skin temperature values representative of dermic and epidermic tumours. The selected equipment, study's population and image acquisition protocol are described in this chapter, as well as the adopted data analysis strategies.

5.1 - Equipment

The equipment used for the collection of thermal data consisted on the thermographic camera FLIR E60sc - Figure 5.1 (adapted from [175]) -, mainly characterized by the properties included in Table 5.1A [176]. To assure the quality of the captured images, the camera was previously calibrated with a blackbody ISOTECH HYPERION R 982. A hygrometer TESTO 175H1 was used to monitor the ambient temperature and relative humidity, guaranteeing optimal conditions for the thermal recordings.

For thermal provocation, an aluminium medal with a diameter and height of 50 and 20 mm, respectively, was used - Figure 5.1B. The selection of this particular metal is justified by the elevated thermal conductivity that it presents, e. g., $237 \text{ W cm}^{-1} \text{ K}^{-1}$ at $298,2 \text{ K}$ [177], providing a high heat transfer rate across the medal.

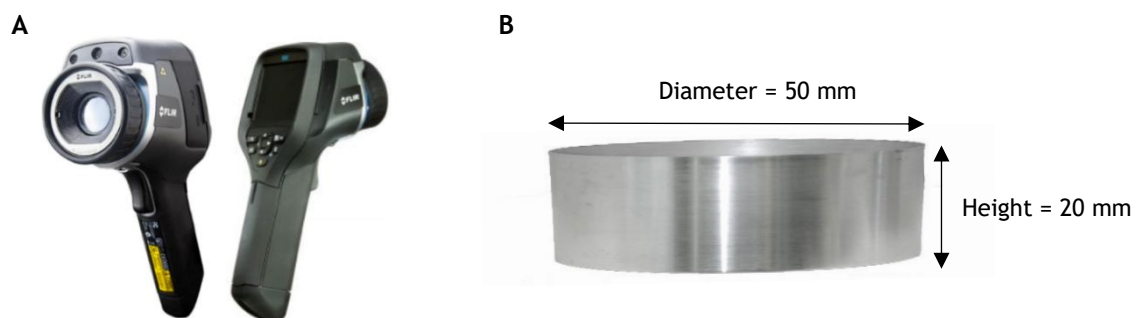


Figure 5.1 - Equipment for image acquisition: A - Thermal imaging camera: FLIR E60sc; B - Aluminium medal.

Table 5.1 - Properties of thermal imaging camera FLIR E60sc.

Property	Property value/specification
Size of focal plane array	320 x 240
Field of view	25° x 19°
Frame rate	60 Hz
NETD	50mK at 30° C
Measurement uncertainty	± 2% of the global reading range
Detector type	Uncooled microbolometer
Focus	Manual
Minimum focus distance	1.3 ft/0.4 m
Measurement correction	Automatic, based on the inputs of ROI's distance, ambient temperature and relative humidity

The software tools for thermogram manipulation, included ThermaCAM Researcher Professional 2.10 [178] and MATLAB R2016a [179]. Excel 2016 was used for gathering and data organization, as well as for statistical calculations. Statistical analysis was also performed in Statistical Package for the Social Sciences (SPSS) v24. Lastly, Waikato Environment for Knowledge Analysis (WEKA) 3.8 [180] was used for classification purposes with machine learning algorithms.

5.2 - Focus group

The study's population group included individuals aged 18 years old or above. No maximum age restriction was specified, being that individuals mentally unfit or legally unable to authorize its participation had the option of being represented by a legal representative. Each subject needed to present, at least, one possible neoplastic lesion for inclusion in this research and non-cooperating individuals, were discarded. Some exclusion criteria regarding necessary precautions before and during the thermal acquisition process were also established - Table 5.2. Image acquisition was performed from October 2017 to May 2018, at a minimum of 3 days a week.

Table 5.2 - Exclusion and inclusion criteria defined for the research study.

Inclusion criteria	Exclusion criteria
	Ingestion of a heavy meal
Age equal or above 18 years old	Partake in tiring and stressful activities
Presence of, at least, one plausible skin neoplasm	Ingestion of alcohol or caffeine-based beverages
	Smoking until 2 hours before thermal capture
	Non-removal of jewelry items
	Applying lotions to the leased area

The thermograms were collected at Instituto Português de Oncologia do Porto Francisco Gentil, E.P.E. (IPO-Porto) after the approval of the ethics Committee - Appendix II. The evaluated lesions were present in patients assigned to the Plastic and Reconstructive Surgery department, being previously diagnosed by a physician at this service. All diagnoses were confirmed by histopathological analysis.

5.3 - Capture protocol

Prior to image capture, the patient was subjected to a period of acclimatization (≈ 10 minutes). During this time, the participant took knowledge of the current investigation work - Appendix III - and filled the necessary documentation, i. e., the informed consent and biometric data questionnaire associated with the pathology - Appendix IV and V, respectively. The biometric data form allowed the registration of patients' skin neoplasm type, age, sex, height, weight, eye colour, Fitzpatrick scale type [181], presence/absence of skin marks and skin neoplasm location.

Following, images of the affected skin area (Image X) and respective contralateral location (Image Y) were captured and, with the aid of the aluminium medal, a cold stimulus, with the duration of 1 minute, was applied to the lesion site. A new thermal image was acquired immediately after the thermal stress (Image 0) and at each following minute, until the 5-minute mark, collecting 5 images representative of the thermal recovery (Images 1, 2, 3, 4 and 5). A summarized scheme of the capture protocol is presented in Figure 5.2.

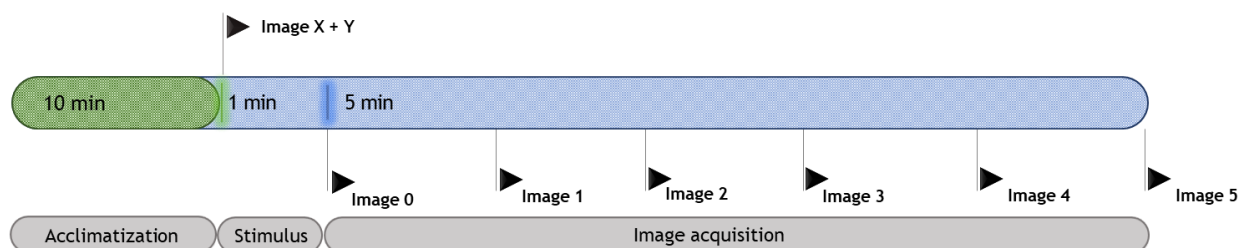


Figure 5.2 - Stages involved in the acquisition protocol.

5.4 - Data analysis

The analysis of thermal data was divided in infrared thermal image analysis, statistical treatment and machine learning classification, using the software tools mentioned in section 5.1. The steps involved in each phase are detailed in the following sub-sections.

5.4.1 - Infrared thermal image analysis

Unlike other diagnostic methods, e. g., dermatoscopy, thermograms provide information concerning the physiological status of the object under evaluation, in preference to anatomic

knowledge [17]. For this reason, a temperature gradient is frequently encountered between the tumour site and the surrounding healthy skin, instead of a precise boundary, making lesion segmentation impossible by the means of algorithms [182]. Thus, an image analysis process that included a user input for lesion localization seemed to be the preferred option.

Before image loading, the thermograms were converted to MAT-files, using ThermoCAM Researcher Professional 2.10.

Following the upload of the file to MATLAB, a pre-processing step was performed, including: image conversion from RGB to grayscale, histogram equalization and resizing. The original image was rescaled for twice its original size, in order to ease the visualization of the lesion site in the user input stage. To guarantee that the average temperature of the thermograms was maintained, the nearest neighbour method was used for the rescaling.

Since the separation of the region of interest (ROI) from the background returns faulty results when performed by segmentation algorithms, a user input was requested in the lesion segmentation stage, to box the leased area. The selected zone was, subsequently, cropped in a 40x40 square, having into account the centre of the original box. The use of a 40x40 matrix was chosen as a standard size to completely include the majority of tumours presented in the thermograms.

The analysis of the thermograms acquired statically and dynamically was performed by two different algorithms, sharing only the previously-mentioned steps - Figure 5.3.

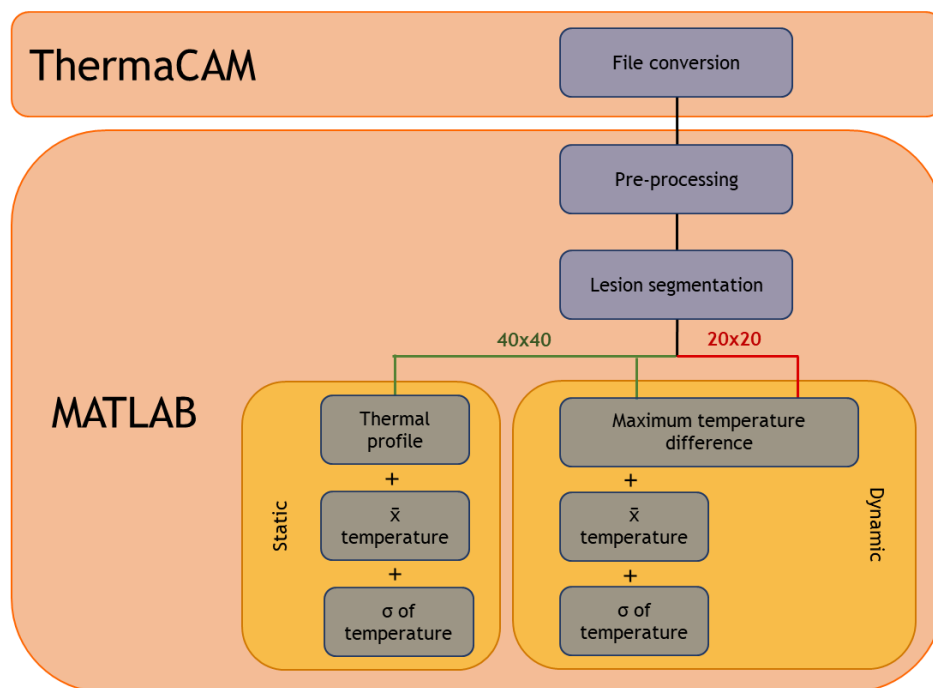


Figure 5.3 - Infrared thermal image analysis scheme of static and dynamic acquired images.

Steady-state

The analysis of the thermograms acquired with static thermography consisted mainly in the construction of a temperature profile representative of the lesion under evaluation. Only

the tumour's thermogram acquired in a steady-state, i. e., Image X, was considered for this stage.

Following lesion segmentation in MATLAB, the temperature values of the two main diagonals of the 40 by 40 squared area - Sd1 and Sd2 - were collected - Figure 5.4A - and, subsequently, multiplied in two manners: top to bottom and left to right - Figure 5.4B. As a result, a vertical (Sv) and a horizontal (Sh) temperature vector, characteristic of the skin lesion, were attained - Figure 5.4C.

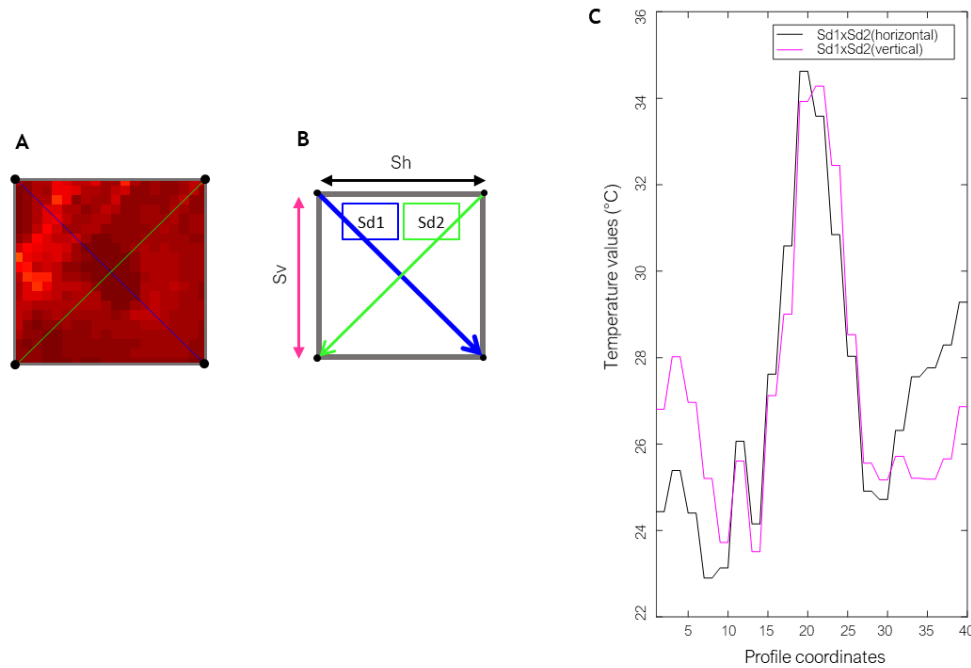


Figure 5.4 - A - Selected skin tumour area; B - Scheme of temperature diagonals and its multiplication; C - Vertical and horizontal temperature vectors.

After concluding from previous work that both temperature vectors supplied meaningful information, an averaging of the values composing the two curves was made, using equation (3), to guarantee the best representation of the lesion's temperature profile.

$$S(x) = \frac{Sv(x) + Sh(x)}{2}, \quad (3)$$

being x horizontal profile coordinates, with $x \in \{1, 2, 3, \dots, 40\}$.

In addition, the average temperature (SM) and standard deviation (SSTD) of the 40x40 lesion area were also collected, for posterior classification purposes, and the average temperature of the healthy collateral region (SMY) was obtained, using Image Y.

The steady-state parameters acquired for each participant are summarized in Table 5.3.

Table 5.3 - Steady-state parameters collected from Image X and Y.

Image		Steady-state variables	
X	S1, S2, ..., S40	SM	SSTD
Y		SMY	

Dynamic state

The dynamic analysis focused on the retrieval of the maximum temperature differences between the central and the peripheral regions of the selected tumour area, before and after thermal recovery.

As seen in Figure 5.5, the lesion was, firstly, divided in 2 regions: a central (C) and a peripheral (P) one. Following, the algorithm searched region C for the 5-connected pixels whose values originated the highest average temperature (\overline{x}_C). The same task was performed in region P, but the 5-connected pixels that resulted in the lowest average temperature were selected instead (\overline{x}_P). The maximum temperature difference (D) was then calculated, using $D = |\overline{x}_C - \overline{x}_P|$.

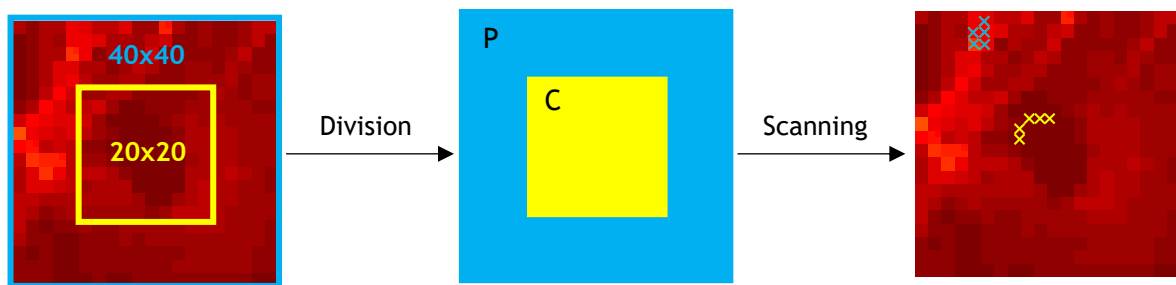


Figure 5.5 - Scheme of image partition and scanning performed by the MATLAB algorithm.

The average temperature (DM) and standard deviation (DSTD) of the 40 by 40 tumour area were also collected.

All of the aforementioned tasks were performed using images X, 0, 1, 2, 3, 4 and 5 of each patient. Table 5.4 summarizing the collected dynamic parameters, according to selected image.

Table 5.4 - Dynamic variables collected from Image X and Y.

Image		Dynamic variables	
X	DX	DMX	DSTDX
0	D0	DM0	DSTD0
1	D1	DM1	DSTD1
2	D2	DM2	DSTD2
3	D3	DM3	DSTD3
4	D4	DM4	DSTD4
5	D5	DM5	DSTD5

5.4.2 - Statistical treatment

Microsoft Excel 2016

The temperature values retrieved during the infrared thermal image analysis stage were used for statistical calculations and chart construction in Microsoft Excel 2016.

Concerning static thermography, the Excel tool was used to acquire the average temperature profile for each skin neoplasm type, using the parameters S1, S2, ..., S40. Separately, the average

tumour temperature (SM) and standard deviation (SSTD) were utilized for the comparison of different skin neoplasm types. The differences between healthy and lesioned skin were also evaluated, using SM and SMD for each skin tumour group.

The dynamic parameters were employed with the same principal, attesting the ongoing changes in tumour temperature difference (DX, D0, ..., D5), average temperature (DMX, DM0, ..., DM5) and standard deviation of lesion temperature (DSTDX, DSTD0, ..., DSTD5), during the dynamic acquisition process.

A frequency histogram concerning lesion location was also constructed, using this tool.

Statistical Package for the Social Sciences (SPSS)

The statistical treatment was primarily performed with Statistical Package for the Social Sciences (SPSS) v24 software. For this, the categories Skin neoplasm, Age group, Sex, Height, Weight, Body Mass Index (BMI), Fitzpatrick scale type, Eye colour and presence/absence of Skin marks, relative to each participant, were considered. The skin neoplasm types were divided into squamous cell carcinoma (SCC), basal cell carcinoma (BCC), melanoma, actinic keratosis (AK), melanocytic nevus (Nevi), seborrheic keratosis (SK), other benign neoplasia (Other) and skin neoplasm scar tissue lesions(Non-neoplastic). The eye colour included blue, green and brown and the Fitzpatrick scale was evaluated from I to V. The factors Age group, Height, Weight and BMI were divided into classes and a label was assigned to each category' component- Table 5.5.

Table 5.5 - Labels assigned to each category.

Label	Skin neoplasm type	Age Group	Sex	Height (m)	Weight (kg)	BMI	Fitzpatrick scale	Eye Colour	Skin marks
0	SCC	[18 - 29]	F	< 1.50	< 50	< 18.5	I	Blue	No
1	BCC	[30 - 39]	M	[1.50 - 1.60]	[50 - 59]	[18.5 - 24.9]	II	Green	Yes
2	Melanoma	[40 - 49]]1.60 - 1.70]]60 - 69]	[25 - 29.9]	III	Brown	
3	AK	[50 - 59]]1.70 - 1.80]]70 - 79]	[30 - 34.9]	IV		
4	Nevi	[60 - 69]		> 1.80]80 - 89]	[35 - 39.9]	V		
5	SK	[70 - 79]			> 90	> 40			
6	Cyst	≥ 80							
7	Other								
8	Non-neoplastic								

In addition to these categories, the parameters collected for each participant, during infrared thermal image analysis, were introduced as variables - Table 5.4. Thus, from the static analysis, 40 temperature values (S1, ..., S40), average lesion temperature (SM) and standard deviation (SSTD) were included, and from the dynamic evaluation 7 values of temperature difference (DTX, DT0, ..., DT5), average lesion temperature (DMX, DM0, ..., DM5) and standard deviation (DSTDX, DSTD0, ..., DSTD5) were considered.

First, a frequency and descriptive analysis was performed to characterize the sample.

Then, the Kolmogorov-Smirnov test was used to assess the normality of the data with a significance level of 0.05.

Due to the k-s test result, non-parametric tests, namely, U-Mann Whitney and Kruskal Wallis test, were applied to verify if the categories representative of the patient biometric data influenced any of the variables collected during the infrared thermal image analysis. The U-Mann Whitney is a non-parametric test equivalent to the parametric independent sample t-test, when the normality of the data is not verified. It is used to test whether two samples belong to the same population, i. e., present the same median value [183]. The Kruskal-Wallis test is the non-parametric alternative to ANOVA for independent samples, not requiring a normality distribution of the data. It compares more than two samples, evaluating if they arise from the same distribution. A significance level of 0.05 was used for both tests.

5.4.3 - Machine learning classification

For the classification stage Waikato Environment for Knowledge Analysis (WEKA) was used.

Six different classification tasks were defined:

- **Lesion type** - Distinction between benign neoplasia, malignant neoplasia¹ and non-neoplastic lesions;
- **Benign** - Distinction between actinic keratosis (AK), melanocytic nevi (Nevi), seborrheic keratosis (SK), cysts (Cyst) and other benign neoplasia (Other);
- **Malignant** - Distinction between squamous cell carcinoma (SCC), basal cell carcinoma (BCC) and melanoma;
- **Melanoma vs Nevi** - Distinction between melanoma and melanocytic nevi lesions;
- **SCC vs AK** - Distinction between squamous cell carcinoma and actinic keratosis lesions;
- **Ben vs Mal** - Distinction between benign and malignant lesions.

In order to compare the classification results obtained with different thermal image acquisition methods, separate data sets were assembled with static and dynamic parameters.

Concerning steady-state thermography, the temperatures composing each lesion thermal profile (S1, S2, ..., S40), average lesion temperature (SM) and standard deviation (SSTD) were used. To assess if one statistical measurement could outperform the other, S1, S2, ..., S40 were, firstly, used as inputs with SM and then tested with SSTD. Thus, each steady-state classification test included 41 input features - Table 5.6.

The dynamic parameters were used with the same logic, coupling, first, maximum temperature differences (DX, D0, ..., D5) with average lesion temperatures (DMX, DM0, ..., DM5) and then with standard deviation values (DSTDX, DSTD0, ..., DSTD5). Therefore, each dynamic classification stage comprised 14 input features - Table 5.6.

¹ Nevi, AK, SK, Cyst and Other lesions were included as benign tumours, while SCC, BCC and melanomas were considered malignant.

Table 5.6 - Possible feature combination for input vector, according to image acquisition process.

Image acquisition method	Input feature vector
Static	S1, S2, ..., S40 \wedge SM \vee SSTD
Dynamic	DX, D0, ..., D5 \wedge DMX, DM0, ..., DM5 \vee DSTDX, DSTD0, ..., DSTD5

For classification the machine learning algorithms Multilayer Perceptron, SMO and iBk were selected. Multilayer perceptron is a type of artificial neural networks (ANN) that classifies instances based on the backpropagation concept [184]. The inputs are processed by a set of functions to obtain the contribution error, of each input neuron, at the output layer. These values are “sent back” and serve as a guidance to adjust the weights of each input, in order to obtain the best classification possible [184], [185]. Sequential Minimal Optimization is used when Support Vector Machine learning is applied to a set of data that is represented by a quadratic function of multiple variables [186]. The main goal is to find the longest distance between each class, which can be time consuming with large data sets [187]. Thus, SMO decomposes the complex quadratic problem into smaller parcels, solving them from the smallest to the greatest [186]. In the iBk classifier the features of a given instance are compared to the features its k-nearest neighbours, based on distance, being the instances labelled as its closest k-neighbour [188].

The classification results were evaluated based on the performance metrics: accuracy (ACC), sensitivity (SN) and specificity (SP). The sensitivity and specificity values were only computed when the classification task included distinction between cancerous and non-cancerous lesions, i. e., Melanoma vs Nevi, SCC vs AK and Ben vs Mal. The accuracy indicates the percentage of instances that were correctly classified by the learner. It is an excellent metric to use when the available data set is balanced, i. e., the number of instances between each class does not differ greatly [190]. In a scenario of an unbalance data set other metrics should be considered. Sensitivity measures the ability of the learner to correctly identify those with the disease, while specificity regards the correct classification of those who don't. These metrics are calculated with equations:

$$\text{Accuracy} = \frac{TP+TN}{TP+FP+TN+FN} \quad (4)$$

$$\text{Sensitivity} = \frac{TP}{TP+FN} \quad (5)$$

$$\text{Specificity} = \frac{TN}{TN+FP} \quad (6),$$

where TP, FP, TN and FN are, respectively, True Positive (malignant lesion classified as malignant), False Positive (benign lesion classified as malignant), True Negative (benign lesion identified as benign) and False Negative (malignant lesion identified as benign). The TP, FP, TN and FN values are commonly displayed using confusion matrices - Figure 5.6.

	a	b
a - Malignant	TP	FN
b - Benign	FP	TN

Figure 5.6 - Confusion matrix model.

According to the selected classifier some parameters were defined. For the support vector classifier two different kernels functions were tested, namely, Radial Basis Function (RBF) and Quadratic Polynomial kernel, since the data set was not linearly separable.

For the implementation of Multilayer Perceptron, the number of hidden units was calculated for each classification task, according to the number of inputs and outputs for that specific trial - Table 5.7. An illustrative example, follows:

Classification task: Malignant - Steady-state data

Number of input features: 41 (S1, S2, ..., S40, SM)

Number of possible classifications: 3 (SCC, BCC, Melanoma)

$$\text{number hidden units} = (41 + 3)/2 = 22$$

Table 5.7 - Number of hidden layers selected for each classification test, according to image acquisition process.

Classification task	Steady-state	Dynamic
Lesion type	22	9
Benign	23	10
Malignant	22	9
Melanoma vs Nevi	22	8
SCC vs AK	22	8
Ben vs Mal	22	8

For the k-nearest neighbour learner 3 different values of k were evaluated²:

- k = 1 - usually delivers the best classification results;
- k = 7 - retrieves a high classification accuracy while keeping the classification error low;
- k = \sqrt{n} - following the “rule of thumb”, the square root of the number of instances (n) used during the training phase should deliver the best result [189] - Table 5.8. An illustrative example follows:

² The values of k=1 and k=7 were selected using cross-validation in previous tests. The correlation between classification accuracy and mean squared error is presented in Appendix VI.

Classification task: Malignant - Steady-state data

Training set size: 185 instances

$$k = \sqrt{n} = \sqrt{185} \approx 14$$

Table 5.8 - Number of nearest neighbours (k) considered for each classification task, according to image acquisition process.

Classification task	Steady-state	Dynamic
Lesion type	9	8
Benign	11	9
Malignant	14	13
Melanoma vs Nevi	5	5
SCC vs AK	6	6
Ben vs Mal	13	12

The default settings of the remaining parameters correspondent to each classifier were kept.

The unsupervised Resample instance filter was selected for the construction of the training and test sets, each with 60% and 40% of instances, respectively.

Chapter 6

Results

This chapter includes the results attained from this research work. First, characterization of the study’ sample is presented, followed by the results acquired from steady-state and dynamic analysis. The influence of participants’ characteristics in the retrieved temperature variables is included. Lastly, the machine learning classification results are presented.

6.1 - Sample characterization

In total, 320 IPO-Porto patients participated in this study, resulting in the thermal evaluation of 320 skin lesions. More than 35% of skin tumour were encountered on the facial region, followed by hands, arms and chest area - Figure 6.1.

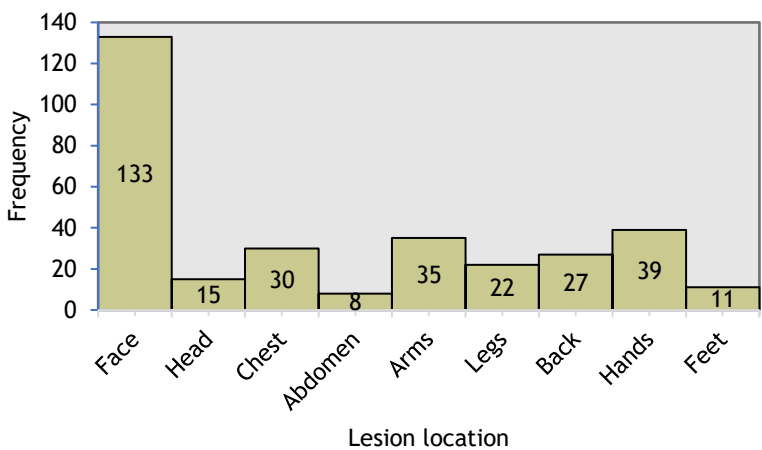


Figure 6.1 Skin neoplasm incidence according to body region.

The majority of lesions corresponded to basal cell carcinoma (BCC) (36.8%), followed by squamous cell carcinoma (SCC), melanocytic nevi (Nevi), actinic keratosis (AK), other benign neoplasia (Other), skin neoplasm scar tissue (Non-neoplastic), melanoma, seborrheic keratosis (SK) and cysts - Figure 6.2A. These lesions were mostly present in patients aged 80 years or above with only 0.6% of participants having 18 to 29 years old - Figure 6.2B. The number of female patients

was fairly proportional to the number of males, surpassing it only by 10% - Figure 6.2C. The characteristics height, weight and BMI tended to follow a normal distribution - Figure 6.2D, E and F - with the most populated classes being 1.50-1.60 m, 60-69 kg and 25-29.9 kg/m², respectively. Concerning, eye colour and the Fitzpatrick scale type, the majority of patients shared typical mediterranean features, namely, brown iris (49.4%) and slightly tan skin and dark hair (48.8%) - Figure 6.2G and H, respectively. Skin marks were absence in most participants - Figure 6.2I. The frequency tables, concerning patients' characteristics are included in Appendix VII.

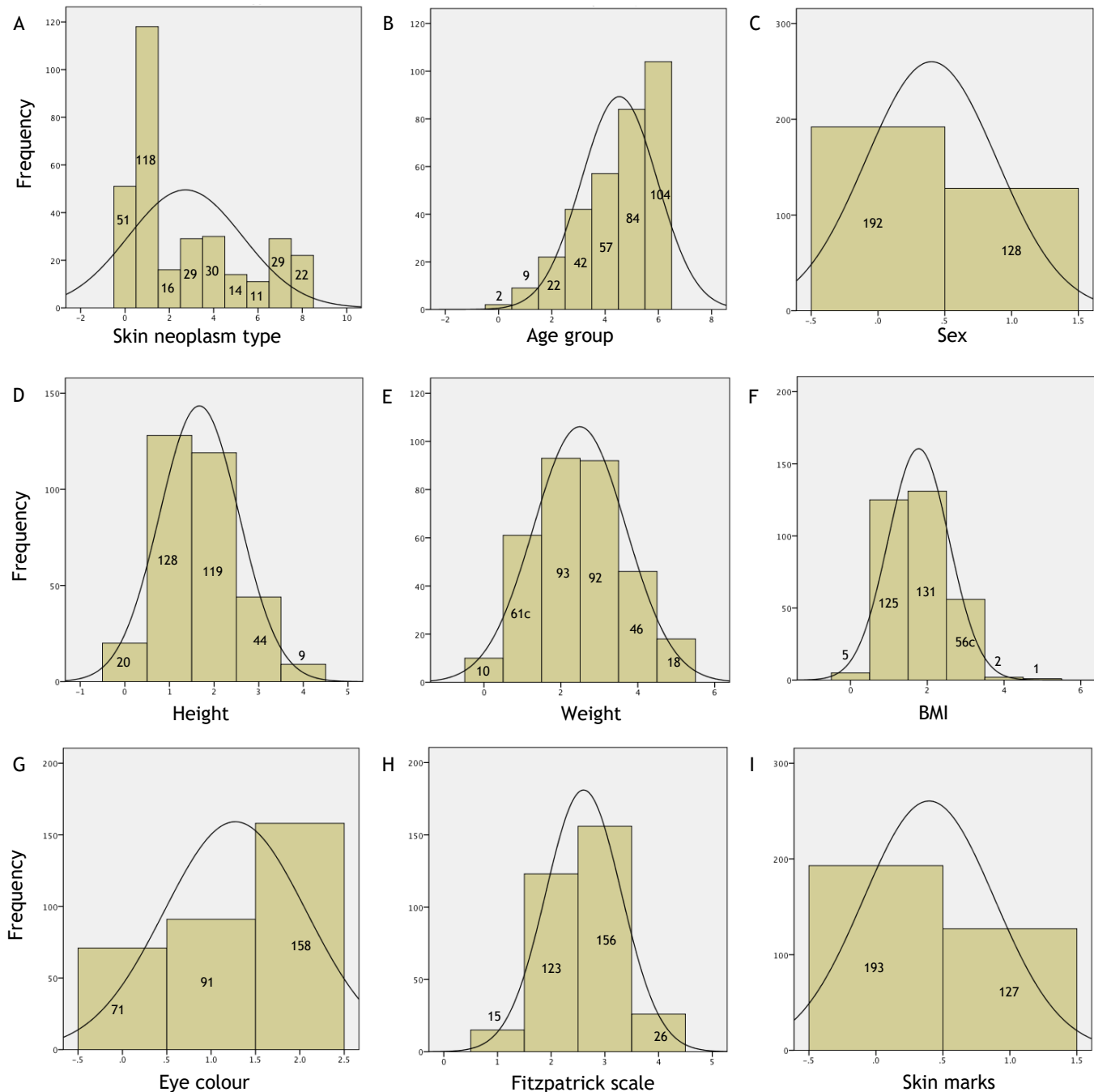


Figure 6.2 - Frequency of patients' characteristics in study's sample.

The descriptive analysis showed that the average patient's age, height, weight and BMI was 70.66 years, 1.62 m, 69.1 kg and 26.1, respectively - Table 6.1.

Table 6.1 - Mean and standard deviation value for patients' age, height, weight and BMI.

Characteristics	Mean \pm Standard deviation
Age (year)	70.66 \pm 7.518
Height (m)	1.62 \pm 0.046
Weight (kg)	69.14 \pm 6.316
BMI (kg/m ²)	26.18 \pm 1.984

6.2 - Steady-state image analysis

In total, 320 lesions were evaluated, including 51 SCC, 118 BCC, 16 melanomas, 29 AK, 30 Nevi, 14 SK, 11 Cysts, 29 other benign neoplasia and 22 scar tissue lesions.

The main goal of static image analysis was the construction of an average temperature profile representative of each skin tumour type. Different thermal profiles were compared, based on the defined classification task groups.

The profiles correspondent to SCC and BCC lesions presented thermal valleys, indicating that the lesion temperature decreased as we move towards its centre. This depression was more accentuated in the squamous cell carcinoma type. Contrarily, melanomas were represented by hyperthermic curves, since a temperature increase was verified as we move away from the periphery. Thus, an overlap occurs between basal and melanoma tumours in the central profile coordinates - Figure 6.3.

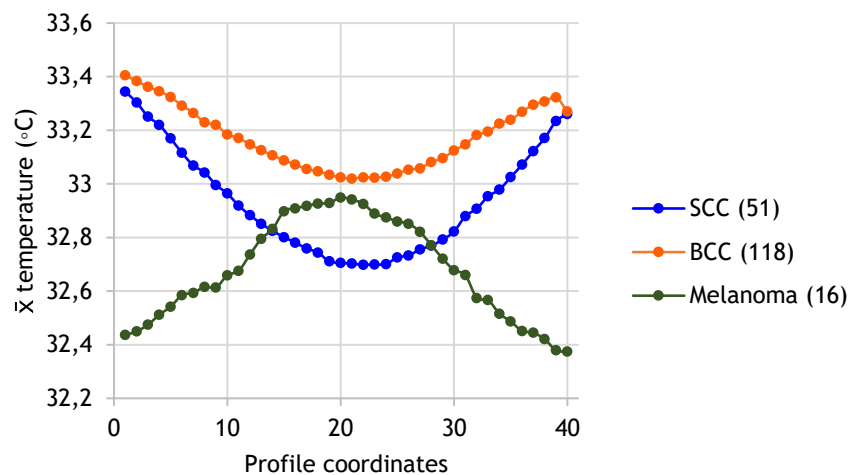


Figure 6.3 - Static thermal profile characteristic of SCC, BCC and melanoma lesions.

The static curves of melanocytic nevi, seborrheic keratosis and cystic tumours were quite similar, with an almost complete overlap in nevi and cyst lesions. The thermal profile of actinic keratosis presented the same shape as these benign tumours, however with lower temperature

values. An accentuated hypothermic curve was obtained for the other benign neoplasia, while actinic lesions showed a smoother thermal profile - Figure 6.4.

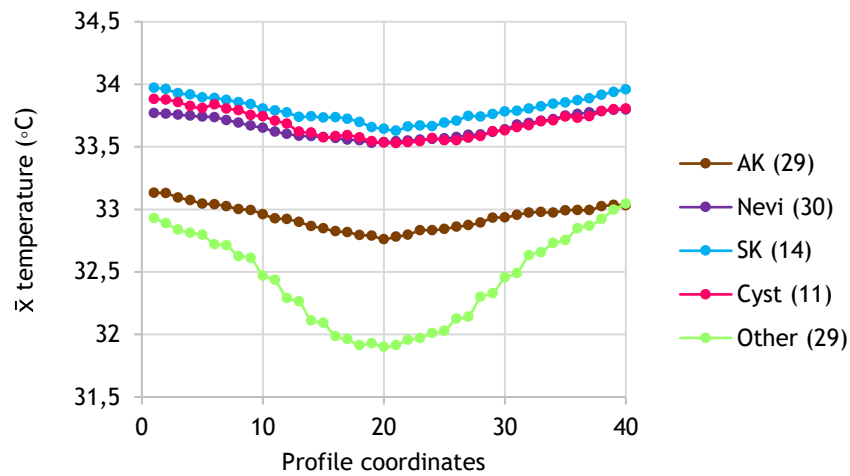


Figure 6.4 - Static thermal profile characteristic of AK, Nevi, SK, Cyst and Other lesions.

The comparison of melanoma and nevi tumours showed a clear distinction between these type of lesions, having melanoma a hyperthermic curve and melanocytic nevi a hypothermic one - Figure 6.5.

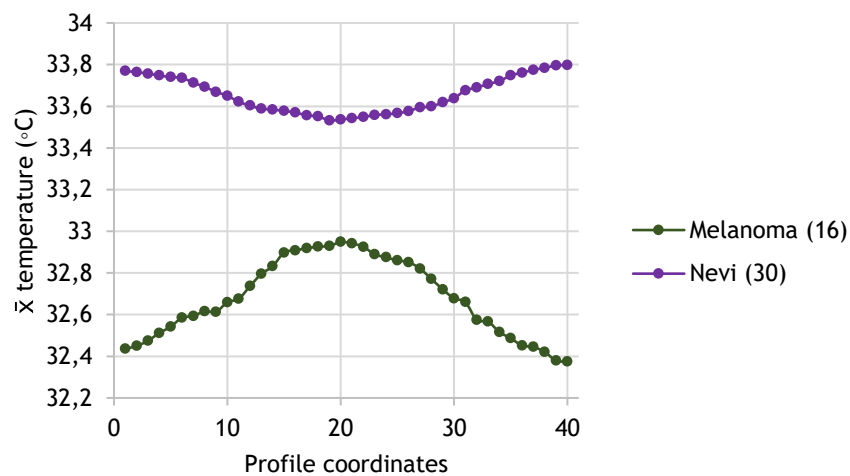


Figure 6.5 - Static thermal profile characteristic of melanoma and melanocytic lesions.

Both SCC and AK displayed hypothermic profiles that overlap in the central region. The hypothermic valley of squamous cell carcinoma is more pronounced, reaching lower temperatures than actinic lesions - Figure 6.6.

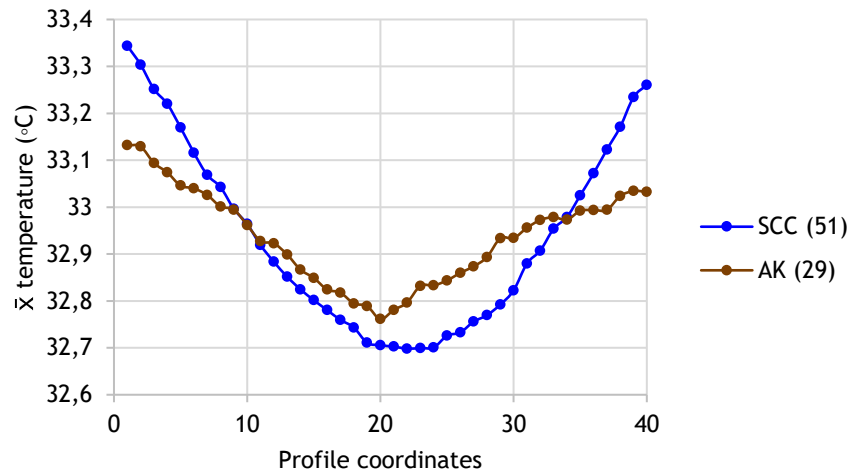


Figure 6.6 - Static thermal profile characteristic of SCC and AK lesions.

Lastly, the benign and malignant lesions were described by thermal curves that decrease its value as the tumour's centre is reached, with the second presenting a smoother depression. The non-neoplastic lesions exhibited an almost stable pattern, with temperatures lower than the neoplastic lesions - Figure 6.7.

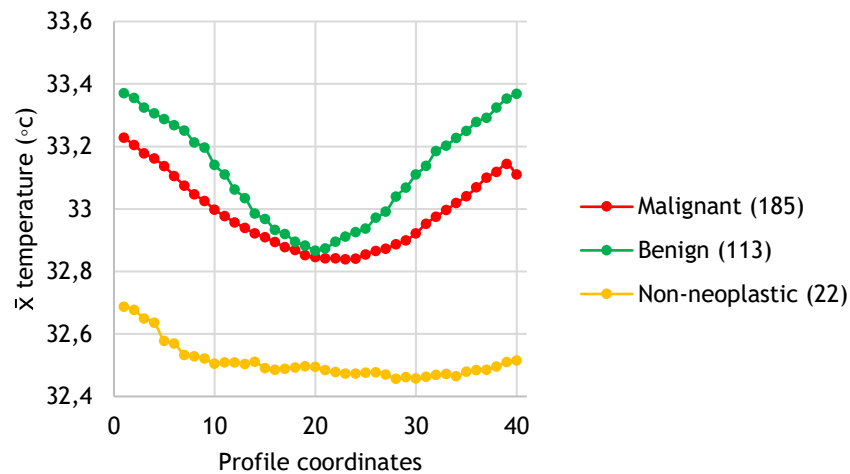


Figure 6.7 - Static thermal profile characteristic of benign, malignant and non-neoplastic lesions.

The average lesion temperature and standard deviation of different skin neoplasm types were also likened for differentiation purposes.

In the case of malignant tumours, the first statistical measurement was higher for BCC lesions and lower for melanomas, while the standard deviation of SCC exceeded the ones of melanoma and BCC - Figure 6.8A and B, respectively.

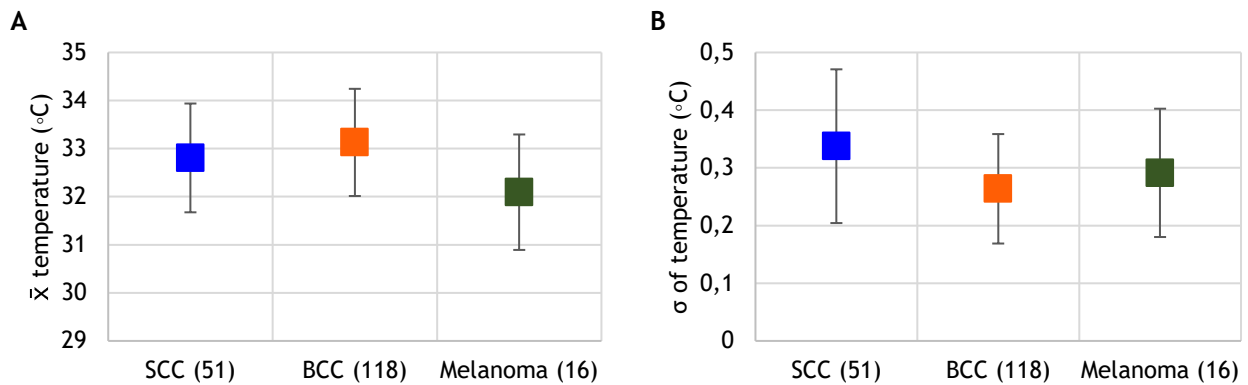


Figure 6.8 - SCC, BCC and melanoma lesions: A - average lesion temperature; B - Standard deviation.

The benign tumours were similar in both average lesion temperature and standard deviation, except for the values correspondent to other benign lesions, that differ greatly in the latter statistical measurement - Figure 6.9B.

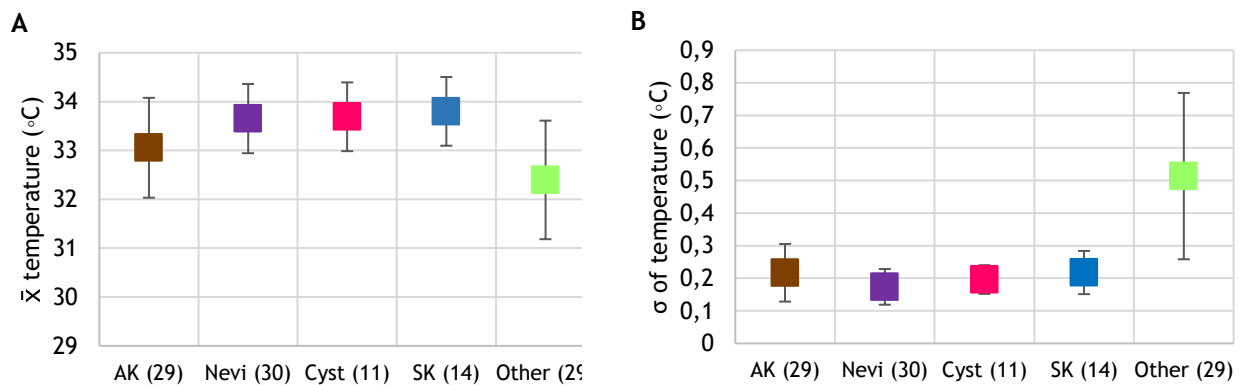


Figure 6.9 - AK, Nevi, Cyst, SK and Other lesions: A - average lesion temperature; B - standard deviation.

In general, melanoma lesions presented lower average temperatures than benign melanocytic tumours. The contrary was verified in the standard deviation measurement - Figure 6.10.

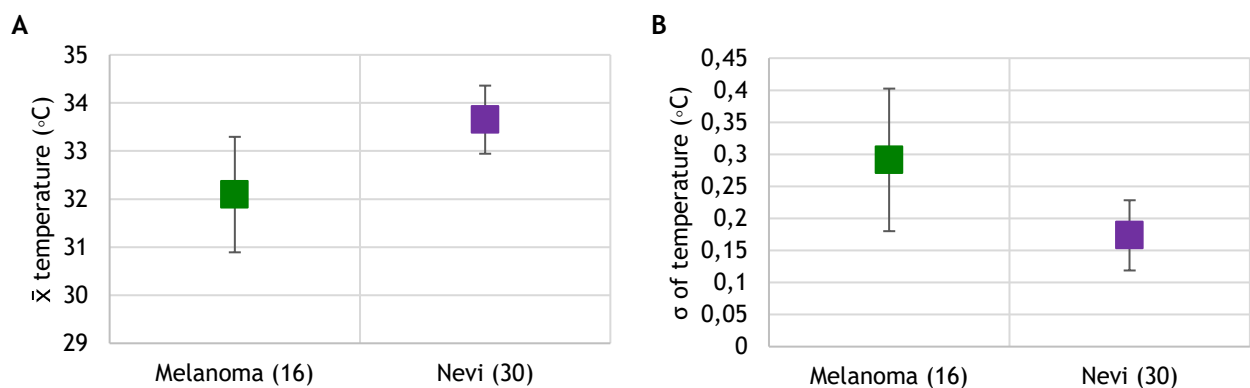


Figure 6.10 - Melanoma and Nevi lesions: A - average lesion temperature; B - standard deviation.

In the comparison of SCC and AK the standard deviation also showed a greater discrepancy than the average - Figure 6.11 A and 6.11B.

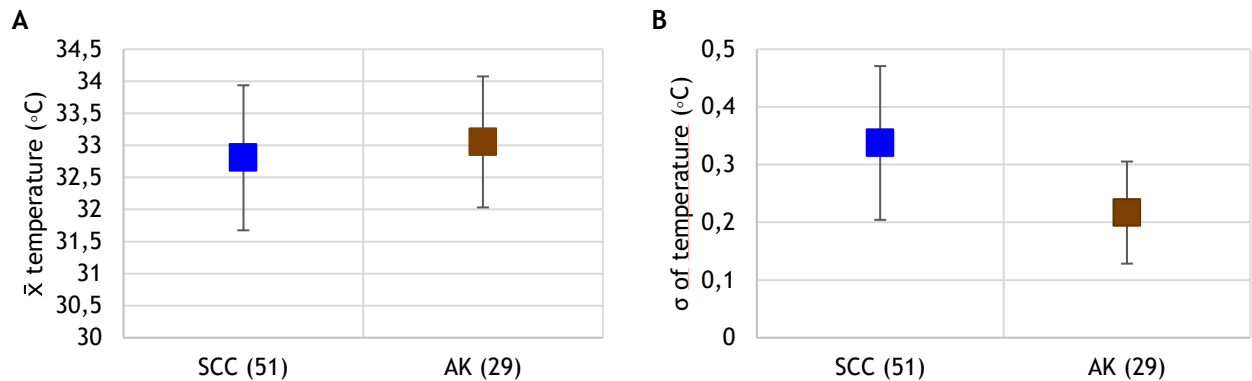


Figure 6.11 - SCC and AK lesions: A - average lesion temperature; B - standard deviation.

When relating different lesion malignancies, non-neoplastic lesions presented the lowest average temperature, followed by malignant and benign neoplasia. For the standard deviation the highest value was attained for malignant lesions and the smallest corresponded to tumours' scared tissue - Figure 6.12.

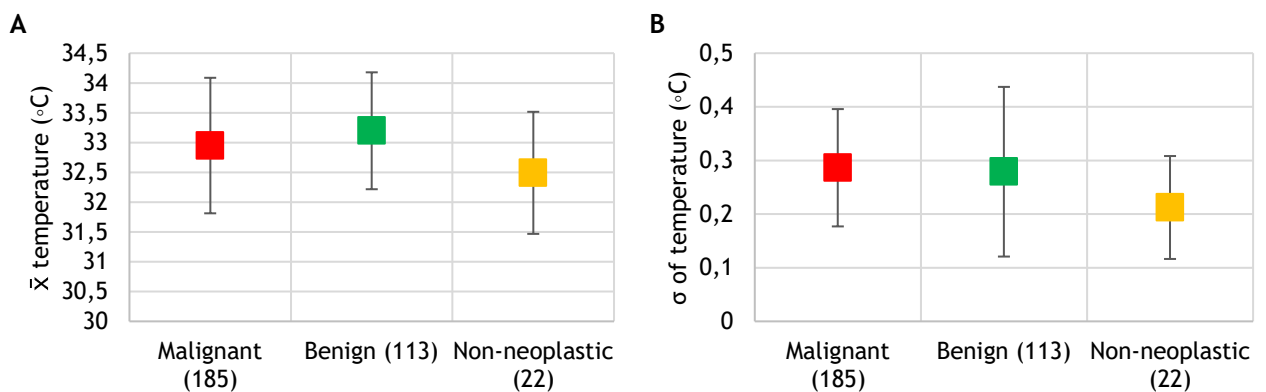


Figure 6.12 - Malignant, benign and Non-neoplastic lesions: A - average lesion temperature; B - standard deviation.

The comparison of leased skin areas and healthy skin tissue showed that the highest temperature difference between these regions was verified in malignant lesions, i. e., SCC, BCC and melanoma, and nevi tumours.

All presented lower temperatures for the tumour region, when compared to the healthy opposite area. The contrary was only verified for cysts and seborrheic tumours - Figure 6.13.

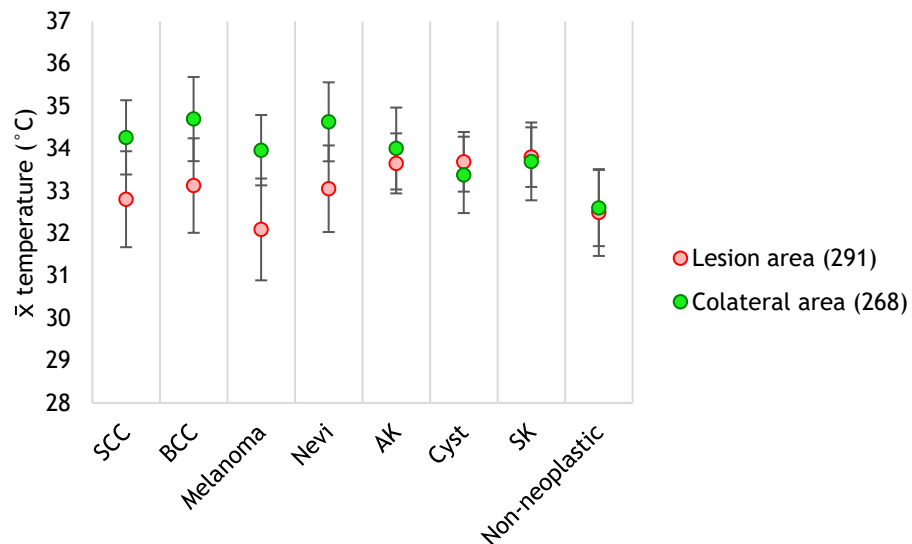


Figure 6.13 - Malignant, benign and non-neoplastic lesions: A - average lesion temperature; B - standard deviation.

6.3 - Dynamic image analysis

The dynamic analysis was performed in 274 tumours, including 30 SCC, 104 BCC, 12 melanomas, 27 actinic keratosis (AK), 29 melanocytic nevi (Nevi), 14 seborrheic keratosis (SK), 11 cysts, 27 other benign neoplasia and 20 scar tissue lesions. Not all 320 skin neoplasms were thermally stressed, since not every lesion was passible of stimulation, due to injury risk or impossible access.

The main goal of this stage was to evaluate the thermal behaviour of different skin neoplasm types after the application of a cold stress. Different thermal recovery curves were compared, based on the established classification task groups.

Concerning malignant lesions, the main differences, during the thermal recovery phase, were verified in Image 0. The highest maximum temperature difference (D) occurred for SCC lesions, followed by BCC and melanomas. The latter also presented the lowest average lesion temperature and standard deviation. After thermal stress, the average temperature of basal lesions decreased greatly and slightly for squamous tumours. Both lesion types displayed similar standard deviations - Figure 6.14.

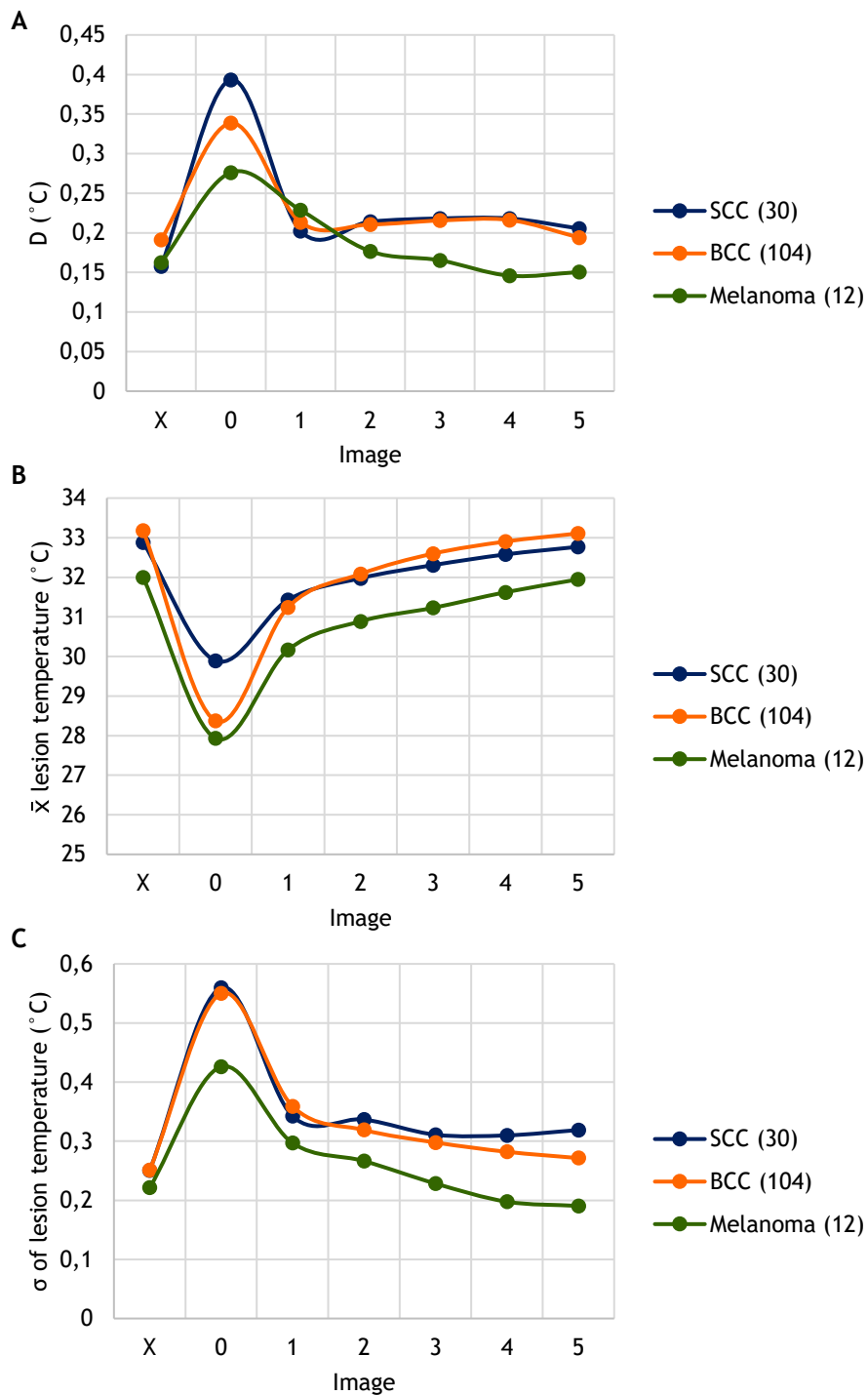


Figure 6.14 - Thermal changes during stimulation process - Malignant: A - Maximum temperature difference; B - Average lesion temperature; C - standard deviation of lesion temperature.

The benign lesion types presented low D , except for cystic lesions. The maximum temperature difference for other benign tumour types was mostly constant during the entire process. The average temperature profile was quite similar for all lesions, with an accentuated decrease on point 0. Lastly, the standard deviation measurement was constantly stable for other benign tumour types and elevated at the 0 time mark for the remaining lesions - Figure 6.15.

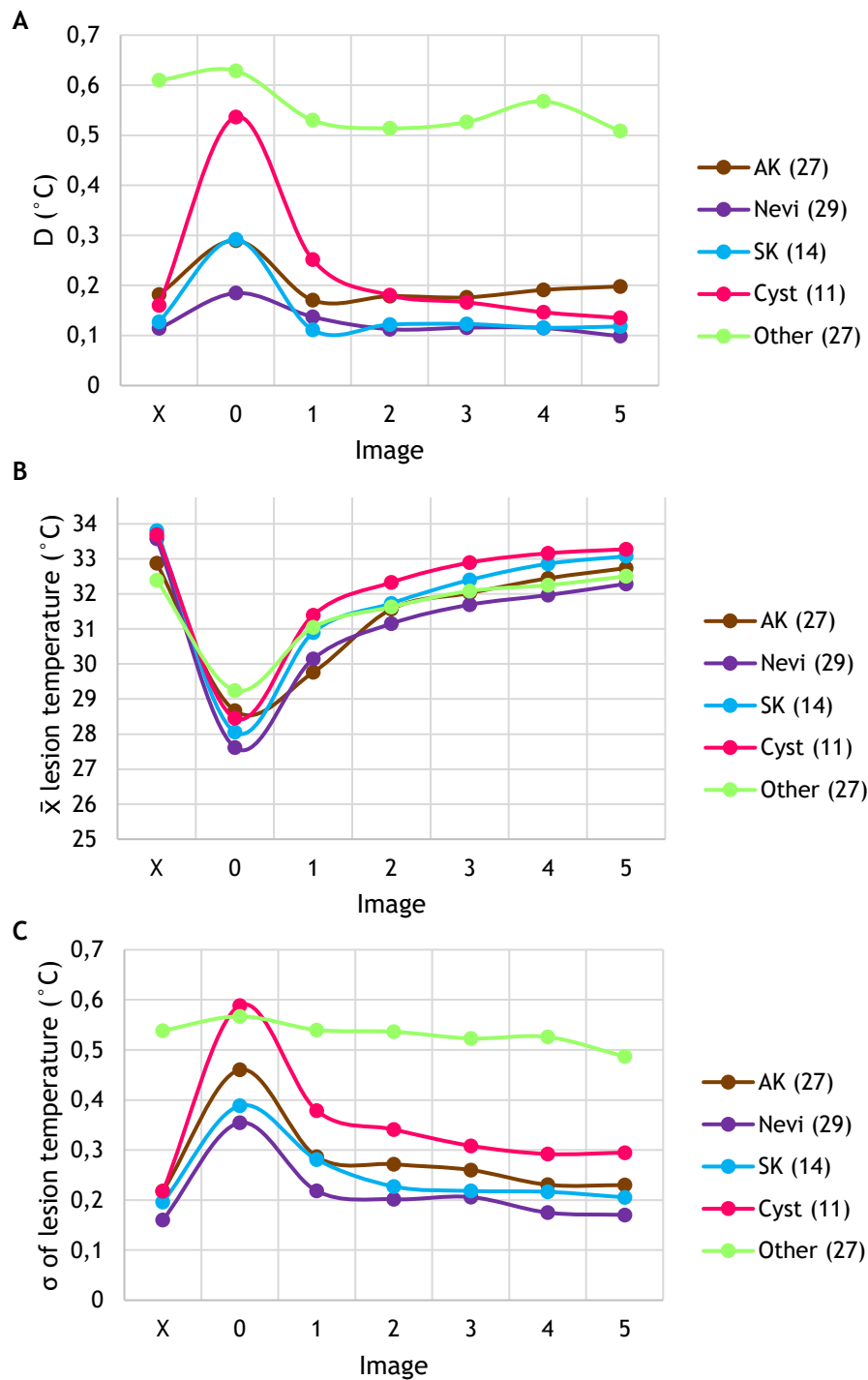


Figure 6.15 - Thermal changes during stimulation process - Benign: A - Maximum temperature difference; B - Average lesion temperature; C - standard deviation of lesion temperature.

The squamous lesions exceeded the actinic tumours in all measurements, specially in the moment immediately after the cooling process. The most significant difference was verified in D, with an increased slope between images X and 0 and images 0 and 1 - Figure 6.16.

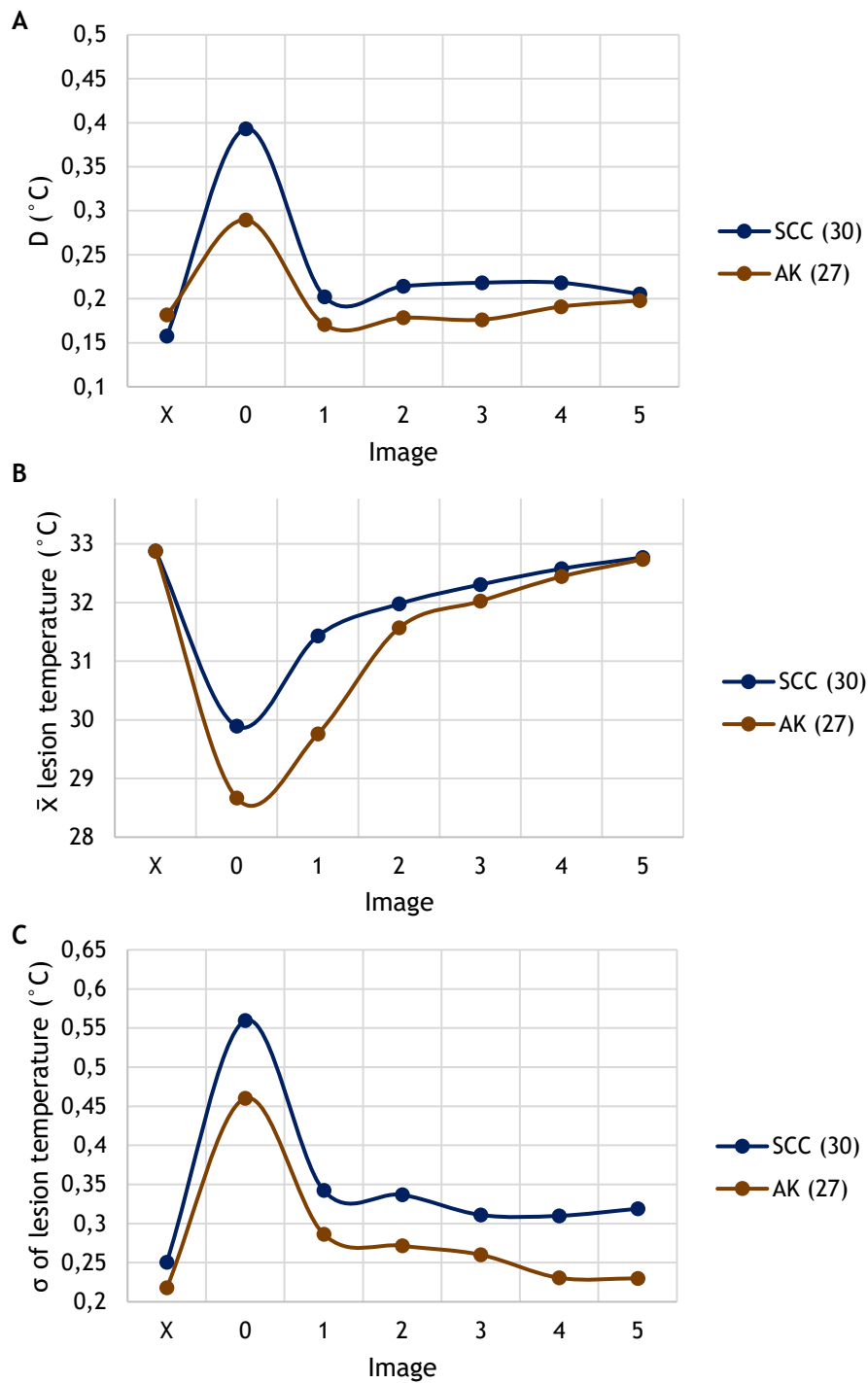


Figure 6.16 - Thermal changes during stimulation process - SCC vs AK: A - Maximum temperature difference; B - Average lesion temperature; C - standard deviation of lesion temperature.

In the evaluation of melanoma and nevi thermal recovery curves it was possible to assess that the malignant lesion type presented higher values for D and standard deviations of temperature than the benign melanocytic lesions. For melanomas the slopes between images X and 0 and images 0 and 1 were also more accentuated than the ones verified in nevi's thermal curve. However, equal temperature values were encountered for the leased area of both types in the majority of the thermal recovery process - Figure 6.17.

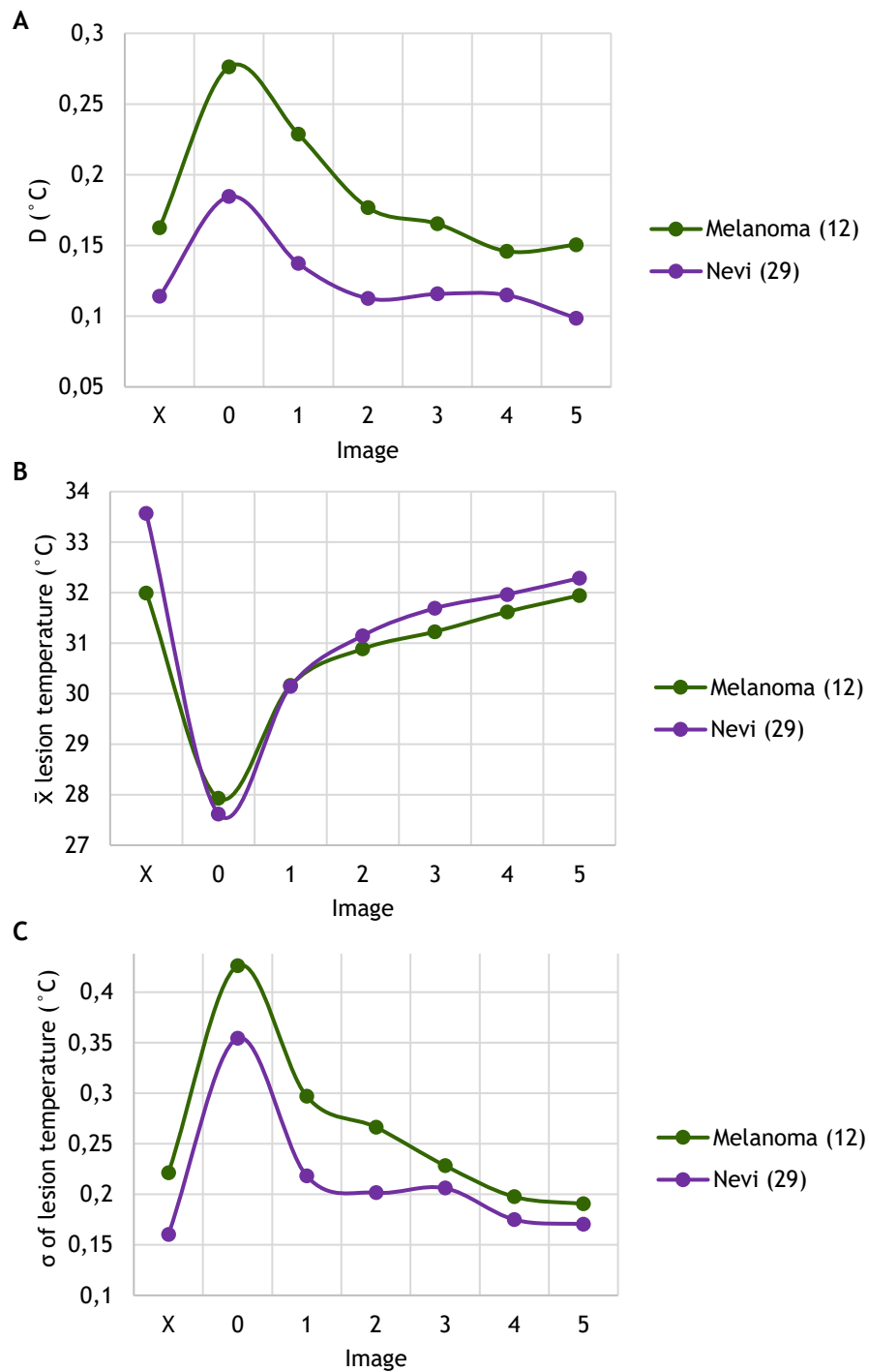


Figure 6.17 - Thermal changes during stimulation process - Melanoma vs Nevi: A - Maximum temperature difference; B - Average lesion temperature; C - standard deviation of lesion temperature.

In the same line, the benign lesions presented smaller curve slopes between images X and 0 and images 0 and 1 than the malignant skin tumours. The standard deviation was also higher for cancerous lesions, followed by non-cancerous pathologies. The overall lesion temperature was slightly higher for malignant tumours - Figure 6.18.

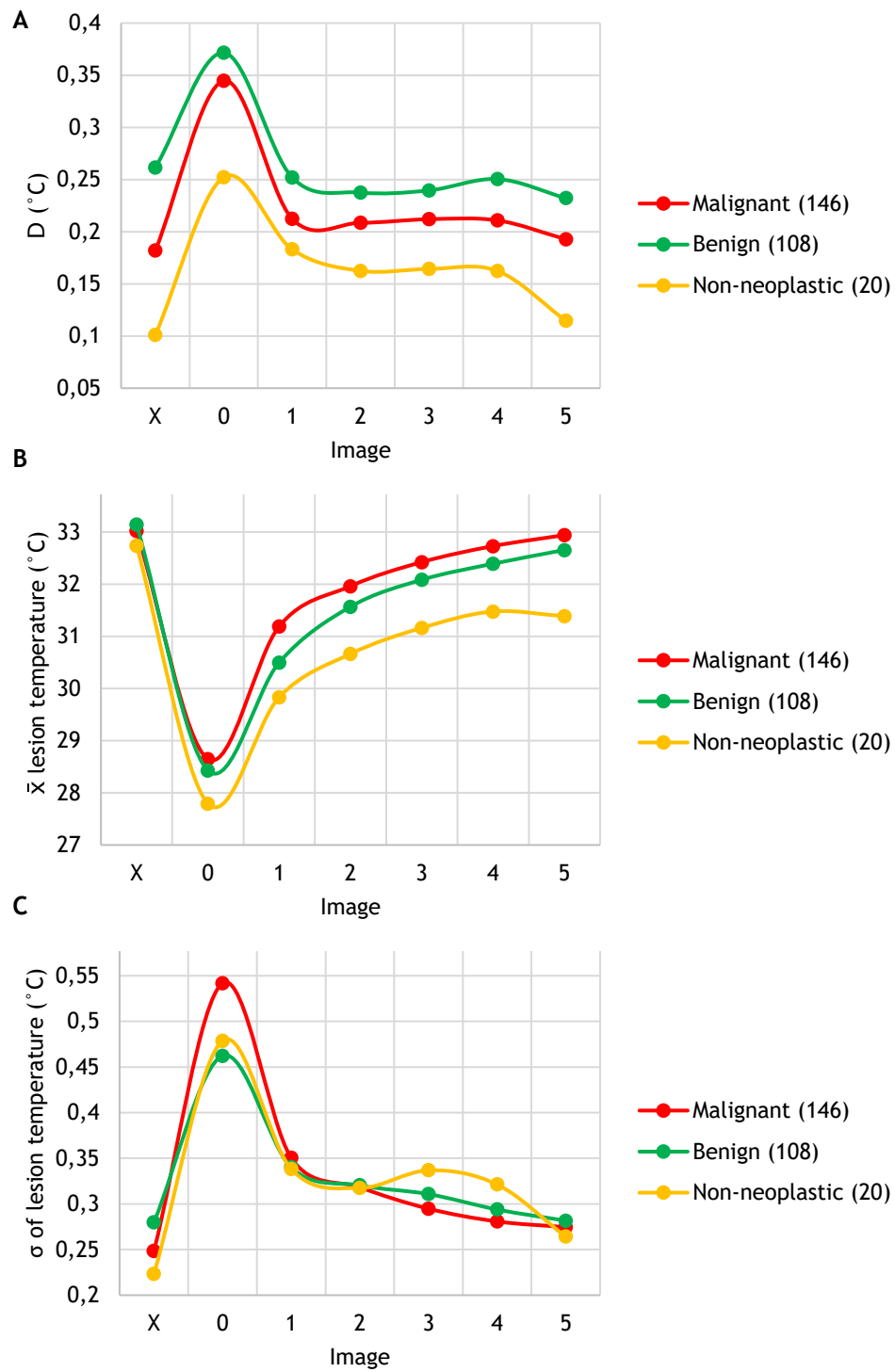


Figure 6.18 Thermal changes during stimulation process - Ben vs Mal vs Non: A - Maximum temperature difference; B - Average lesion temperature; C - standard deviation of lesion temperature.

6.4 - Statistical analysis

The statistical analysis included all the 320 participants and the correspondent biometric information and static and dynamic data collected during the infrared thermal image analysis stage.

The Kolmogorov-Smirnov test showed that not all variables followed a normal distribution, so the non-parametric tests U-Mann Whitney and Kruskal Wallis were applied with the purpose of assessing the influence of the factors Skin neoplasm type, Age group, Sex, Height, Weight, BMI, Eye colour, Fitzpatrick scale type and Skin marks in the steady-state (S1, S2, ..., S40; SM; SSTD) and dynamic variables (DX, DO, ..., D5; DMX, DM0, ..., DM5; DSTDX, DSTD0, ..., DSTD5).

For the Kruskal-Wallis test, the skin neoplasm type was predominantly associated with standard deviation, maximum temperature difference and average variables, while the age group was only linked to standard deviation measurements. Both test showed statistical evidence of rejecting the null hypothesis ($p < 0.05$) in the Sex class, which demonstrated the influence of such in variables D2 and DSTD4. The Eye colour characteristic was only connected to STD0 by the Kruskal-Wallis test - Table 6.2.

No other factor was considered to influence any variable.

Table 6.2 - Results of U-Mann Whitney and Kruskal-Wallis test: variables influenced by patients' factors.

Category	U-Mann Whitney	Kruskal-Wallis
Skin neoplasm type	-	SSTD, DX, D0, D1, D2, D4, DM0, DM1, DM2, DM3, DM4, DM5, DSTD4, DSTD5
Age group	-	DSTDX, DSTD0, DSTD1, DSTD2, DSTD4, DSTD5
Sex	D2, DSTD4	D2, DSTD4
Eye colour	-	DSTD0

6.5 - Machine learning classifiers

The classification stage had the primary goal of differentiating distinct skin neoplasm types, using different machine learning algorithms, e. g., Sequential Minimal Optimization (SMO), Multilayer Perceptron and instance Based k-nearest neighbour (iBk). For this, the acquired static (S1, S2, ..., S40; SM; SSTD) and dynamic variables (DX, DO, ..., D5; DMX, DM0, ..., DM5; DSTDX, DSTD0, ..., DSTD5) were used for different classification tasks.

Steady-state: S1, S2, ..., S40 and SM feature vector

The classification results based on lesion profile temperature values (S1, S2, ..., S40) and average lesion temperature (SM) are displayed in Figures 6.19-6.21 and Table 6.3-6.5.

The correct classification of different skin lesion types (benign, malignant and non-neoplastic lesions) was more difficult to achieve, than the distinction of benign and malignant tumours alone.

The differentiation among the benign lesion group was inconceivable, with accuracy (ACC) values of 19-29%, while different malignant lesions were more easily distinguished by the majority of classifiers, with the best accuracy corresponding to SMO-RBF and iBk (K=7) (ACC=60.8%).

The SMO learner with a quadratic polynomial kernel outperformed other classifiers in the task Melanoma vs Nevi (ACC=84.2%), while the highest correct classification of instances for SCC vs AK was achieved by the SMO with RBF and iBk ($k=\sqrt{n}$) algorithms (ACC=71.9%) - Figure 6.19 and Table 6.3.

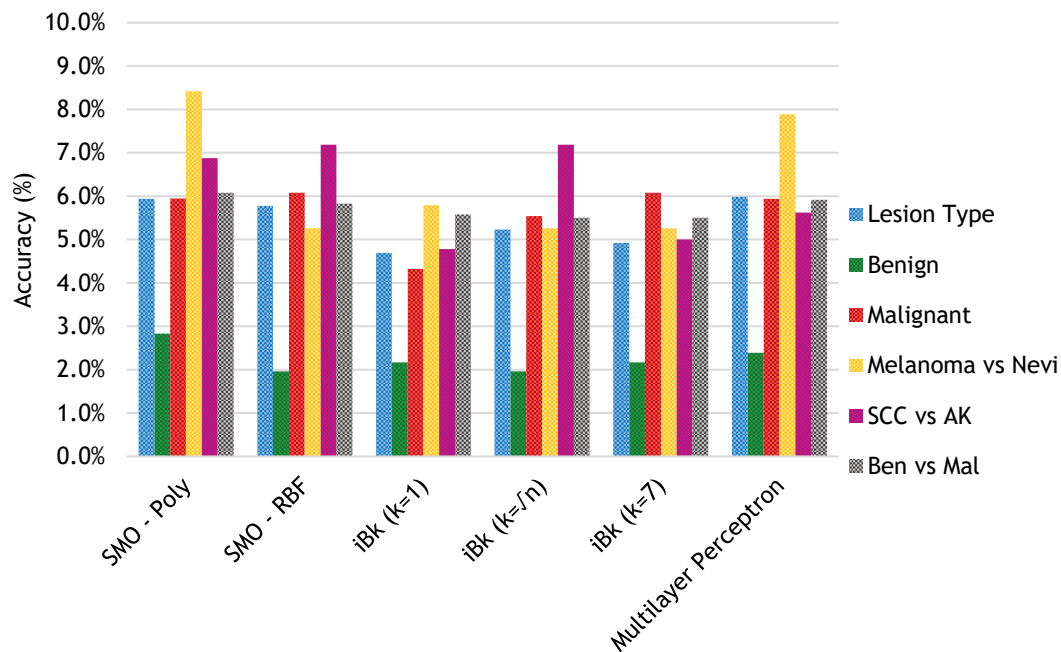


Figure 6.19 - Accuracy results for different classification tasks with SMO, iBk and Multilayer perceptron classifiers with S1, S2, ..., S40 and SM constituting the input vector.

Table 6.3 - Accuracy values for different classification tasks with SMO, iBk and Multilayer perceptron classifiers with S1, S2, ..., S40 and SM constituting the input vector.

Classifier	Lesion Type	Benign	Malignant	Melanoma vs Nevi	SCC vs AK	Ben vs Mal
SMO - Poly	59.4%	<u>28.3%</u>	59.5%	<u>84.2%</u>	68.8%	<u>60.8%</u>
SMO - RBF	57.8%	19.6%	<u>60.8%</u>	52.6%	<u>71.9%</u>	58.3%
iBk (k=1)	46.9%	21.7%	43.2%	57.9%	47.8%	55.8%
iBk (k=√n)	52.3%	19.6%	55.4%	52.6%	<u>71.9%</u>	56.7%
iBk (k=7)	49.2%	21.7%	<u>60.8%</u>	52.6%	50.0%	55.0%
Multilayer Perceptron	<u>59.8%</u>	23.9%	59.4%	78.9%	56.2%	59.2%

The best sensitivity values (SN) for the Melanoma vs Nevi, SCC vs AK and Ben vs Mal tasks were encountered, using SMO-Poly and iBk(k=1) (SN=66.7%), SMO-Poly and iBk (k= \sqrt{n}) (91.3%) and SMO with RBF (100.0%), respectively - Figure 6.20 and Table 6.4.

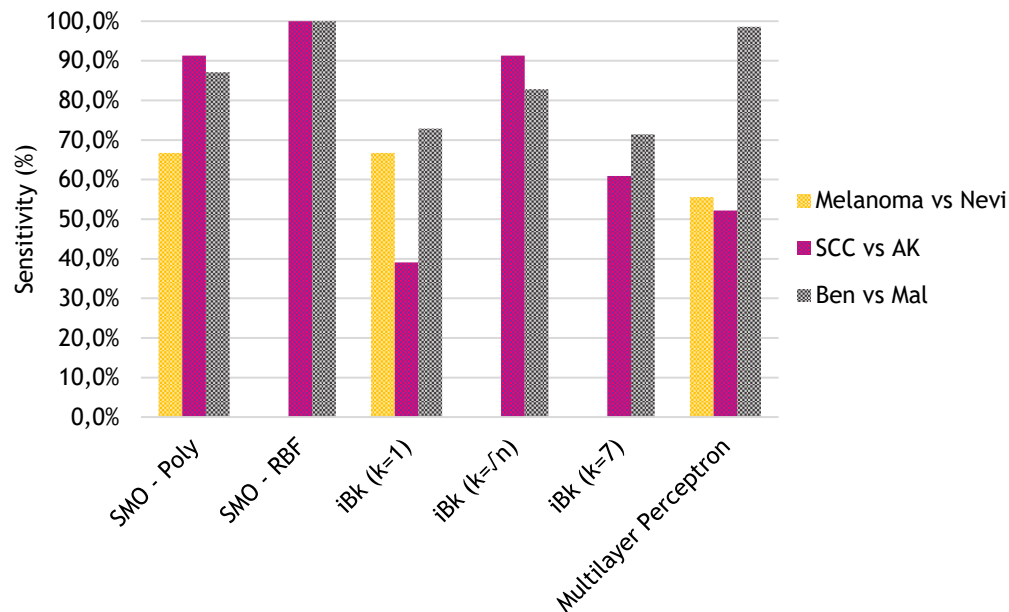


Figure 6.20 - Sensitivity results for different classification tasks with SMO, iBk and Multilayer perceptron classifiers with S1, S2, ..., S40 and SM constituting the input vector.

Table 6.4 - Sensitivity values for different classification tasks with SMO, iBk and Multilayer perceptron classifiers with S1, S2, ..., S40 and SM constituting the input vector.

Classifier	Lesion Type	Benign	Malignant	Melanoma vs Nevi	SCC vs AK	Ben vs Mal
SMO - Poly	-	-	-	<u>66.7%</u>	<u>91.3%</u>	87.1%
SMO - RBF	-	-	-	0.0%	100.0%	<u>100.0%</u>
iBk (k=1)	-	-	-	<u>66.7%</u>	39.1%	72.9%
iBk (k= \sqrt{n})	-	-	-	0.0%	<u>91.3%</u>	82.9%
iBk (k=7)	-	-	-	0.0%	60.9%	71.4%
Multilayer Perceptron	-	-	-	55.6%	52.2%	98.6%

The best specificity values (SP) for the Melanoma vs Nevi, SCC vs AK and Ben vs Mal tasks were achieved by all the classifiers, except iBk (k=1) (SP=100.0%), Multilayer perceptron (66.7%) and iBk (k=1 and k=7) (SP=32.0%), respectively - Figure 6.21 and Table 6.5.

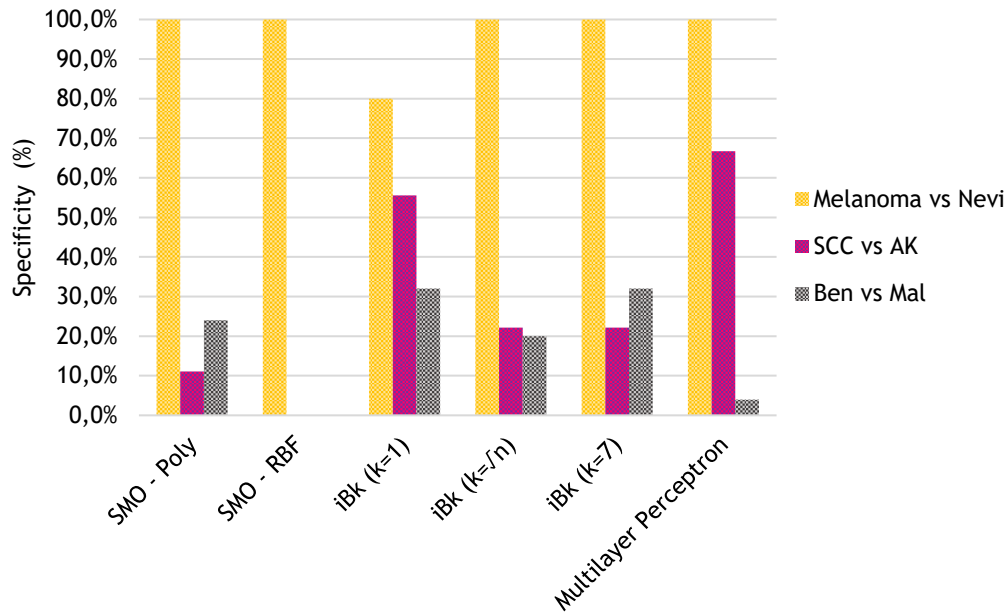


Figure 6.21 - Specificity results for different classification tasks with SMO, iBk and Multilayer perceptron classifiers with S1, S2, ..., S40 and SM constituting the input vector.

Table 6.5 - Specificity values for different classification tasks with SMO, iBk and Multilayer perceptron classifiers with S1, S2, ..., S40 and SM constituting the input vector.

Classifier	Lesion Type	Benign	Malignant	Melanoma vs Nevi	SCC vs AK	Ben vs Mal
SMO - Poly	-	-	-	<u>100.0%</u>	11.1%	24.0%
SMO - RBF	-	-	-	<u>100.0%</u>	0.0%	0.0%
iBk (k=1)	-	-	-	80.0%	55.6%	<u>32.0%</u>
iBk (k=vn)	-	-	-	<u>100.0%</u>	22.2%	20.0%
iBk (k=7)	-	-	-	<u>100.0%</u>	22.2%	<u>32.0%</u>
Multilayer Perceptron	-	-	-	<u>100.0%</u>	<u>66.7%</u>	4.0%

Steady-state: S1, S2, ..., S40 and SSTD feature vector

The classification results using lesion profile temperature values (S1, S2, ..., S40) and average lesion standard deviation (SSTD) as inputs for the feature vector are displayed in Figure 6.22-6.24 and Table 6.6-6.8.

Like in the previous mentioned classification results, the distinction between different lesion types was worse than the solo differentiation between benign and malignant lesions. The benign classification task was also poorly performed. The separation of different malignant types was best achieved by the learner SMO-RBF (ACC=60.8%), the melanoma task displayed a high accuracy with Multilayer perceptron (ACC=84.2%) and the best SCC vs AK result was encountered with the SMO-Poly (ACC=75.0%) - Figure 6.22 and Table 6.6.

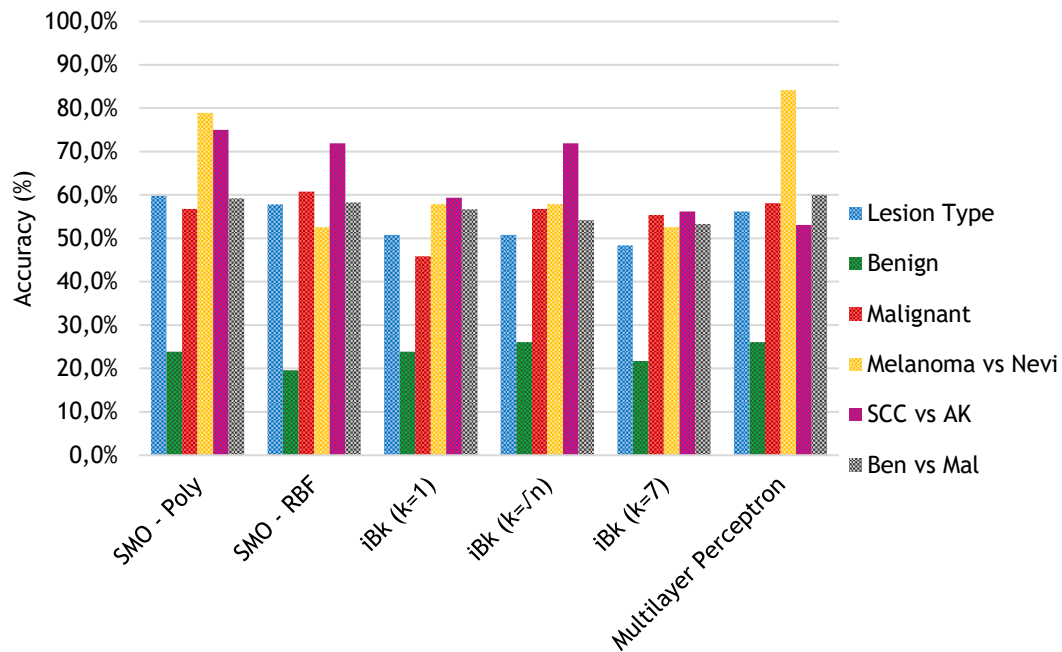


Figure 6.22 - Accuracy results for different classification tasks with SMO, iBk and Multilayer perceptron classifiers with S1, S2, ..., S40 and SSTD constituting the input vector.

Table 6.6 - Accuracy values for different classification tasks with SMO, iBk and Multilayer perceptron classifiers with S1, S2, ..., S40 and SSTD constituting the input vector.

Classifier	Lesion Type	Benign	Malignant	Melanoma vs Nevi	SCC vs AK	Ben vs Mal
SMO - Poly	<u>59.8%</u>	23.9%	56.8%	78.9%	<u>75.0%</u>	59.2%
SMO - RBF	57.8%	19.6%	<u>60.8%</u>	52.6%	71.9%	58.3%
iBk (k=1)	50.8%	23.9%	45.9%	57.9%	59.4%	56.7%
iBk (k=vn)	50.8%	<u>26.1%</u>	56.8%	57.9%	71.9%	54.2%
iBk (k=7)	48.4%	21.7%	55.4%	52.6%	56.2%	53.3%
Multilayer Perceptron	56.2%	<u>26.1%</u>	58.1%	<u>84.2%</u>	53.1%	<u>60.0%</u>

The sensitivity values (SN) for the Melanoma vs Nevi task reached the 77.8% mark with the classifier Multilayer perceptron. The sensitivity for the tasks SCC vs AK and Ben vs Mal reached the 100.0% mark with the learners SMO-RBF and SMO-Poly - Figure 6.23 and Table 6.7.

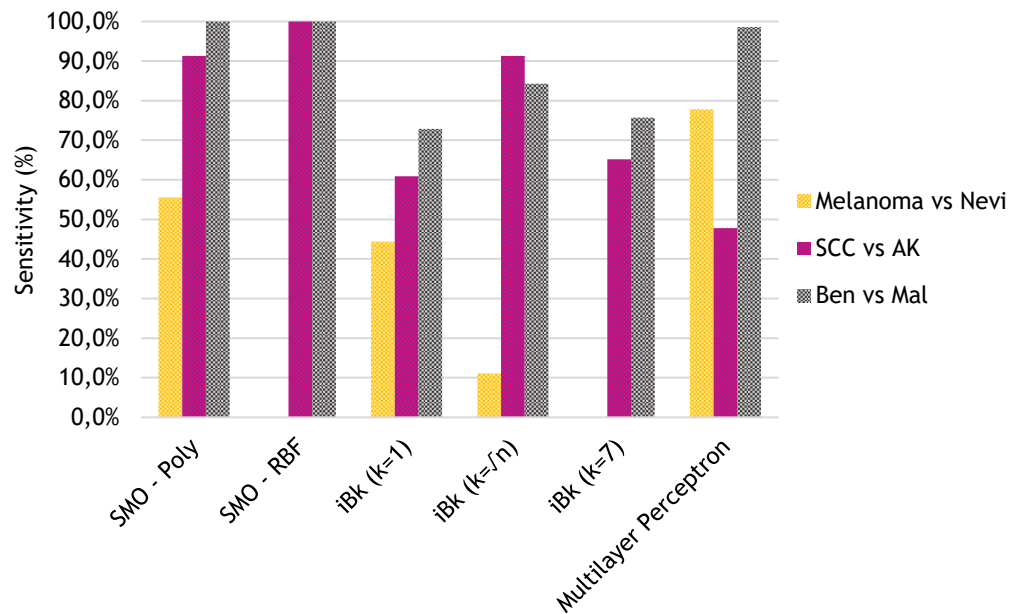


Figure 6.23 - Sensitivity results for different classification tasks with SMO, iBk and Multilayer perceptron classifiers with S1, S2, ..., S40 and SSTD constituting the input vector.

Table 6.7 - Sensitivity values for different classification tasks with SMO, iBk and Multilayer perceptron classifiers with S1, S2, ..., S40 and SSTD constituting the input vector.

Classifier	Lesion Type	Benign	Malignant	Melanoma vs Nevi	SCC vs AK	Ben vs Mal
SMO - Poly	-	-	-	55.6%	91.3%	<u>100.0%</u>
SMO - RBF	-	-	-	0.0%	<u>100.0%</u>	<u>100.0%</u>
iBk (k=1)	-	-	-	44.4%	60.9%	72.9%
iBk (k=vn)	-	-	-	11.1%	91.3%	84.3%
iBk (k=7)	-	-	-	0.0%	65.2%	75.7%
Multilayer Perceptron	-	-	-	<u>77.8%</u>	47.8%	98.6%

The 100% specificity value was reached by several classifiers for the differentiation of melanoma and nevi lesions. The Multilayer perceptron algorithm outperformed the others for the distinction of SCC and AK (SP=66.7%) and the iBk (k=1) gave the best, even though low, result (SP=34.0%) for the Ben vs Mal classification task - Figure 6.24 and Table 6.8.

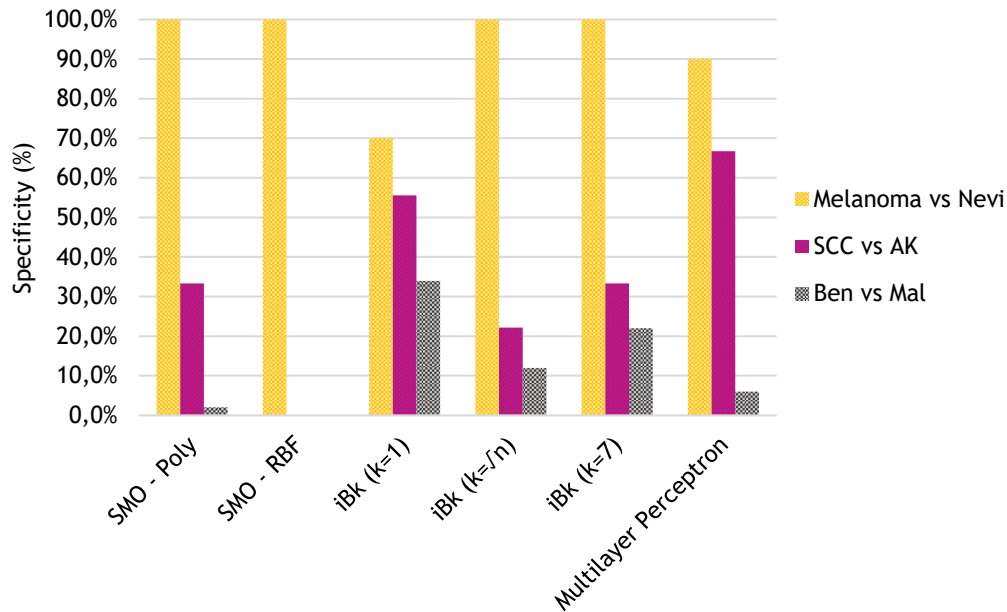


Figure 6.24 - Specificity results for different classification tasks with SMO, iBk and Multilayer perceptron classifiers with S1, S2, ..., S40 and SSTD constituting the input vector.

Table 6.8 - Specificity values for different classification tasks with SMO, iBk and Multilayer perceptron classifiers with S1, S2, ..., S40 and SSTD constituting the input vector.

Classifier	Lesion Type	Benign	Malignant	Melanoma vs Nevi	SCC vs AK	Ben vs Mal
SMO - Poly	-	-	-	<u>100.0%</u>	33.3%	2.0%
SMO - RBF	-	-	-	<u>100.0%</u>	0.0%	0.0%
iBk (k=1)	-	-	-	70.0%	55.6%	<u>34.0%</u>
iBk (k=√n)	-	-	-	<u>100.0%</u>	22.2%	12.0%
iBk (k=7)	-	-	-	<u>100.0%</u>	33.3%	22.0%
Multilayer Perceptron	-	-	-	90.0%	<u>66.7%</u>	6.0%

Dynamic: DX, DO, ..., D5 and DMX, DM0, ..., DM5 feature vector

The classification results using maximum temperature differences (DX, DO, ..., D5) and average lesion temperature (DMX, DM0, ..., DM5) are displayed in Figure 6.25 -6.27 and Table 6.9-6.11.

The percentage of correct classified instances for Lesion Type and Ben vs Mal was more balanced, with some classifiers performing better in the first, e.g., iBk (k=√n) and iBk (k=7), and others in the second task, namely, SMO-Poly, SMO-RBF, iBk (k=1) and Multilayer perceptron. The accuracy for Benign improved slightly when compared with the static results. Even though lower, the accuracy reached 45.4% with the iBk (k=√n). The Malignant task followed the same tendency presenting all accuracy values above 60.0%. Contrarily, the distinction of melanoma and nevi tumours worsened, having the Multilayer perceptron learner reached an accuracy of 70.6%. The iBk (k=√n) classifier was the best performer in SCC vs AK (ACC=78.3%) - Figure 6.25 and Table 6.9.

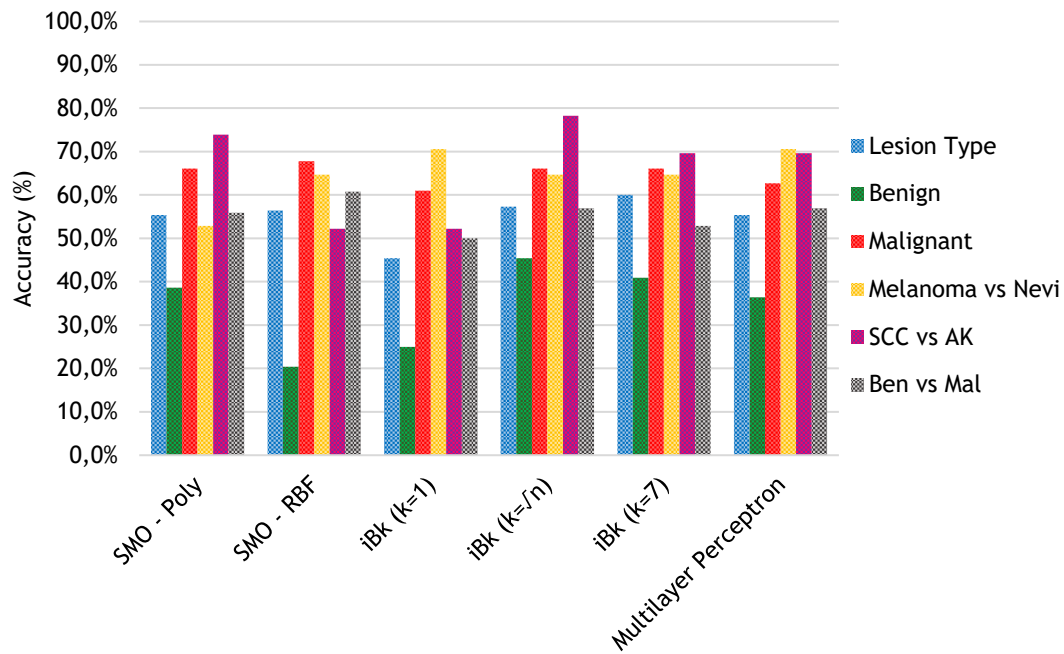


Figure 6.25 - Accuracy results for different classification tasks with SMO, iBk and Multilayer perceptron classifiers with DX, DO, ..., D5 and DMX, DM0, ..., DM5 constituting the input vector.

Table 6.9 - Accuracy values for different classification tasks with SMO, iBk and Multilayer perceptron classifiers with DX, DO, ..., D5 and DMX, DM0, ..., DM5 constituting the input vector.

Classifier	Lesion Type	Benign	Malignant	Melanoma vs Nevi	SCC vs AK	Ben vs Mal
SMO - Poly	55.4%	38.6%	66.1%	52.9%	73.9%	55.9%
SMO - RBF	56.4%	20.4%	<u>67.8%</u>	64.7%	52.2%	<u>60.8%</u>
iBk (k=1)	45.4%	25.0%	61.0%	70.6%	52.2%	50.0%
iBk (k=vn)	57.3%	<u>45.4%</u>	66.1%	64.7%	<u>78.3%</u>	56.9%
iBk (k=7)	<u>60.0%</u>	40.9%	66.1%	64.7%	69.6%	52.9%
Multilayer Perceptron	55.4%	36.4%	62.7%	<u>70.6%</u>	69.6%	56.9%

The distinction of melanoma and nevi tumours presented low sensitivity values, varying from 0.0% to 34%. In contrast the SCC vs AK task obtained high sensitivity values, with SMO with RBF kernel reaching the 100%. The same result was reached with the same classifier for the distinction of benign and malignant lesions - Figure 6.26 and Table 6.10.

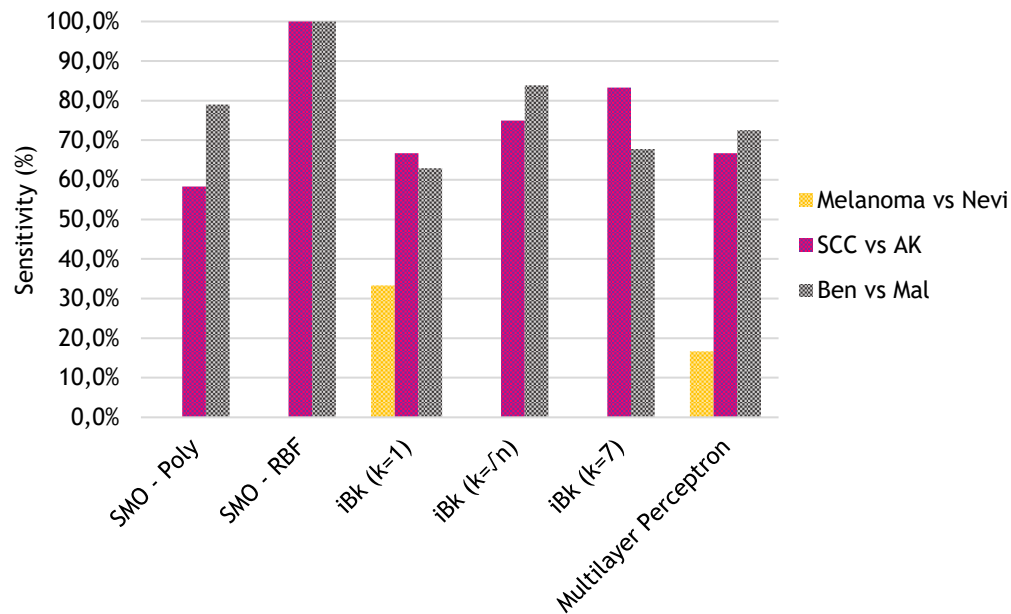


Figure 6.26 - Sensitivity results for different classification tasks with SMO, iBk and Multilayer perceptron classifiers with DX, DO, ..., D5 and DMX, DM0, ..., DM5 constituting the input vector.

Table 6.10 - Sensitivity values for different classification tasks with SMO, iBk and Multilayer perceptron classifiers with DX, DO, ..., D5 and DMX, DM0, ..., DM5 constituting the input vector.

Classifier	Lesion Type	Benign	Malignant	Melanoma vs Nevi	SCC vs AK	Ben vs Mal
SMO - Poly	-	-	-	0.0%	58.3%	79.0%
SMO - RBF	-	-	-	0.0%	<u>100.0%</u>	<u>100.0%</u>
iBk (k=1)	-	-	-	<u>33.3%</u>	66.7%	62.9%
iBk (k=∞)	-	-	-	0.0%	75.0%	83.9%
iBk (k=7)	-	-	-	0.0%	83.3%	67.7%
Multilayer Perceptron	-	-	-	16.7%	66.7%	72.6%

The maximum specificity was reached by several classifiers in the Melanoma vs Nevi task, while poor performance was encountered for the Ben vs Mal one. The best SP for the differentiation of squamous cell carcinomas and actinic keratosis lesions was achieved with SMO-Poly (SP=90.9%) - Figure 6.27 and Table 6.11.

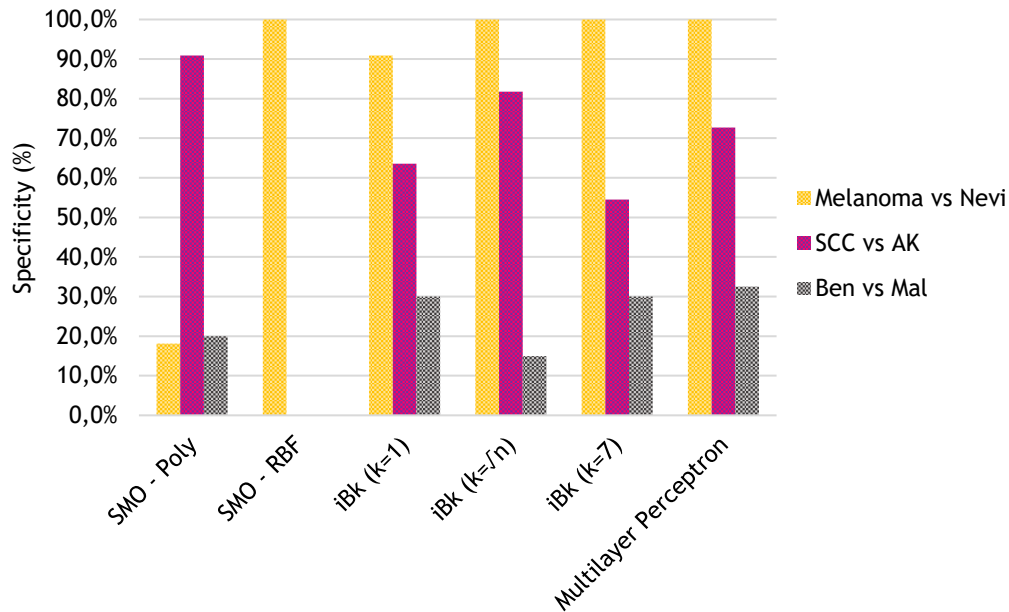


Figure 6.27 - Specificity results for different classification tasks with SMO, iBk and Multilayer perceptron classifiers with DX, DO, ..., D5 and DMX, DM0, ..., DM5 constituting the input vector.

Table 6.11 - Specificity values for different classification tasks with SMO, iBk and Multilayer perceptron classifiers with DX, DO, ..., D5 and DMX, DM0, ..., DM5 constituting the input vector.

Classifier	Lesion Type	Benign	Malignant	Melanoma vs Nevi	SCC vs AK	Ben vs Mal
SMO - Poly	-	-	-	18.1%	<u>90.9%</u>	20.0%
SMO - RBF	-	-	-	<u>100.0%</u>	0.0%	0.0%
iBk (k=1)	-	-	-	90.9%	63.6%	30.0%
iBk (k=∞)	-	-	-	<u>100.0%</u>	81.8%	15.0%
iBk (k=7)	-	-	-	<u>100.0%</u>	54.5%	30.0%
Multilayer Perceptron	-	-	-	<u>100.0%</u>	72.7%	<u>32.5%</u>

Dynamic: DX, DO, ..., D5 and STD_X, STD₀, ..., STD₅ feature vector

The accuracy (ACC), sensitivity and specificity values acquired using maximum temperature differences (DX, DO, ..., D5) and standard deviation of lesion temperature (STD_X, STD₀, ..., STD₅) are presented in Figure 6.28 -6.30 and Table 6.12-6.14.

The accuracy results for Lesion type and Ben vs Mal classification tasks were, once again close, with both reaching accuracies values around 60.0%. Improvements in the Benign and Malignant tasks were also verified when compared to the steady-state accuracies. Like in the previous dynamic results the Melanoma vs Nevi only reached the 70.6% mark, but with the SMO-Poly learner. The distinction of squamous cell carcinomas and actinic lesions only achieved accuracy values of 52.2%, with the implementation of SMO-RBF and iBk (k=1) - Figure 6.28 and Table 6.12.

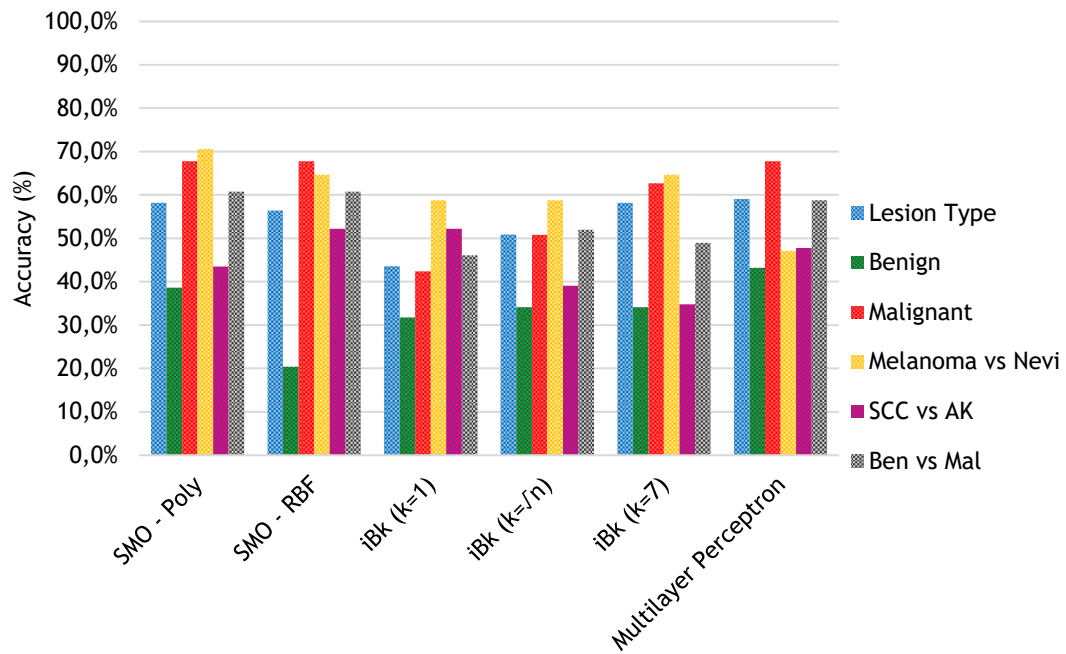


Figure 6.28 - Accuracy results for different classification tasks with SMO, iBk and Multilayer perceptron classifiers with DX, DO, ..., D5 and DSTDX, DSTDO, ..., DSTD5 constituting the input vector.

Table 6.12 - Accuracy values for different classification tasks with SMO, iBk and Multilayer perceptron classifiers with DX, DO, ..., D5 and DSTDX, DSTDO, ..., DSTD5 constituting the input vector.

Classifier	Lesion Type	Benign	Malignant	Melanoma vs Nevi	SCC vs AK	Ben vs Mal
SMO - Poly	58.2%	38.6%	<u>67.8%</u>	<u>70.6%</u>	43.5%	<u>60.8%</u>
SMO - RBF	56.4%	20.4%	<u>67.8%</u>	64.7%	<u>52.2%</u>	<u>60.8%</u>
iBk (k=1)	43.6%	31.8%	42.4%	58.8%	<u>52.2%</u>	46.1%
iBk (k=vn)	50.9%	34.1%	50.8%	58.8%	39.1%	52.0%
iBk (k=7)	58.2%	34.1%	62.7%	64.7%	34.8%	49.0%
Multilayer Perceptron	<u>59.1%</u>	<u>43.2%</u>	<u>67.8%</u>	47.1%	47.8%	58.8%

The sensitivity values for Melanoma vs Nevi were very low, with a best sensitivity of 20.0%. Contrarily, the remaining classification tasks presented maximum sensitivities with the classifier SMO-RBF - Figure 6.29 and Table 6.13.

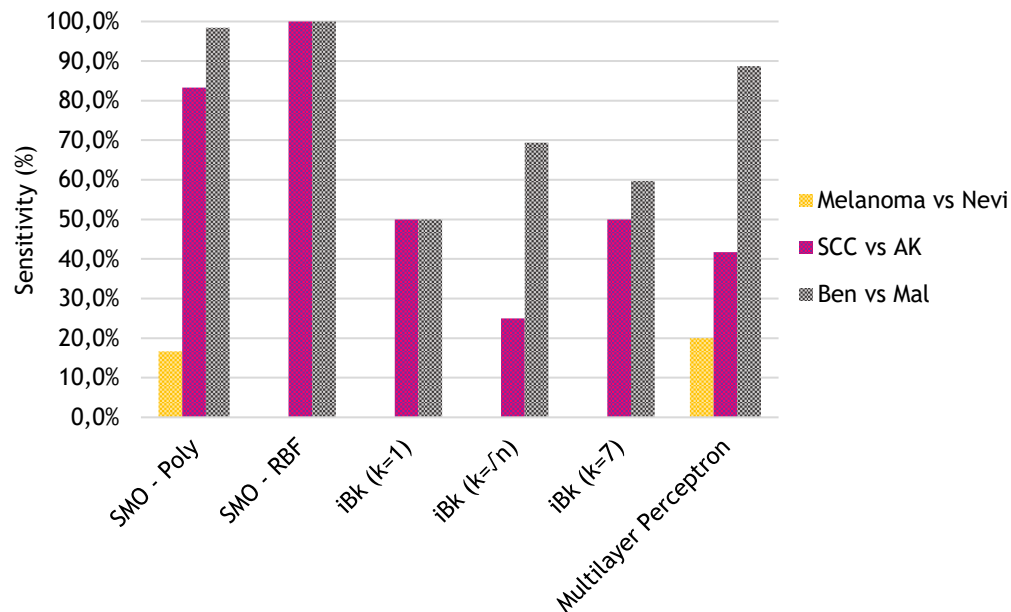


Figure 6.29 - Sensitivity results for different classification tasks with SMO, iBk and Multilayer perceptron classifiers with DX, DO, ..., D5 and DSTDX, DSTDO, ..., DSTD5 constituting the input vector.

Table 6.13 - Sensitivity values for different classification tasks with SMO, iBk and Multilayer perceptron classifiers with DX, DO, ..., D5 and DSTDX, DSTDO, ..., DSTD5 constituting the input vector.

Classifier	Lesion Type	Benign	Malignant	Melanoma vs Nevi	SCC vs AK	Ben vs Mal
SMO - Poly	-	-	-	16.7%	83.3%	98.4%
SMO - RBF	-	-	-	0.0%	<u>100.0%</u>	<u>100.0%</u>
iBk (k=1)	-	-	-	0.0%	50.0%	50.0%
iBk (k=∞)	-	-	-	0.0%	25.0%	69.4%
iBk (k=7)	-	-	-	0.0%	50.0%	59.7%
Multilayer Perceptron	-	-	-	<u>20.0%</u>	41.7%	88.7%

A maximum specificity was reached for the Melanoma vs. Nevi and SCC vs AK tasks with the SMO-Poly classifier. The SP values for the differentiation between benign and malignant lesions was somewhat low, with values from 0.0% (SMO-RBF) to 40.0% (iBk (k=1)) - Figure 6.30 and Table 6.14.

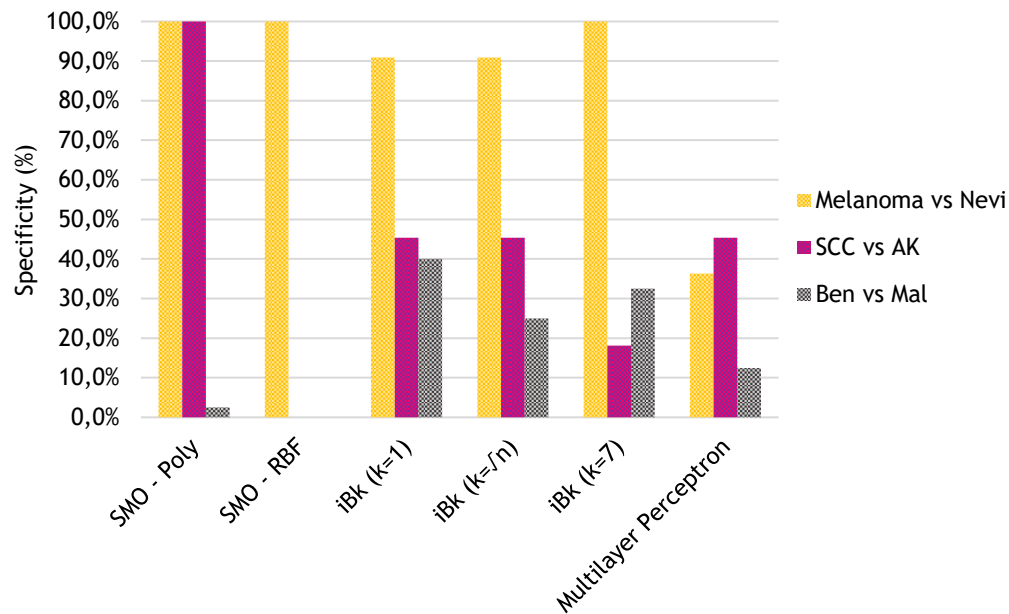


Figure 6.30 - Specificity results for different classification tasks with SMO, iBk and Multilayer perceptron classifiers with DX, DO, ..., D5 and DSTDX, DSTDO, ..., DSTD5 constituting the input vector.

Table 6.14 - Specificity values for different classification tasks with SMO, iBk and Multilayer perceptron classifiers with DX, DO, ..., D5 and DSTDX, DSTDO, ..., DSTD5 constituting the input vector.

Classifier	Lesion Type	Benign	Malignant	Melanoma vs Nevi	SCC vs AK	Ben vs Mal
SMO - Poly	-	-	-	<u>100.0%</u>	<u>100.0%</u>	2.5%
SMO - RBF	-	-	-	<u>100.0%</u>	0.0%	0.0%
iBk (k=1)	-	-	-	90.9%	45.4%	<u>40.0%</u>
iBk (k=√n)	-	-	-	90.9%	45.4%	25.0%
iBk (k=7)	-	-	-	<u>100.0%</u>	18.1%	32.5%
Multilayer Perceptron	-	-	-	36.3%	45.4%	12.5%

The True Positive (TP), True Negative (TN), False Positive (FP) and False Negative (FN) values obtained for the classification tasks Melanoma vs Nevi, SCC vs AK and Ben vs Mal are included in Appendix VIII, according to the features selected for the input vector.

The best overall classification results for each classification task are summarized in Table 6.15 and will be discussed in the following chapter.

Table 6.15 - Best overall classification results.

Classification task	Classifier	Input vector	ACC	SN	SP
Lesion type	Multilayer perceptron	DX, DO, ..., D5 DMX, DM0, ..., DM5	60.0%	-	-
Benign	iBk (k=vn)	DX, DO, ..., D5 DMX, DM0, ..., DM5	45.4%	-	-
Malignant	SMO-Poly or Multilayer perceptron	DX, DO, ..., D5 DSTDx, DSTD0, ..., DSTD5	67.8%	-	-
Melanoma vs Nevi	SMO-Poly	S1, S2, ..., S40 SM	84.2%	91.3%	11.1%
SCC vs AK	iBk=(vn)	DX, DO, ..., D5 DMX, DM0, ..., DM5	78.3%	75.0%	81.8%
Ben vs Mal	SMO-Poly	S1, S2, ..., S40 SM	60.8%	87.1%	24.0%

Chapter 7

Discussion

This chapter includes the discussion of results acquired with steady-state image analysis, dynamic image analysis, influence of patient's characteristics in the collected variables and classification using machine learning classifiers.

7.1 - Steady-state image analysis

The static analysis included the evaluation of 320 lesions, with the goal of attaining the lesions' average temperature profile, average lesion temperature and standard deviation for differentiation purposes.

Concerning malignant lesions, the concavity encountered in squamous cell carcinoma (SCC) tumours can be justified by the characteristic anatomy of this type of skin cancer. In fact, SCC tend to grow on height, due to the accumulation of a crust in the lesion site. This structure causes an insulated environment, leading to the depression verified in the resultant temperature profile. The concavity encountered for basal lesions could be explained not by anatomical features, but rather by physiological alterations that take place when this cancerous tumour is formed [191], [192]. The melanoma hyperthermic profile was expected, being reported several times in the literature. It is commonly associated with the increased vasculature on the lesion site, that results, ultimately, in an increase of tumour temperature when compared to the surrounding healthy skin [80], [193].

Looking at the benign tumours' temperature profiles, it is expected for its distinction to be difficult, due to lesion overlap and profile shape similarity. The only type of benign neoplasia more easily identifiable is the other benign lesion group, that presents an accentuated valley, suggesting that most neoplasm that compose it have a hypothermic nature.

The static curves of melanomas and nevi shows that its differentiation should be easier than the abovementioned situations, so better classification results can be anticipated. The overlap of SCC and AK in the central region indicates that the differentiation of these tumours might only be achievable when focusing on peripheral temperature values. Since actinic tumours are precursor

lesions of SCC, the valley found for this type of skin neoplasms is justified by the same anatomical alterations. Even though a scale-like structure is also encountered in this type of lesion, the thermal insulation process is weaker, due to the low thickness of the formed crust. Hence, the less accentuated depression in the thermal profile of AK.

The resemblance of benign and malignant temperature curves could difficult its distinction, while non-neoplastic lesions should be more easily separated from the remaining others. The constant temperature of this group validates the absence of any skin physiological alteration, i. e., the complete removal of the skin cancer.

The comparison of average and standard deviation of lesion temperature could provide information regarding the performance of one or another statistical measurement in the classification tasks that followed. For Malignant, Benign and Lesion type groups, both parameters presented overlaps, indicating that similar classification results should be achieved. The discrepancy verified in the average lesion temperature values for melanoma and nevi neoplasms suggest better classification results with the use of this statistical measurements. The contrary is expected for SCC vs AK.

Lastly, the higher contralateral temperatures for SCC and BCC are justified by the previously mentioned reasons, while melanomas were expected to exceed the temperature of healthy skin areas. Since most evaluated melanoma lesions were of small size, the average temperature of the 40x40 area could have included a great portion of healthy skin, resulting in an overall lower temperature value. The melanocytic nevi showed a greater temperature for healthy skin, confirming the cold pattern previously verified. The remaining lesion types did not display substantial differences between these two regions, indicating that no significant physiological and/or anatomical alterations occur in this area.

7.2 - Dynamic image analysis

The dynamic analysis was performed to assess the thermoregulatory behaviour of different skin lesion types after the application of a thermal stress. Contrarily to steady-state analysis, only 274 tumours were evaluated. The fact that not all lesions were passable of being stimulated, indicates that other cooling methods could be tested. Strategies based on convection, like a fan, instead of conduction, could be used to diminish the risk of injury caused by the contact between the aluminium medal and the skin tumour, and facilitate access to areas that the medal cannot reach, e. g., inner ear and eye corner. However, that method would also have disadvantages such as not reaching all the surface in the same manner and may cause the spread of bacteria's infecting the areas of injury.

Like in static analysis, the evaluation of the statistical measurements, average and standard deviation of lesion temperature, was also performed to estimate the best classification outcome.

Concerning the Malignant group, the presence of lower D values for melanoma tumours is somewhat unexpected. This feature could indicate that some skin lesion types recover more rapidly than others. In the particular case of melanomas, the encountered low value of D, shows

that the high vasculature of the lesion site rapidly heats the tumour area, decreasing the temperature difference between the centre and the periphery, even before the thermal acquisition of image 0. A better distinction between SCC, BCC and melanomas was verified in the average lesion temperature curves, suggesting that this parameter might be more suited for classification purposes.

Similarly to static results, the other benign curves outstanded in the benign lesion group, with standard deviation appearing to be the best option for lesion distinction. The constant curves attained for D and standard deviation of temperature in the other benign lesion category, is justified by the fact that this sample group encompasses tumours that are commonly hyperthermic, i. e., angiomas, and hypothermic, e. g., lipomas, cancelling each other profiles.

Concerning SCC vs AK any of the statistical measurements could be allied to the maximum temperature differences, while for Melanoma vs Nevi the latter parameter seems to be the most adequate.

Looking at the Lesion type group, the distinction of benign, malignant and non-neoplastic lesions appears to be more easily achieved with the dynamic parameters, instead of the static ones, since that, even though similar, a clearer separation between the different sets is encountered. The use of average lesion temperature coupled with maximum temperature difference seems to give the highest separation.

7.3 - Statistical treatment

All 320 participants were considered for statistical treatment with the goal of attesting the influence of different patient characteristics in the variables collected during static and thermal image analysis.

The statistical analysis results showed that the distinction of different skin neoplasms types would be very difficult to achieve with statistical methods, since a very small number of variables was connected to the patient's categories.

Nonetheless, the verification that most of the dynamic values were considered to be influenced by the skin neoplasm type is a good indication that these parameters could be of value for classification purposes.

The linking of lesion standard deviation to age group is also curious and could indicate that skin imperfections associated with age, contribute with noisy information during thermogram formation.

7.4 - Machine learning classifiers

For the classification of different skin neoplasm types, the classifiers Sequential Minimal Optimization (SMO), Multilayer Perceptron and instance Based for k-nearest neighbour (iBk) were

applied, using the variables collected during static (S1, S2, ..., S40; SM; SSTD) and dynamic (DX, DO, ..., D5; DMX, DM0, ..., DM5; DSTDX, DSTDO, ..., DSTD5) image analysis.

When evaluating the performance of a machine learning algorithm several aspects need to be considered. Thus, in this work, accuracy (ACC), sensitivity (SN) and specificity (SP) were chosen to select the learner that best performed in each classification task.

Focusing on the Lesion Type task, the best classification accuracy (60.0%) was acquired with the implementation of iBk ($k=7$), using the dynamic variables DX, DO, ..., D5 and DMX, DM0, ..., DM5. This result validates the conclusions retrieved from the dynamic analysis.

The SMO with quadratic polynomial kernel was considered to be the learner that best performed in the Ben vs Mal task, since it presented the best balance between accuracy (60.8%), sensitivity (87.1%) and specificity (24.0%), using the static variables S1, S2, ..., S40 and SM. With the same accuracy values, maximum sensitivity was achieved with the SMO - RBF learner in the dynamic tests, indicating that the classifier was able to identify all malignant lesion as such. However, a SP value of 0.0% was obtained, meaning, it failed to recognise any of the benign lesions, which is not acceptable in a medical diagnosis scenario. A similar situation was also verified with the Multilayer perceptron when the feature input vector included S1, S2, ..., S40 and SSTD. Even though some k-nearest neighbour-based methods exceeded the specificity of the SMO-Poly learner, lower sensitivity and accuracy values were presented, hence, the preference for Sequential Minimal Optimization.

As anticipated, the distinction among different types of benign lesions was the task that presented poorer results, due to profile overlap. A maximum accuracy of 45.4%, using maximum temperature differences and average lesion temperature as input features for the feature vector, was reached with iBk ($k=\sqrt{n}$). Nonetheless, an improvement with the use of dynamic variables occurred, when compared to the results acquired with the static parameters, validating the conclusions previously reached.

In the same line, the Malignant task was best performed when dynamic input values were used (67.8%), particularly, DX, DO, ..., D5 with DSTDX, DSTDO, ..., DSTD5. This value was achieved by the classifiers SMO-Poly, SMO-RBF and Multilayer perceptron. However, since SMO with radial basis function kernel seems to result in a high number of false positives, the other classifier options are advised.

Again, the classifiers SMO-Poly and Multilayer perceptron presented the best overall results, retrieving accuracy values of 84.2% for the differentiation of melanoma and nevi lesions, with the S1, S2, ..., S40 with SM and S1, S2, ..., S40 with SSTD, respectively. The first learner performed better in melanoma detection ($SN=91.3\%$), while the second achieved better results in the identification of benign lesions ($SP=66.7\%$). Even though with a low specificity value (11.1%), SMO-Poly was considered the top learner for this task, since the correct classification of cancerous lesions was considered of more importance.

Lastly, the SCC vs AK classification task was best accomplished with the iBk ($k=\sqrt{n}$), using DX, DO, ..., D5 with DMX, DM0, ..., DM5. A good balance was achieved for the classification metrics, with accuracy, sensitivity and specificity of 78.3%, 75.0% and 81.8%, respectively.

Chapter 8

Conclusion

The presented research work focused on the use of medical infrared imaging for characterization of skin oncological conditions. This goal was achieved with the construction of an acquisition protocol for static and dynamic images, and image analysis algorithms allied with machine learning techniques for classification purposes.

The developed methodology, concerning thermal assessment, proved to be doable in a clinical scenario, allowing the retrieval of several parameters that reflect thermophysiological alterations characteristic of different skin tumour types.

Its distinction was accomplished varying classifiers and features used for input vectors, with classification results that showed the relevance of dynamic parameters over steady ones. It is worth highlight the classification results of classification tasks that involve the differentiation of benign and malignant tumours, particularly, the distinction of melanoma from nevi lesions, with accuracy, sensitivity and specificity values reaching 84.2%, 91.3% and 11.1%, respectively, with the learner based on support vector machines. Some needed improvements include:

- reduction of false negatives to raise sensitivity;
- reduction of false positives to raise specificity.

Nonetheless, the dynamic application of medical infrared thermography proved to be a potential tool for the assessment of skin neoplasms, aiding in medical diagnosis.

8.1 - Future work

In order to surpass some limitations and progress towards better results, a few tasks are suggested:

- combination of thermal characterization data with clinical and visual characterization information, for better classification;

- the use of feature selection methods to guarantee the best representation of the data set;
- construction of a multi-classifier based on SVM, ANN and k-NN methods to improve the final classification outcomes.
- expand the correlations of these findings with the biopsies histology results.
- the use of upcoming high definition, mobile devices attachable infrared cameras, to ease the implementation of the presented methodology in a medical environment.

References

- [1] U. Leit, T. Eigentler, and C. Garbe, "Epidemiology of Skin Cancer," in *Sunlight. Vitamin D and Skin Cancer*, 2nd ed., J. Reichrath, Ed. Landes Bioscience and Springer Science+Business Media, 2014.
- [2] "Skin Cancers," *World Health Organization*, 2017. [Online]. Available: <http://www.who.int/uv/faq/skincancer/en/index1.html>. [Accessed: 01-Oct-2017].
- [3] J. Ferlay *et al.*, "Cancer incidence and mortality patterns in Europe: Estimates for 40 countries in 2012," *Eur. J. Cancer*, vol. 49, no. 6, pp. 1374-1403, Apr. 2013.
- [4] J. Hunter, J. Savin, and M. Dahl, "The function and structure of the skin," in *Clinical Dermatology*, 3rd ed., Blackwell Science, 2002, pp. 7-28.
- [5] J. Reichrath, "Apoptosis and Pathogenesis of Melanoma and Nonmelanoma Skin Cancer," in *Sunlight, Vitamin D and Skin Cancer*, J. Reichrath, Ed. Springer Science+Business Media, LLC Landes Bioscience, 2014, p. 284.
- [6] P. C. Nasca and H. Pastides, "Basic Terminology - Benign and Malignant Neoplasms," in *Fundamentals of Cancer Epidemiology*, Aspen Publishers. Inc., 2001, pp. 23-38.
- [7] L. V Crowley, "Neoplastic Disease," in *An Introduction to Human Disease: Pathology and Pathophysiology Correlations*, 9th ed., Jones and Bartlett Learning, 2013, pp. 192-209.
- [8] W. P. Tseng, "Effects and dose response relationships of skin cancer and blackfoot disease with arsenic," *Environ. Health Perspect.*, vol. Vol.19, no. August, pp. 109-119, 1977.
- [9] B. Krynitz *et al.*, "Risk of skin cancer and other malignancies in kidney, liver, heart and lung transplant recipients 1970 to 2008 - A Swedish population-based study," *Int. J. Cancer*, vol. 132, no. 6, pp. 1429-1438, 2013.
- [10] V. Madan, J. T. Lear, and R.-M. Szeimies, "Non-melanoma skin cancer," *Lancet*, vol. 375, no. 9715, pp. 673-685, 2010.
- [11] M. L. Valentine, "Cancer Screening and Prevention," in *The Well-Woman Visit*, D. Chelmsow, A. Blanchard, and L. Learman, Eds. Cambridge University Press, 2017, p. 204.
- [12] J. Reichrath and K. Rass, "UV Damage and DNA Repair in Malignant Melanoma and Nonmelanoma Skin Cancer," in *Sunlight, Vitamin D and Skin Cancer*, J. Reichrath, Ed. New York, NY: Springer New York, 2014, pp. 162-178.
- [13] R. A. Schwartz, "Introduction," in *Skin Cancer*, Blackwell Publishing, 2008, pp. 1-4.
- [14] M. Mogensen and G. B. E. Jemec, "Diagnosis of nonmelanoma skin cancer/keratinocyte carcinoma: A review of diagnostic accuracy of nonmelanoma skin cancer diagnostic tests and technologies," *Dermatologic Surg.*, vol. 33, no. 10, pp. 1158-1174, 2007.
- [15] D. Leffell, K. Lee, and H. W. Higgins, "Point of care cutaneous imaging technology in melanoma screening and mole mapping," *F1000Prime Rep.*, vol. 6, May 2014.
- [16] C. Fink and H. A. Haenssle, "Non-invasive tools for the diagnosis of cutaneous melanoma," *Ski. Res. Technol.*, pp. 1-11, 2017.
- [17] I. A. Nola and D. Kolanc, "Thermography in biomedicine," in *2015 57th International Symposium ELMAR (ELMAR)*, 2015, pp. 17-20.
- [18] C. Herman, "The role of dynamic infrared imaging in melanoma diagnosis," *Expert Rev. Dermatol.*, vol. 8, no. 2, pp. 177-184, 2013.
- [19] E. F. J. Ring and K. Ammer, "Infrared thermal imaging in medicine," *Physiol. Meas.*, vol. 33, no. 3, pp. R33-R46, Mar. 2012.
- [20] M. Pirtini Çetingül and C. Herman, "The Assessment of Melanoma Risk Using the Dynamic Infrared Imaging Technique," *J. Therm. Sci. Eng. Appl.*, 2011.
- [21] I. Kononenko, "Machine learning for medical diagnosis: history, state of the art and

- perspective,” *Artif. Intell. Med.*, vol. 23, no. 1, pp. 89-109, Aug. 2001.
- [22] M. De Falco, M. M. Pisano, and A. De Luca, “Embryology and Anatomy of the Skin,” in *Skin Cancer*, A. Baldi, P. Pasquali, and E. P. Spugnini, Eds. New York, NY: Springer New York, 2014, pp. 1-15.
- [23] A. A. Romanovsky, “Skin temperature: its role in thermoregulation,” *Acta Physiol.*, vol. 210, no. 3, pp. 498-507, Mar. 2014.
- [24] “Anatomia da pele,” 2015. [Online]. Available: <http://www.istockphoto.com/pt/foto/anatomia-da-pele-gm499693703-42756446>. [Accessed: 25-Oct-2017].
- [25] J. A. McGrath, R. A. J. Eady, and F. M. Pope, “Anatomy and Organization of Human Skin,” in *Rook’s Textbook of Dermatology*, no. May 2010, 2010, pp. 1-53.
- [26] S. Kusuma, R. K. Vuthoori, M. Piliang, and J. E. Zins, “Skin Anatomy and Physiology,” in *Plastic and Reconstructive Surgery*, London: Springer London, 2010, pp. 161-171.
- [27] “Células de gordura,” 2014. [Online]. Available: <http://www.istockphoto.com/pt/foto/células-de-gordura-gm478351717-35940588>. [Accessed: 25-Oct-2017].
- [28] A. M. J. Claessens, “Human Thermoregulation Individual differences in cold induced thermogenesis,” Maastricht, 2008.
- [29] E. Arens and H. A. Zhang, “The skin’s role in human thermoregulation and comfort,” in *Thermal and Moisture Transport in Fibrous Materials*, N. Pan and P. Gibson, Eds. Cambridge, England: Woodhead Publishing Limited, 2006, pp. 560-602.
- [30] W. I. Cranston, “Thermoregulation and the Skin,” in *Handbook of Pharmacology of the Skin I Pharmacology of Skin Systems*, I., vol. 87, M. W. Greaves and S. Shuster, Eds. Berlin, Heidelberg: Springer Berlin Heidelberg, 1989, pp. 213-221.
- [31] C. L. Lim, C. Byrne, and J. K. W. Lee, “Human thermoregulation and measurement of body temperature in exercise and clinical settings,” *Ann. Acad. Med. Singapore*, vol. 37, no. 4, pp. 347-353, 2008.
- [32] M. J. Tipton, “Thermoregulation,” United Kingdom.
- [33] P. Gillam, “2.89 Skin - A* understanding for iGCSE Biology,” 2014. [Online]. Available: <https://pmgbiology.com/tag/vasoconstriction/>.
- [34] T. Everson, “Cutaneous thermoreception,” *Part I: Thermoreception*. [Online]. Available: <http://web.pdx.edu/~zelickr/sensory-physiology/articles/2014-articles/05-21-wednesday/thermo-only.pdf>. [Accessed: 10-Dec-2017].
- [35] S. Fonseca, “Fisiopatologia da dor,” in *Termografia: Imagem Médica e Síndromes Dolorosas*, 1 st., Lisbon: Lidel, 2016, pp. 32-43.
- [36] B. Park and S. J. Kim, “Cooling the Skin: Understanding a Specific Cutaneous Thermosensation,” *J. Lifestyle Med.*, vol. 3, no. 2, pp. 91-97, 2013.
- [37] K. Parsons, “Human Thermal Environments,” in *Human Thermal Environments*, 2nd ed., London: Taylor & Francis, 2003, pp. 1-29.
- [38] L. Morbidelli, S. Donnini, and M. Ziche, “Role of Nitric Oxide in Tumor Angiogenesis,” in *Angiogenesis in Brain Tumors*, M. Kirsch and P. M. Black, Eds. Boston, MA: Springer, 2004, pp. 155-167.
- [39] M. Kaczmarek and A. Nowakowski, “Active IR-Thermal Imaging in Medicine,” *J. Nondestruct. Eval.*, vol. 35, no. 19, Mar. 2016.
- [40] D. Ribatti, T. Annese, and V. Longo, “Angiogenesis and Melanoma,” *Cancers (Basel)*, vol. 2, no. 1, pp. 114-132, 2010.
- [41] K. E. Johnson and T. A. Wilgus, “Multiple Roles for VEGF in Non-Melanoma Skin Cancer: Angiogenesis and Beyond,” *J. Skin Cancer*, vol. 2012, pp. 1-6, 2012.
- [42] R.-J. Schröder *et al.*, “Vascularization of malignant and benign skin tumours measured by d-galactose-based signal-enhanced colour doppler sonography,” *Acta radiol.*, vol. 42, no. 3, pp. 294-301, May 2001.
- [43] L. Laino *et al.*, “The efficacy of a photolyase-based device on the cancerization field: a clinical and thermographic study,” *J. Exp. Clin. Cancer Res.*, vol. 34, no. 1, p. 84, Dec. 2015.
- [44] J. Hunter, J. Savin, and M. Dahl, “Skin Tumours,” in *Clinical Dermatology*, 3rd ed., Blackwell Science, 2002, pp. 253-282.
- [45] R. A. Schwartz, “Melanoma,” in *Skin Cancer: Recognition and Management*, 2nd ed., Newark, New Jersey: Blackwell Publishing, 2008, pp. 153-199.
- [46] C. Ricotti, N. Bouzari, A. Agadi, and C. J. Cockerell, “Malignant Skin Neoplasms,” *Med. Clin. North Am.*, vol. 93, no. 6, pp. 1241-1264, 2009.

- [47] R. A. Schwartz, "Basal cell carcinoma," in *Skin Cancer: Recognition and Management*, 2nd ed., Newark, New Jersey: Blackwell Publishing, 2008, pp. 87-104.
- [48] R. A. Schwartz, "Squamous Cell Carcinoma," in *Skin Cancer: Recognition and Management*, 2nd ed., Newark, New Jersey: Blackwell Publishing, 2008, pp. 47-65.
- [49] R. A. Schwartz, "Merkel cell carcinoma," in *Skin Cancer: Recognition and Management*, 2nd ed., Newark, New Jersey: Blackwell Publishing, 2008, pp. 220-226.
- [50] D. L. S. Mark C. Lubam, Scott A. Bangs, Andrew M. Mohler, "Common Benign Skin Tumors," *Am. Fam. Physician*, vol. 67, no. 4, pp. 729-738, 2003.
- [51] R. A. Schwartz, "Dysplastic nevus and dysplastic nevus syndrome," in *Skin Cancer: Recognition and Management*, 2nd ed., Newark, New Jersey: Blackwell Publishing, 2008, pp. 141-151.
- [52] R. A. Schwartz, "Actinic keratosis," in *Skin Cancer Facts & Statistics*, 2nd ed., Newark, New Jersey: Blackwell Publishing, 2008, pp. 5-15.
- [53] L. Rose, "Recognizing Neoplastic Skin Lesions: A Photo Guide," *Am. Fam. Physician*, vol. 58, no. 4, pp. 873-884, Sep. 1998.
- [54] M. Bonmarin and F.-A. Le Gal, "Lock-in thermal imaging for the early-stage detection of cutaneous melanoma: A feasibility study," *Comput. Biol. Med.*, vol. 47, pp. 36-43, Apr. 2014.
- [55] "Skin Cancer Death Rate Per 100,000," *World Health Rankings*, 2014. [Online]. Available: <http://www.worldlifeexpectancy.com/cause-of-death/skin-cancers/by-country/>. [Accessed: 01-Oct-2017].
- [56] RORENO, "Registo Oncológico Nacional," *Instituto Português de Oncologia do Porto Francisco Gentil - EPE*, 2016. [Online]. Available: <http://www.ipoport.pt/universo-ipo-porto/>. [Accessed: 08-Dec-2017].
- [57] G. Tinghög, P. Carlsson, I. Synnerstad, and I. Rosdahl, "Societal Cost of Skin Cancer in Sweden in 2005," *Acta Derm. Venereol.*, vol. 88, no. 5, pp. 467-473, 2008.
- [58] G. P. Guy, S. R. Machlin, D. U. Ekwueme, and K. R. Yabroff, "Prevalence and Costs of Skin Cancer Treatment in the U.S., 2002-2006 and 2007-2011," *Am. J. Prev. Med.*, vol. 48, no. 2, pp. 183-187, Feb. 2015.
- [59] C. M. Doran *et al.*, "Estimating the economic costs of skin cancer in New South Wales, Australia," *BMC Public Health*, vol. 15, no. 1, p. 952, 2015.
- [60] L. G. Gordon and D. Rowell, "Health system costs of skin cancer and cost-effectiveness of skin cancer prevention and screening: a systematic review.," *Eur. J. Cancer Prev.*, vol. 24, pp. 141-149, 2015.
- [61] R. A. Schwartz, "Dermoscopy for skin cancer," in *Skin Cancer: Recognition and Management*, 2nd ed., Newark, New Jersey: Blackwell Publishing, 2008, pp. 200-219.
- [62] "Melanoma Detection," *Fraunhofer Portugal*, 2017. [Online]. Available: https://www.fraunhofer.pt/en/fraunhofer_aicos/projects/internal_research/melanoma_detection.html. [Accessed: 08-Dec-2017].
- [63] J. Hunter, J. Savin, and M. Dahl, "Diagnosis of skin disorders," in *Clinical Dermatology*, 3rd ed., Blackwell Science, 2002, pp. 29-40.
- [64] G. Argenziano, H. Soyer, S. Chimenti, R. Talamini, R. Corona, and F. Sera, "Dermoscopy of pigmented skin lesions: results of a consensus meeting via the Internet," *J. Am. Acad. Dermatol.*, vol. 48, no. 5, pp. 679-693, 2003.
- [65] H. Kittler, C. Rosendahl, A. Cameron, and P. Tschandl, "General principles," in *Dermatoscopy. An algorithmic method based on pattern analysis*, 2nd ed., Viena: Facultas Verlags und Buchhandels, AG, 2016, pp. 3-26.
- [66] S. Kockara, T. Halic, C. Hudson, A. Loney, and A. Crawford, "Portable malignant lesion detection with low cost mobile infrared thermography," in *2014 IEEE Innovations in Technology Conference*, 2014, pp. 1-5.
- [67] C. Moulin, N. Poulalhon, G. Duru, S. Debarbieux, S. Dalle, and L. Thomas, "Dermoscopy use by French private practice dermatologists: A nationwide survey," *Br. J. Dermatol.*, vol. 168, no. 1, pp. 74-79, 2013.
- [68] A. Burke-Smith, J. Collier, and I. Jones, "A comparison of non-invasive imaging modalities: Infrared thermography, spectrophotometric intracutaneous analysis and laser Doppler imaging for the assessment of adult burns," *Burns*, vol. 41, no. 8, pp. 1695-1707, Dec. 2015.
- [69] R. E. Hunger, R. Della Torre, A. Serov, and T. Hunziker, "Assessment of melanocytic skin lesions with a high-definition laser Doppler imaging system," *Ski. Res. Technol.*, vol. 18, no. 2, pp. 207-211, 2012.

- [70] M. Ulrich, E. Stockfleth, J. Roewert-Huber, and S. Astner, "Noninvasive diagnostic tools for nonmelanoma skin cancer," *Br. J. Dermatol.*, vol. 157, no. SUPPL. 2, pp. 56-58, 2007.
- [71] E. Stockfleth, T. Rosen, and S. Shumack, *Managing skin cancer*. Berlin, Heidelberg: Springer Berlin Heidelberg, 2010.
- [72] J. Hunter, J. Savin, and M. Dahl, "Physical forms of treatment," in *Clinical Dermatology*, 3rd ed., Blackwell Science, 2002, pp. 321-327.
- [73] J.-C. Martinez and C. C. Otley, "The Management of Melanoma and Nonmelanoma Skin Cancer: A Review for the Primary Care Physician," *Mayo Clin. Proc.*, vol. 76, no. 12, pp. 1253-1265, Dec. 2001.
- [74] R. A. Schwartz, "Cryosurgery," in *Skin Cancer: Recognition and Management*, 2nd ed., Newark, New Jersey: Blackwell Publishing, 2008, pp. 376-384.
- [75] R. A. Schwartz, "Topical immunotherapy," in *Skin Cancer: Recognition and Management*, 2nd ed., Newark, New Jersey: Blackwell Publishing, 2008, pp. 465-476.
- [76] J. Reichrath, "Treatment of Melanoma and Nonmelanoma Skin Cancer," in *Sunlight, Vitamin D and Skin Cancer*, J. Reichrath, Ed. New York, NY: Springer New York, 2014, pp. 298-318.
- [77] R. B. Barnes, "Thermography of the Human Body: Infrared-radiant energy provides new concepts and instrumentation for medical diagnosis," *Science (80-.)*, vol. 140, no. 3569, pp. 870-877, May 1963.
- [78] R. Berz and H. Sauer, "The Medical Use of Infrared-Thermography History and Recent Applications," in *Termografia Kolloquium 2007*, 2007, pp. 1-12.
- [79] R. Vardasca, "Bases da termografia: Fundamentos de física médica," in *Termografia: Imagem Médica e Síndromes Dolorosas*, 1 st., Lisbon: Lidel, 2016, pp. 11-16.
- [80] A. Di Carlo, "Thermography and the Possibilities for Its Applications in Clinical and Experimental Dermatology," *Clin. Dermatol.*, vol. 13, pp. 329-336, 1995.
- [81] A. Cholewka *et al.*, "Proposal of thermal imaging application in photodynamic therapy—Preliminary report," *Photodiagnosis Photodyn. Ther.*, vol. 14, pp. 34-39, Jun. 2016.
- [82] R. Vardasca, C. Ramalhão, and J. Gabriel, "Bases da termografia: Enquadramento da termografia com outras técnicas de imagem médica," in *Termografia: Imagem Médica e Síndromes Dolorosas*, 1 st., Lisbon: Lidel, 2016, pp. 3-10.
- [83] M. Pirtini Çetingül and C. Herman, "Quantification of the thermal signature of a melanoma lesion," *Int. J. Therm. Sci.*, vol. 50, no. 4, pp. 421-431, Apr. 2011.
- [84] A. Liberati *et al.*, "The PRISMA Statement for Reporting Systematic Reviews and Meta-Analyses of Studies That Evaluate Health Care Interventions: Explanation and Elaboration," *PLoS Med.*, vol. 6, no. 7, p. e1000100, Jul. 2009.
- [85] D. Moher, A. Liberati, J. Tetzlaff, D. Altman, and The PRISMA Group, "Preferred reporting items for systematic reviews and meta-analyses: The PRISMA statement," *PLoS One*, vol. 6, no. 7, pp. 1-6, 2009.
- [86] S. E. Godoy *et al.*, "Dynamic infrared imaging for skin cancer screening," *Infrared Phys. Technol.*, vol. 70, pp. 147-152, May 2015.
- [87] M. Hashemiyan, F. Valipoori Goodarzi, and J. Haddadnia, "Diagnosis of malignant melanoma based on tissue changes in spatial thermography images," *J. Dermatology Cosmet.*, vol. 6, no. 4, pp. 221-226, 2016.
- [88] M. D. Stringasci, L. T. Moriyama, A. G. Salvio, V. S. Bagnato, and C. Kurachi, "Thermographic diagnostics to discriminate skin lesions: a clinical study," in *Biophotonics South America Proc. of SPIE Proc. of SPIE*, 2015, vol. 9531.
- [89] A. Di Carlo, F. Elia, F. Desiderio, C. Catricalà, F. M. Solivetti, and L. Laino, "Can video thermography improve differential diagnosis and therapy between basal cell carcinoma and actinic keratosis?," *Dermatol. Ther.*, vol. 27, no. 5, pp. 290-297, Sep. 2014.
- [90] F. M. Solivetti *et al.*, "HF ultrasound vs PET-CT and telethermography in the diagnosis of In-transit metastases from melanoma: a prospective study and review of the literature," *J. Exp. Clin. Cancer Res.*, vol. 33, no. 1, p. 96, Dec. 2014.
- [91] C. Laurino and B. Palmieri, "Wide instrumental screening in monitoring early melanoma," *Eur. J. Oncol.*, vol. 20, no. 1, pp. 41-52, 2015.
- [92] J. Li, C. Guo, Z. Wang, K. Gao, X. Shi, and J. Liu, "Electrical stimulation towards melanoma therapy via liquid metal printed electronics on skin," *Clin. Transl. Med.*, vol. 5, no. 1, p. 21, Dec. 2016.
- [93] A. Bhowmik, R. Repaka, and S. C. Mishra, "Thermographic evaluation of early melanoma within the vascularized skin using combined non-Newtonian blood flow and bioheat models," *Comput. Biol. Med.*, vol. 53, pp. 206-219, Oct. 2014.

- [94] A. Bhowmik, R. Repaka, R. Mulaveesala, and S. C. Mishra, "Suitability of frequency modulated thermal wave imaging for skin cancer detection—A theoretical prediction," *J. Therm. Biol.*, vol. 51, pp. 65-82, Jul. 2015.
- [95] E. Agyingi, T. Wiandt, and S. Maggelakis, "A Quantitative Model of Cutaneous Melanoma Diagnosis Using Thermography," in *Mathematical and Computational Approaches in Advancing Modern Science and Engineering*, Cham: Springer International Publishing, 2016, pp. 167-175.
- [96] T. Y. Cheng and C. Herman, "Analysis of skin cooling for quantitative dynamic infrared imaging of near-surface lesions," *Int. J. Therm. Sci.*, vol. 86, pp. 175-188, 2014.
- [97] K. Grzesiak-Kopeć, M. Ogorzałek, and L. Nowak, "Computational Classification of Melanocytic Skin Lesions," in *Artificial Intelligence and Soft Computing*, vol. 9693, 2016, pp. 169-178.
- [98] "k -Nearest Neighbor Algorithm," in *Discovering Knowledge in Data*, Hoboken, NJ, USA: John Wiley & Sons, Inc., 2005, pp. 90-106.
- [99] M. M. Rahman and P. Bhattacharya, "An integrated and interactive decision support system for automated melanoma recognition of dermoscopic images," *Comput. Med. Imaging Graph.*, vol. 34, no. 6, pp. 479-486, 2010.
- [100] A. Pennisi, D. D. Bloisi, D. Nardi, A. R. Giampetruzzi, C. Mondino, and A. Facchiano, "Skin lesion image segmentation using Delaunay Triangulation for melanoma detection," *Comput. Med. Imaging Graph.*, vol. 52, pp. 89-103, 2016.
- [101] D. Ruiz, V. Berenguer, A. Soriano, and B. Sánchez, "A decision support system for the diagnosis of melanoma: A comparative approach," *Expert Syst. Appl.*, vol. 38, no. 12, pp. 15217-15223, 2011.
- [102] A. Abraham, "Artificial Neural Networks," in *Handbook of Measuring System Design*, Chichester, UK: John Wiley & Sons, Ltd, 2005.
- [103] R. Vardasca, L. Vaz, and J. Mendes, "Classification and Decision Making of Medical Infrared Thermal Images," in *Lecture Notes in Computational Vision and Biomechanics*, vol. 26, 2018, pp. 79-104.
- [104] K. Narasimhan and V. Elamaram, "Wavelet-based energy features for diagnosis of melanoma from dermoscopic images," *Int. J. Biomed. Eng. Technol.*, vol. 20, no. 3, p. 243, 2016.
- [105] C. Barata, M. Ruela, M. Francisco, T. Mendonca, and J. S. Marques, "Two Systems for the Detection of Melanomas in Dermoscopy Images Using Texture and Color Features," *IEEE Syst. J.*, vol. 8, no. 3, pp. 965-979, Sep. 2014.
- [106] A. Masood, A. Al-Jumaily, and K. Anam, "Self-supervised learning model for skin cancer diagnosis," *Int. IEEE/EMBS Conf. Neural Eng. NER*, vol. 2015-July, pp. 22-24, 2015.
- [107] G. Schaefer, B. Krawczyk, M. E. Celebi, H. Iyatomi, and A. E. Hassanien, "Melanoma Classification Based on Ensemble Classification of Dermoscopy Image Features," in *Advanced Machine Learning Technologies and Applications. AMLTA 2014. Communications in Computer and Information Science*, A. E. Hassanien, M. F. Tolba, and A. Taher Azar, Eds. Springer, Cham, 2014, pp. 291-298.
- [108] M. A. Hearst, S. T. Dumais, E. Osuna, J. Platt, and B. Scholkopf, "Support vector machines," *IEEE Intell. Syst. their Appl.*, vol. 13, no. 4, pp. 18-28, Jul. 1998.
- [109] H. Castillejos-fernández and O. López-ortega, "An Intelligent System for the Diagnosis of Skin Cancer on Digital Images taken with Dermoscopy," vol. 14, no. 3, pp. 169-185, 2017.
- [110] M. Faal, M. H. Miran Baygi, and E. Kabir, "Improving the diagnostic accuracy of dysplastic and melanoma lesions using the decision template combination method," *Ski. Res. Technol.*, vol. 19, no. 1, pp. 113-122, 2013.
- [111] M. Rastgoo, O. Morel, F. Marzani, and R. Garcia, "Ensemble approach for differentiation of malignant melanoma," *Proc. SPIE - Int. Soc. Opt. Eng.*, vol. 9534, 2015.
- [112] M. Rastgoo, R. Garcia, O. Morel, and F. Marzani, "Automatic differentiation of melanoma from dysplastic nevi," *Comput. Med. Imaging Graph.*, vol. 43, pp. 44-52, 2015.
- [113] F. Xie, H. Fan, Y. Li, Z. Jiang, R. Meng, and A. Bovik, "Melanoma classification on dermoscopy images using a neural network ensemble model," *IEEE Trans. Med. Imaging*, vol. 36, no. 3, pp. 849-858, 2017.
- [114] Q. Abbas, M. Sadaf, and A. Akram, "Prediction of Dermoscopy Patterns for Recognition of both Melanocytic and Non-Melanocytic Skin Lesions," *Computers*, vol. 5, no. 3, p. 13, Jun. 2016.
- [115] R. Amelard, J. Glaister, A. Wong, and D. A. Clausi, "High-Level Intuitive Features (HLIFs) for Intuitive Skin Lesion Description," *IEEE Trans. Biomed. Eng.*, vol. 62, no. 3, pp. 820-

- 831, Mar. 2015.
- [116] E. Almansour and M. A. Jaffar, "Classification of Dermoscopic Skin Cancer Images Using Color and Hybrid Texture Features," *IJCSNS Int. J. Comput. Sci. Netw. Secur.*, vol. 16, no. 4, pp. 135-139, 2016.
 - [117] F. Adjed, I. Faye, F. Ababsa, S. J. Gardezi, and S. C. Dass, "Classification of skin cancer images using local binary pattern and SVM classifier," in *4th International Conference on Fundamental and Applied Sciences (ICFAS 2016)*, 2016, vol. 1787.
 - [118] T. Y. Tan, L. Zhang, and M. Jiang, "An intelligent decision support system for skin cancer detection from dermoscopic images," in *2016 12th International Conference on Natural Computation, Fuzzy Systems and Knowledge Discovery (ICNC-FSKD)*, 2016, pp. 2194-2199.
 - [119] J. Jaworek-Korjakowska, "Computer-Aided Diagnosis of Micro-Malignant Melanoma Lesions Applying Support Vector Machines," *Biomed Res. Int.*, vol. 2016, pp. 1-8, 2016.
 - [120] E. La Torre, B. Caputo, and T. Tommasi, "Learning methods for melanoma recognition," *Int. J. Imaging Syst. Technol.*, vol. 20, no. 4, pp. 316-322, 2010.
 - [121] N. C. F. Codella *et al.*, "Deep learning ensembles for melanoma recognition in dermoscopy images," *IBM J. Res. Dev.*, vol. 61, no. 4/5, p. 5:1-5:15, Jul. 2017.
 - [122] M. E. Celebi *et al.*, "A methodological approach to the classification of dermoscopy images," *Comput. Med. Imaging Graph.*, vol. 31, no. 6, pp. 362-373, Sep. 2007.
 - [123] A. Masood and A. Al-Jumaily, "SA-SVM based automated diagnostic system for skin cancer," in *Proceedings of SPIE - The International Society for Optical Engineering*, 2015, vol. 9443.
 - [124] M. A. Wahba, A. S. Ashour, S. A. Napoleon, M. M. Abd Elnaby, and Y. Guo, "Combined empirical mode decomposition and texture features for skin lesion classification using quadratic support vector machine," *Heal. Inf. Sci. Syst.*, vol. 5, no. 1, p. 10, 2017.
 - [125] X. Yuan, Z. Yang, G. Zouridakis, and N. Mullani, "SVM-based Texture Classification and Application to Early Melanoma Detection," in *2006 International Conference of the IEEE Engineering in Medicine and Biology Society*, 2006, pp. 4775-4778.
 - [126] R. Suganya, "An automated computer aided diagnosis of skin lesions detection and classification for dermoscopy images," in *2016 International Conference on Recent Trends in Information Technology (ICRTIT)*, 2016, pp. 1-5.
 - [127] S. Joseph and J. R. Panicker, "Skin lesion analysis system for melanoma detection with an effective hair segmentation method," in *2016 International Conference on Information Science (ICIS)*, 2016, pp. 91-96.
 - [128] M. Messadi, A. Bessaid, and A. Taleb-Ahmed, "New characterization methodology for skin tumors classification," *J. Mech. Med. Biol.*, vol. 10, no. 3, pp. 467-477, Sep. 2010.
 - [129] R. B. Aswin, J. A. Jaleel, and S. Salim, "Hybrid genetic algorithm - Artificial neural network classifier for skin cancer detection," in *2014 International Conference on Control, Instrumentation, Communication and Computational Technologies (ICICCT)*, 2014, pp. 1304-1309.
 - [130] B. Cheng *et al.*, "Analysis of clinical and dermoscopic features for basal cell carcinoma neural network classification," *Ski. Res. Technol.*, vol. 19, no. 1, pp. 217-222, 2013.
 - [131] L. K. Ferris *et al.*, "Computer-aided classification of melanocytic lesions using dermoscopic images," *J. Am. Acad. Dermatol.*, vol. 73, no. 5, pp. 769-776, Nov. 2015.
 - [132] P. Kharazmi, H. Lui, Z. J. Wang, and T. K. Lee, "Automatic detection of basal cell carcinoma using vascular-extracted features from dermoscopy images," in *2016 IEEE Canadian Conference on Electrical and Computer Engineering (CCECE)*, 2016, pp. 1-4.
 - [133] P. Kharazmi, M. I. AlJasser, H. Lui, Z. J. Wang, and T. K. Lee, "Automated Detection and Segmentation of Vascular Structures of Skin Lesions Seen in Dermoscopy, With an Application to Basal Cell Carcinoma Classification," *IEEE J. Biomed. Heal. Informatics*, vol. 21, no. 6, pp. 1675-1684, Nov. 2017.
 - [134] H. Ganster, P. Pinz, R. Rohrer, E. Wildling, M. Binder, and H. Kittler, "Automated melanoma recognition," *IEEE Trans. Med. Imaging*, vol. 20, no. 3, pp. 233-239, Mar. 2001.
 - [135] A. Gerger *et al.*, "Sensitivity and specificity of confocal laser-scanning microscopy for in vivo diagnosis of malignant skin tumors," *Cancer*, vol. 107, no. 1, pp. 193-200, Jul. 2006.
 - [136] A. Lorber *et al.*, "Correlation of image analysis features and visual morphology in melanocytic skin tumours using in vivo confocal laser scanning microscopy," *Ski. Res. Technol.*, vol. 15, no. 2, pp. 237-241, May 2009.
 - [137] A. Gerger *et al.*, "Diagnostic image analysis of malignant melanoma in in vivo confocal laser-scanning microscopy: a preliminary study," *Ski. Res. Technol.*, vol. 14, no. 3, pp. 359-363, Aug. 2008.

- [138] S. Koller *et al.*, "In vivo reflectance confocal microscopy: automated diagnostic image analysis of melanocytic skin tumours," *J. Eur. Acad. Dermatology Venereol.*, vol. 25, no. 5, pp. 554-558, May 2011.
- [139] S. M. Odeh, F. de Toro, I. Rojas, and M. J. Saéz-Lara, "Evaluating Fluorescence Illumination Techniques for Skin Lesion Diagnosis," *Appl. Artif. Intell.*, vol. 26, no. 7, pp. 696-713, Aug. 2012.
- [140] S. M. Odeh and A. K. M. Baareh, "A comparison of classification methods as diagnostic system: A case study on skin lesions," *Comput. Methods Programs Biomed.*, vol. 137, pp. 311-319, Dec. 2016.
- [141] L. Li, Q. Zhang, Y. Ding, H. Jiang, B. H. Thiers, and J. Z. Wang, "Automatic diagnosis of melanoma using machine learning methods on a spectroscopic system," pp. 1-12, 2014.
- [142] Z. Liu, J. Sun, M. Smith, L. Smith, and R. Warr, "Incorporating clinical metadata with digital image features for automated identification of cutaneous melanoma," *Br. J. Dermatol.*, vol. 169, no. 5, pp. 1034-1040, Nov. 2013.
- [143] S. Tomatis *et al.*, "Automated melanoma detection with a novel multispectral imaging system: Results of a prospective study," *Phys. Med. Biol.*, vol. 50, no. 8, pp. 1675-1687, 2005.
- [144] S. Tomatis *et al.*, "Automated melanoma detection: Multispectral imaging and neural network approach for classification," *Med. Phys.*, vol. 30, no. 2, pp. 212-221, 2003.
- [145] P. Mohr *et al.*, "Electrical impedance spectroscopy as a potential adjunct diagnostic tool for cutaneous melanoma," *Ski. Res. Technol.*, vol. 19, no. 2, pp. 75-83, 2013.
- [146] P. Åberg, U. Birgersson, P. Elsner, P. Mohr, and S. Ollmar, "Electrical impedance spectroscopy and the diagnostic accuracy for malignant melanoma," *Exp. Dermatol.*, vol. 20, no. 8, pp. 648-652, Aug. 2011.
- [147] V. H. Maciel, W. R. Correr, C. Kurachi, V. S. Bagnato, and C. da Silva Souza, "Fluorescence spectroscopy as a tool to in vivo discrimination of distinctive skin disorders," *Photodiagnosis Photodyn. Ther.*, vol. 19, pp. 45-50, 2017.
- [148] M. H. Jafari, S. Samavi, N. Karimi, S. M. R. Soroushmehr, K. Ward, and K. Najarian, "Automatic detection of melanoma using broad extraction of features from digital images," in *2016 38th Annual International Conference of the IEEE Engineering in Medicine and Biology Society (EMBC)*, 2016, no. August, pp. 1357-1360.
- [149] J. Eslava and C. Druzgalski, "Differential Feature Space in Mean Shift Clustering for Automated Melanoma Assessment," in *IFMBE Proceedings*, vol. 51, D. A. Jaffray, Ed. Cham: Springer International Publishing, 2015, pp. 1401-1404.
- [150] M. Takruri, M. W. Rashad, and H. Attia, "Multi-classifier decision fusion for enhancing melanoma recognition accuracy," *Int. Conf. Electron. Devices, Syst. Appl.*, pp. 0-4, 2017.
- [151] R. B. Oliveira, N. Marranghello, A. S. Pereira, and J. M. R. S. Tavares, "A computational approach for detecting pigmented skin lesions in macroscopic images," *Expert Syst. Appl.*, vol. 61, pp. 53-63, Nov. 2016.
- [152] P. Spyridonos, G. Gaitanis, A. Likas, and I. D. Bassukas, "Automatic discrimination of actinic keratoses from clinical photographs," *Comput. Biol. Med.*, vol. 88, no. June, pp. 50-59, Sep. 2017.
- [153] W. Abbes, D. Sellami, A. Control, and E. E. Departement, "High-Level features for automatic skin lesions neural network based classification," *Int. Image Process. Appl. Syst. Conf.*, pp. 1-7, 2016.
- [154] N. Karami and A. Esteki, "Automated Diagnosis of Melanoma Based on Nonlinear Complexity Features," in *5th Kuala Lumpur International Conference on Biomedical Engineering 2011*, N. A. A. Osman, W. A. B. W. Abas, A. K. A. Wahab, and H. Ting, Eds. Berlin, Heidelberg: Springer, 2011, pp. 270-274.
- [155] I. Sanchez and S. Agaian, "Computer aided diagnosis of lesions extracted from large skin surfaces," in *2012 IEEE International Conference on Systems, Man, and Cybernetics (SMC)*, 2012, pp. 2879-2884.
- [156] K. Tabatabaie and A. Esteki, "Independent Component Analysis as an Effective Tool for Automated Diagnosis of Melanoma," in *2008 Cairo International Biomedical Engineering Conference*, 2008, pp. 1-4.
- [157] M. H. Jafari, S. Samavi, S. M. R. Soroushmehr, H. Mohaghegh, N. Karimi, and K. Najarian, "Set of descriptors for skin cancer diagnosis using non-dermoscopic color images," in *2016 IEEE International Conference on Image Processing (ICIP)*, 2016, pp. 2638-2642.
- [158] K. Przystaliski, "Decision Support System for Skin Cancer Diagnosis," *Oper. Res.*, pp. 406-413, 2010.

- [159] P. G. Cavalcanti and J. Scharcanski, "Automated prescreening of pigmented skin lesions using standard cameras," *Comput. Med. Imaging Graph.*, vol. 35, no. 6, pp. 481-491, Sep. 2011.
- [160] N. Noroozi and A. Zakerolhosseini, "Computer assisted diagnosis of basal cell carcinoma using Z-transform features," *J. Vis. Commun. Image Represent.*, vol. 40, pp. 128-148, Oct. 2016.
- [161] N. Noroozi and A. Zakerolhosseini, "Differential diagnosis of squamous cell carcinoma in situ using skin histopathological images," *Comput. Biol. Med.*, vol. 70, pp. 23-39, Mar. 2016.
- [162] A. Masood and A. Al-Jumaily, "Semi-advised learning model for skin cancer diagnosis based on histopathological images," in *2016 38th Annual International Conference of the IEEE Engineering in Medicine and Biology Society (EMBC)*, 2016, pp. 631-634.
- [163] B. C. Q. Truong, H. D. Tuan, V. P. Wallace, A. J. Fitzgerald, and H. T. Nguyen, "The Potential of the Double Debye Parameters to Discriminate between Basal Cell Carcinoma and Normal Skin," *IEEE Trans. Terahertz Sci. Technol.*, vol. 5, no. 6, pp. 990-998, 2015.
- [164] S. Kia, S. Setayeshi, M. Shamsaei, and M. Kia, "Computer-aided diagnosis (CAD) of the skin disease based on an intelligent classification of sonogram using neural network," *Neural Comput. Appl.*, vol. 22, no. 6, pp. 1049-1062, May 2013.
- [165] Y. Ding, N. W. John, L. Smith, J. Sun, and M. Smith, "Combination of 3D skin surface texture features and 2D ABCD features for improved melanoma diagnosis," *Med. Biol. Eng. Comput.*, vol. 53, no. 10, pp. 961-974, Oct. 2015.
- [166] U. R. Acharya, E. Y. K. Ng, J.-H. Tan, and S. V. Sree, "Thermography Based Breast Cancer Detection Using Texture Features and Support Vector Machine," *J. Med. Syst.*, vol. 36, no. 3, pp. 1503-1510, 2012.
- [167] A. Lashkari, F. Pak, and M. Firouzmand, "Full Intelligent Cancer Classification of Thermal Breast Images to Assist Physician in Clinical Diagnostic Applications.," *J. Med. Signals Sens.*, vol. 6, no. 1, pp. 12-24, 2016.
- [168] S. V. Francis, M. Sasikala, and S. D. Jaipurkar, "Detection of Breast Abnormality Using Rotational Thermography," in *Application of Infrared to Biomedical Sciences*, E. Y. K. Ng and M. Etehadtavakol, Eds. Singapore: Springer Nature, 2017, pp. 133-158.
- [169] S. G. Kandlikar *et al.*, "Infrared imaging technology for breast cancer detection - Current status, protocols and new directions," *Int. J. Heat Mass Transf.*, vol. 108, pp. 2303-2320, 2017.
- [170] J. R. González, C. Damião, and A. Conci, "An infrared thermal images database and a new technique for thyroid nodules analysis," *Stud. Health Technol. Inform.*, vol. 245, pp. 384-387, 2017.
- [171] M. B. Lopez, C. R. Del-Blanco, and N. Garcia, "Detecting exercise-induced fatigue using thermal imaging and deep learning," in *2017 Seventh International Conference on Image Processing Theory, Tools and Applications (IPTA)*, 2017, pp. 1-6.
- [172] S. Umapathy, S. Vasu, and N. Gupta, "Computer Aided Diagnosis Based Hand Thermal Image Analysis : A Potential Tool for the Evaluation of Rheumatoid Arthritis," *J. Med. Biol. Eng.*, 2017.
- [173] J. Ramesh and J. Thiruvengadam, "Application of Dynamic Thermogram for Diagnosis of Hypertension," in *International Journal of Advanced Research in Computer Science and Software Engineering*, vol. 2, no. 2, Springer Singapore, 2018, pp. 129-137.
- [174] M. Strąkowska, R. Strąkowski, M. Strzelecki, G. De Mey, and B. Więcek, "Thermal modelling and screening method for skin pathologies using active thermography," *Biocybern. Biomed. Eng.*, vol. 8, pp. 0-8, 2018.
- [175] "FLIR E60 Thermal Imaging Camera," RS. [Online]. Available: <http://uk.rs-online.com/web/p/thermal-imaging-cameras/8481404/>. [Accessed: 16-Nov-2017].
- [176] "FLIR E-Series," FLIR Systems, 2013. [Online]. Available: http://www.flir.com/uploadedFiles/Thermography_USA/Products/Product_Literature/flir-e-series-datasheet.pdf. [Accessed: 16-Nov-2017].
- [177] J. E. Hatch, "Properties of pure aluminum," in *Aluminum: Properties and Physical Metallurgy*, J. E. Hatch, Ed. ASM International, 1984, pp. 1-24.
- [178] FLIR, "ThermaCAM Researcher," 2018. [Online]. Available: <http://www.flir.co.uk/cs/display/?id=42404>.
- [179] MathWorks, "Image Processing Toolbox," 2018. [Online]. Available: <https://www.mathworks.com/products/image.html>.
- [180] F. Eibe, A. H. Mark, and J. P. Chris, "Data Mining: Practical Machine Learning Tools and

- Techniques,” *The WEKA Workbench*, 2016. .
- [181] S. Sachdeva, “Fitzpatrick skin typing: Applications in dermatology,” *Indian J. Dermatol. Venereol. Leprol.*, vol. 75, no. 1, p. 93, 2009.
 - [182] S. Shaikh, H. Gite, R. R. Manza, K. V. Kale, and N. Akhter, “Segmentation of Thermal Images Using Thresholding-Based Methods for Detection of Malignant Tumours,” in *Advances in Intelligent Systems and Computing*, Springer, 2016, pp. 131-146.
 - [183] A. Hart, “Mann-Whitney test is not just a test of medians: differences in spread can be important,” *BMJ*, vol. 323, no. 7309, pp. 391-393, Aug. 2001.
 - [184] H. Pokharna, “The Introduction to Neural Networks we all need ! (Part 2),” *Medium2*, 2016. [Online]. Available: <https://medium.com/technologymadeeasy/for-dummies-the-introduction-to-neural-networks-we-all-need-part-2-1218d5dc043>. [Accessed: 08-Jan-2018].
 - [185] H. Pokharna, “The Introduction to Neural Networks we all need ! (Part 1),” *Medium*, 2016. [Online]. Available: <https://medium.com/technologymadeeasy/for-dummies-the-introduction-to-neural-networks-we-all-need-c50f6012d5eb>. [Accessed: 08-Jan-2018].
 - [186] J. Miguel, “[SVM Matlab code implementation] SMO (Sequential Minimal Optimization) and Quadratic Programming explained,” *Lipman’s Artificial Intelligence Directory*, 2015. [Online]. Available: <http://laid.delanover.com/svm-matlab-code-implementation-smo-sequential-minimal-optimization-and-quadratic-programming-explained/>. [Accessed: 08-Jan-2018].
 - [187] J. Miguel, “[Supervised Learning] SVM - Support Vector Machine explained with examples,” *Lipman’s Artificial Intelligence Directory*, 2015. [Online]. Available: <http://laid.delanover.com/supervised-learning-svm-support-vector-machine-explained-with-examples/>. [Accessed: 08-Jan-2018].
 - [188] S. Thirumuruganathan, “A Detailed Introduction to K-Nearest Neighbor (KNN) Algorithm,” 2010. [Online]. Available: <https://saravananthirumuruganathan.wordpress.com/2010/05/17/a-detailed-introduction-to-k-nearest-neighbor-knn-algorithm/>. [Accessed: 08-Oct-2018].
 - [189] R. O. Duda, P. E. Hart, and D. G. Stork, “The Nearest-Neighbor Rule,” in *Pattern Classification*, 2nd ed., John Wendeley & Sons, Inc., 2001, pp. 177-186.
 - [190] L. A. Jeni, J. F. Cohn, and F. De La Torre, “Facing Imbalanced Data--Recommendations for the Use of Performance Metrics,” in *2013 Humaine Association Conference on Affective Computing and Intelligent Interaction*, 2013, pp. 245-251.
 - [191] T. M. Buzug, S. Schumann, L. Pfaffmann, U. Reinhold, and J. Ruhlmann, “Functional Infrared Imaging for Skin-Cancer Screening,” in *2006 International Conference of the IEEE Engineering in Medicine and Biology Society*, 2006, pp. 2766-2769.
 - [192] F. J. González, C. Castillo-Martínez, R. Valdes-Rodríguez, E. S. Kolosovas-Machuca, U. Villela-Segura, and B. Moncada, “Thermal signature of melanoma and non-melanoma skin cancers,” in *Proceedings of the 2012 International Conference on Quantitative InfraRed Thermography*, 2012.
 - [193] C. Herman and M. Pirtini Cetingul, “Quantitative Visualization and Detection of Skin Cancer Using Dynamic Thermal Imaging,” *J. Vis. Exp.*, no. 51, pp. 2-5, 2011.

Appendixes

Appendix I - Scientific publications.

Appendix II - Approved ethics Committee document.

Appendix III - Volunteer information.

Appendix IV - Informed consent.

Appendix V - Biometric data associated with the pathology.

Appendix VI - Mean absolute error and accuracy values as the number of neighbours (k) varies. (classification tests with 10-fold cross-validation for steady-state parameters).

Appendix VII - Frequency table, concerning patients' characteristics.

Appendix VIII - True Positive (TP), True Negative (TN), False Positive (FP) and False Negative (FN) values obtained for the classification tasks Melanoma vs Nevi, SCC vs AK and Ben vs Mal., according to the features selected for input vector.

Classifying Skin Neoplasms with Infrared Thermal Images

by C. Magalhaes*, R. Vardasca **, J. Mendes**

* Faculdade de Engenharia, Universidade do Porto, Rua Dr. Roberto Frias S/N 4200-465 Porto, Portugal

** LABIOMEP, INEGI-LAETA, Faculdade de Engenharia, Universidade do Porto, Rua Dr. Roberto Frias S/N 4200-465 Porto, Portugal, rvardasca@fe.up.pt

Abstract

The cases of benign and malignant skin neoplasms have been rising over the last decades. They are an esthetical and health threat and require prompt attention, the current diagnostic methods are the biopsy (expensive and invasive) and the dermatoscopy (experience dependent), so new objective methods are needed. The growth of neoplasms is influenced by blood flow, influencing, thereby, skin temperature. Infrared thermal images were taken from 85 patients at the cancer hospital, being analysed and classified with different intelligent data methods. The method that outperformed the other was the k-Nearest Neighbour with 60% accuracy.

1. Introduction

According to the 2012 statistics, in Europe there is an incidence rate for melanomas of 11.1 per 100 000 population. Comprehensive statistics on the occurrence of non-melanoma skin neoplasia are scarce but is well acknowledged that its number exceeds largely those of melanoma [1].

The increased number of skin cancer cases has been connected to excessive exposure to ultraviolet radiation, particularly during child and young adult years. Poor recurrent lifestyle choices, e.g., use of tanning beds and non-use of sunscreen, of younger individuals, indicates that these values are likely to rise [2]. Hence, special attention is required.

The available diagnostic methods for skin neoplasia are dermatoscopy, used in the evaluation of melanocytic lesions, and biopsy, mainly performed when the malignancy of a skin tumor is doubtful. Both methods present disadvantages, being the first a subjective technique, due to its' dependence on physician experience, and the second an invasive and costly procedure that is frequently associated with increased patient stress and unaesthetic scars [3]. Thus, it is important to explore new methodologies that provide a prompt diagnosis without the disadvantages encountered in common strategies.

Infrared thermal imaging (IRT) is able to monitor the temperature variations of a given skin area, through the use of infrared thermal cameras. This imaging technique can be implemented actively – dynamic thermography – with the application of a cold or hot stimulus to disturb the thermal balance, or passively – static thermography – when thermograms are acquired without any temperature stress [4]. The emitted skin heat is highly dependent on the peripheral blood flow, an anatomical characteristic that is largely affected when a physiological alteration, such as the growth of a skin neoplasm, takes place [5]. Considering that malignant tumors present metabolic activities that exceed the ones of benign lesions, different temperature disturbances should be expected for different neoplasia, namely, hyperthermic patterns for the first and hypothermic for the second. This factor associated with the various advantages of IRT, e. g., non-invasiveness, contactless, inexpensive, fast and non-ionizing [6], have made authors explore the use of IRT for skin cancer diagnosis over the last years [7].

The strategy adopted for image analysis and processing is the key to retrieved temperature values and/or parameters that allow a distinctive characterization of the skin lesion under evaluation. Artificial intelligence computational classification methods are frequently associated with this process and have been employed in medical IRT since 2002 with several applications, being the k-Nearest Neighbor (k-NN) the technique that provided better results, followed by Support Vector Machines (SVM) and Artificial Neural Networks (ANN) [8].

In this study a MATLAB application for the collection of temperature values, of a given skin area, was constructed with the goal of attaining the temperature profile of different skin neoplasm types, through thermal images acquired with steady-state thermography, for posterior classification.

2. Methodology

The collection of thermal images was performed at Instituto Português de Oncologia do Porto Francisco Gentil, EPE, cancer dedicated hospital, being the research project approved by the hospital ethical committee. A total of 85 skin oncological patients participated in this study after reading the Participant Information sheet and signing the Informed Consent. The lesions were present in several locations such as the face, upper limbs, back, thorax and lower limbs.

The data collection followed the international guidelines [9], [10] using a 10 minute acclimatization period and the room being acclimatized in a ambient temperature around 22°C with a relative humidity of <50%. The Infrared camera used to acquire the thermograms was the FLIR E60sc, with a FPA sensor size of 320x240, a Noise-Equivalent



Temperature Difference (NETD) of 50mK at 30°C and a measurement uncertainty of $\pm 2\%$ of the overall reading range. The population studied included 85 skin lesions: 35 Basal Cell Carcinomas (BCC), 26 Melanomas, 10 Melanocytic Nevus (MN), 7 Squamous Cell Carcinoma (SCC), 2 Seborrheic Keratosis (SK), 2 Actinic Keratosis (AK), 1 Atypical Nevus (AN), 1 Merkel Cell Carcinoma (MCC) and 1 Chondritis. All the neoplasia diagnoses were confirmed by a dermatologist and histopathologic results, i.e., biopsy.

The thermal images were opened in the FLIR ThermoCAM Researcher Pro 2.10 software to convert the temperature matrix format to MATLAB files. A MATLAB application was developed to read the loaded temperature matrix and display the image (Figure 1). A user input was requested to draw a square encompassing the entire lesion. The selected area was then dimensioned to a 40 by 40-pixel size (Figure 2A) and the temperature values of the 2 cross-sections of the diagonals over the normalized square were multiplied (Figure 2B) to obtain the characteristic thermal profiles (Figure 2C) of the lesion under evaluation.

These curves were primarily used for statistical calculations, where the average temperature profile was obtained, first, by groups of benign – Melanocytic Nevus, Seborrheic Keratosis, AK and Atypical Nevus – and malignant – Melanoma, BCC, SCC and Merkel Cell Carcinoma – neoplasms and second, for each type of skin tumour, separately. All 85 skin lesions were included in this analysis.

Then, the profiles were applied as inputs to the advanced data classification methods: Multilayer Perceptron, a feedforward ANN model of interconnected nodes that maps, in a non-linear way, the connections between the input and the output data [11], a more practical Support Vector Machine (SVM) algorithm that simplifies the calculations performed when the number of variables is higher [12], and Instance Based for K-Nearest neighbour (k-NN), that assigns each instance to a given group according to the similarity with the majority of its neighbour [13]. The classification methods were run into the open-source suite of machine learning software Weka (<https://www.cs.waikato.ac.nz/ml/weka>). The standard values of WEKA parameters were used. Considering the small number of samples for Seborrheic Keratosis, AK, Atypical Nevus, Merkel Cell Carcinoma and Chondritis, in this classification stage only 50 lesion profiles were selected: 26 BCC, 14 Melanomas, 6 Melanocytic Nevus and 4 SCC. The samples were randomly divided into training and test sets of 25 instances, each.

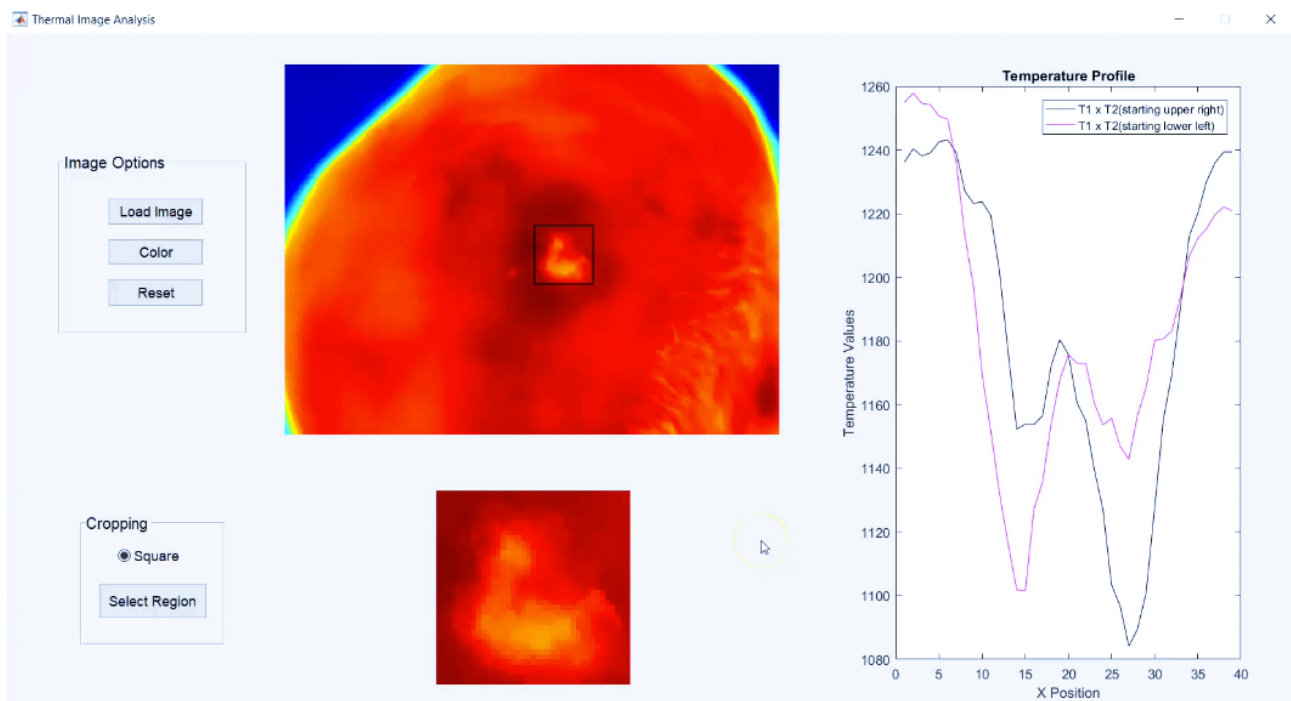


Fig. 1. The Graphic User Interface to process the thermal images of the skin neoplasms developed on Matlab.

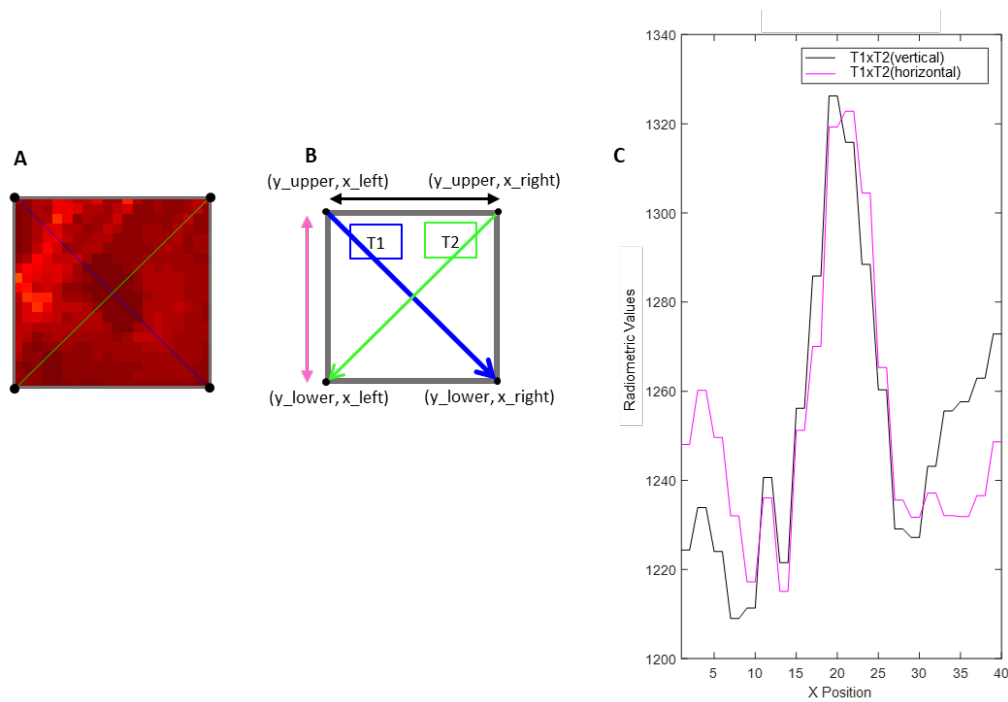


Fig. 2. Thermal cross-section profile methodology: A – User selected 40x40 area; B – Multiplication of cross-sections of the diagonals over the normalized square; C – Characteristic thermal profiles.

3. Results

In total, 85 skin lesions were examined, being 35 Basal Cell Carcinomas (BCC), 26 Melanomas, 10 Melanocytic Nevus (MN), 7 Squamous Cell Carcinoma (SCC), 2 Seborrheic Keratosis (SK), 2 Actinic Keratosis (AK), 1 Atypical Nevus (AN), 1 Merkel Cell Carcinoma (MCC) and 1 Chondritis.

A clear separation between the average radiometric values of malignant and benign neoplasms was observed (Figure 3). Furthermore, the characteristic thermal profiles, for the same malignancy, were not significantly different.

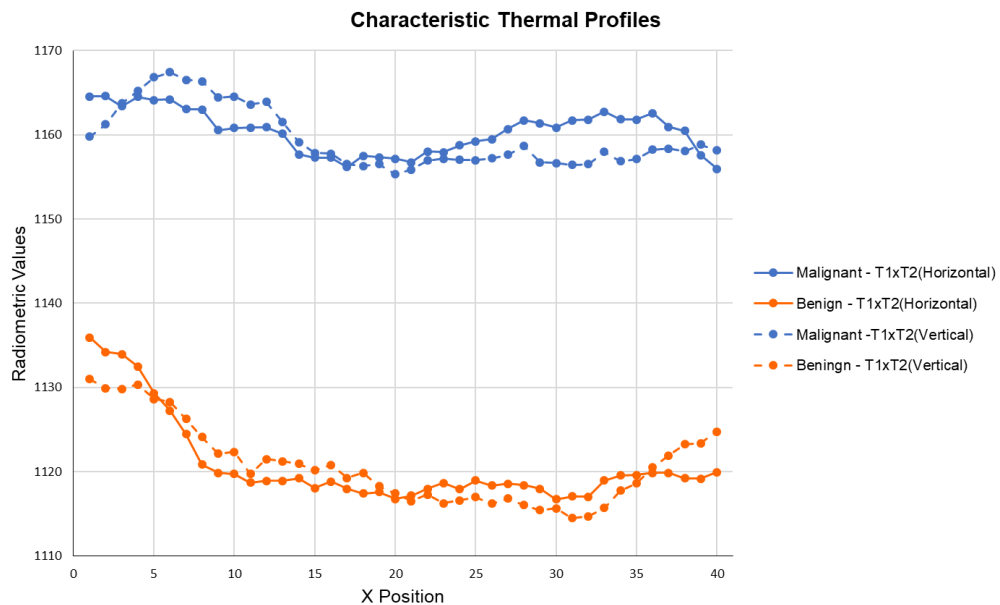


Fig. 3. Characteristic thermal profiles – T1xT2 (Horizontal) and T1xT2(Vertical) – for benign and malignant groups of neoplasia.

The temperature profiles acquired for each skin neoplasm type were also fairly similar (Figure 4 and 5). The curves corresponding to malignant lesions, e.g., BCC, Melanoma, SCC and Merkel Cell Carcinoma, presented, in general, higher values than the benign ones. Only the radiometric values of AK and Seborrheic Keratosis samples exceed the ones of malignant neoplasia. Two temperature valleys were identified, one for SCC and another for Chondritis.

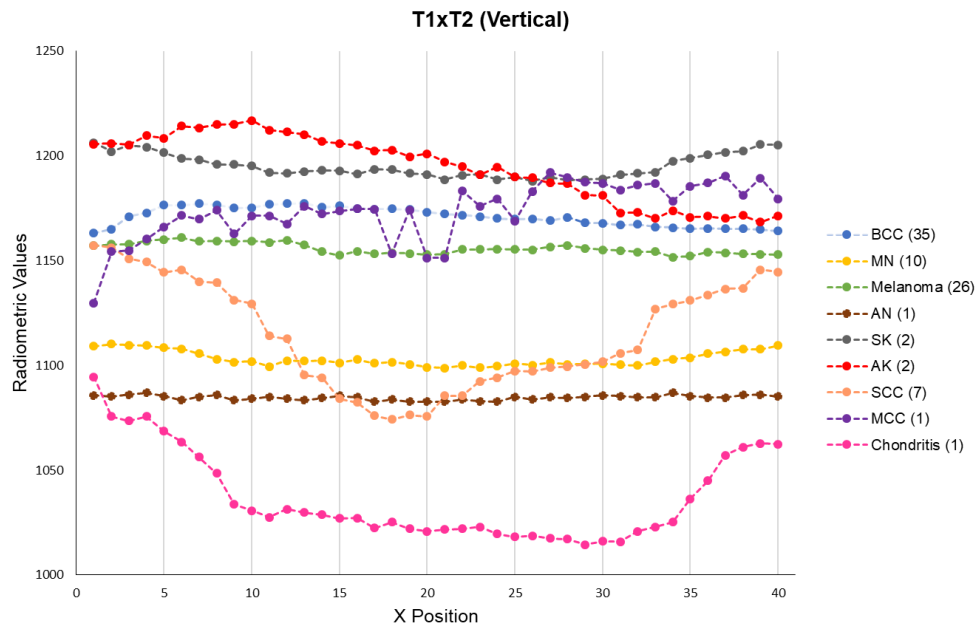


Fig. 4. Characteristic thermal profiles for each skin neoplasm type – T1xT2 (Vertical).

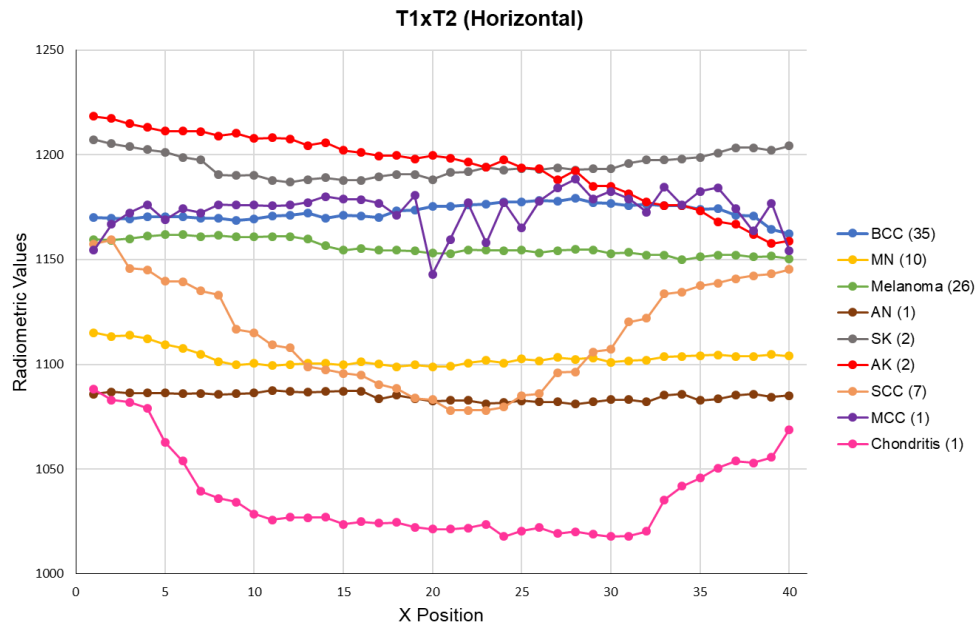


Fig. 5. Characteristic thermal profiles for each skin neoplasm type – T1xT2 (Horizontal).

The obtained classification accuracies are shown in table 1, from which it can be seen that the k-NN classifier was the classification method with best accuracy (60%), followed by ANN (52%) and the worst result was achieved by the SVN (44%).

Table 1. Results from the data classification accuracy at Weka.

Classifiers	ANN	SVM	k-NN
Accuracy	52%	44%	60%

4. Discussion

The minor differences observed between the thermal curves T1xT2 (Vertical) and T1xT2 (Horizontal) suggest that either one of the profiles could be used for the identification and classification of skin lesions in thermographic studies (Figure 2, 3 and 4). As expected the curves obtained for malignant neoplasms showed, in general, higher temperature values when compared to the benign ones (Figure 3, 4 and 5). However, SCC, a malignant lesion, displayed a hypothermic pattern, instead of a hyperthermic one (Figure 4 and 5). This profile can be justified by the characteristic anatomy of this type of skin cancer, since a thick crust is commonly encountered on top of the lesion, acting as a thermal insulator. Furthermore, the profiles obtained for actinic and seborrheic keratosis – benign neoplasms – were higher than the malignant ones (Figure 4 and 5). Concerning the first, the explanation might be in the fact that this lesion type is usually portrayed as a pre-cancerous lesion, so it is possible that some of the actinic keratosis lesions were misdiagnosed, being in a more advanced state and having, therefore, higher temperature values. A hypothermic pattern should be characteristic of seborrheic keratosis' lesions. Thus, the contradictory outcome could only be explained by the lack of samples (two) for this type of lesion.

The obtained classification results were not very satisfactory. However, the number of participants enrolled is small and it is expected a rise in the accuracy with the increase of sample size. The enhancement of temperature differences between the lesion site and healthy skin might also contribute to better classification results.

5. Conclusion

The temperature values of thermal skin neoplasm images, acquired using steady-state thermography, were analyzed with a MATLAB application and used for statistical evaluation and sample classification.

The temperature profile of each skin tumor type was successfully obtained by either one of the main lesion diagonals, being as expected, except for SCC and actinic and seborrheic keratosis. The k-NN classifier was the one that attained the best classification results, even though unsatisfactory. The improvement of this results could be achieved with the increase of the number of samples included in the data set. For a future approach, instead of a static thermogram over the lesion, a cold thermal provocation stimulus with the analysis of its recovery might be more interesting. If successfully applied and with good classification results, it could, in most cases, provide a cheaper and faster result than biopsies and in an objective manner, contrasting with the dermatoscopy method.

6. Acknowledgments

The authors gratefully acknowledge the partial funding of project NORTE-01-0145-FEDER-000022 - SciTech - Science and Technology for Competitive and Sustainable Industries, co-financed by Programa Operacional Regional do Norte (NORTE2020), through Fundo Europeu de Desenvolvimento Regional (FEDER) and of project LAETA - UID/EMS/50022/2013.

REFERENCES

- [1] J. Ferlay *et al.*, "Cancer incidence and mortality patterns in Europe: Estimates for 40 countries in 2012," *Eur. J. Cancer*, vol. 49, no. 6, pp. 1374–1403, Apr. 2013.
- [2] Linos E., S. SM., C. MG., C. GA., and C. CA., "Increasing burden of melanoma in the United States," *J. Invest. Dermatol.*, vol. 129, no. 7, pp. 1666–74, 2009.
- [3] D. A. Weinstein, S. Konda, and B. M. Coldiron, "Use of Skin Biopsies Among Dermatologists," *Dermatologic Surg.*, vol. 43, no. 11, pp. 1348–1357, Nov. 2017.
- [4] M. Pirtini Çetingül and C. Herman, "Quantification of the thermal signature of a melanoma lesion," *Int. J. Therm. Sci.*, vol. 50, no. 4, pp. 421–431, Apr. 2011.
- [5] I. A. Nola and D. Kolanc, "Thermography in biomedicine," in *2015 57th International Symposium ELMAR (ELMAR)*, 2015, pp. 17–20.
- [6] E. F. J. Ring and K. Ammer, "Infrared thermal imaging in medicine," *Physiol. Meas.*, vol. 33, no. 3, pp. R33–R46, Mar. 2012.
- [7] C. Magalhães, R. Vardasca, and J. Mendes, "Recent use of medical infrared thermography in skin neoplasms," *Ski. Res. Technol.*, vol. 0, pp. 1–5, 2018.
- [8] R. Vardasca, L. Vaz, and J. Mendes, "Classification and Decision Making of Medical Infrared Thermal Images," in

- Lecture Notes in Computational Vision and Biomechanics*, vol. 26, 2018, pp. 79–104.
- [9] K. Ammer and K. Ammer, “The Glamorgan Protocol for recording and evaluation of thermal images of the human body,” *Thermol. Int.*, vol. 18, no. 4, pp. 125–129, 2008.
- [10] E. Ring and K. Ammer, “The technique of infrared imaging in medicine,” in *Infrared Imaging*, IOP Publishing, 2015, pp. 1–10.
- [11] M. . Gardner and S. . Dorling, “Artificial neural networks (the multilayer perceptron)—a review of applications in the atmospheric sciences,” *Atmos. Environ.*, vol. 32, no. 14–15, pp. 2627–2636, 1998.
- [12] L. J. Cao *et al.*, “Parallel sequential minimal optimization for the training of support vector machines,” *IEEE Trans. Neural Networks*, vol. 17, no. 4, pp. 1039–1049, 2006.
- [13] C. Hulett, A. Hall, and G. Qu, “Dynamic Selection of k Nearest Neighbors in Instance-based Learning,” pp. 85–92, 2012.

Towards the Diabetic Foot Ulcers Classification with Infrared Thermal Images

by R. Vardasca*, L. Vaz**, C. Magalhães**, A. Seixas***, ****, J. Mendes*

* LABIOMEPE, INEGI-LAETA, Faculdade de Engenharia, Universidade do Porto, Rua Dr. Roberto Frias S/N 4200-465 Porto, Portugal, rvardasca@fe.up.pt

** Faculdade de Engenharia, Universidade do Porto, Rua Dr. Roberto Frias S/N 4200-465 Porto, Portugal

*** Escola Superior de Saúde, Universidade Fernando Pessoa, Rua Carlos da Maia, 296, 4200-150 Porto, Portugal

**** LABIOMEPE, CIFI2D, Faculdade de Desporto, Universidade do Porto, R. Dr. Plácido da Costa, 91, 4200-450 Porto, Portugal

Abstract

Diabetes Mellitus is a top 10 deadly health condition worldwide, one of its consequences is the diabetic foot ulcers (DFU) that in severe cases can lead to amputations and death. Preventive measures are required, a rise in skin temperature is one of the early signs of a DFU formation. Infrared thermal images were taken from 56 DFU patients at early stage, being processed and classified using an intelligent data method (k- Nearest Neighbour), an accuracy of 92.5% was achieved. A larger sample is required to improve the results, so it can be used at daily practice for DFU prevention.

1. Introduction

According to the International Diabetes Federation [1] a total of 485 million people is affected with Diabetes Mellitus (DM) worldwide and 1 in 2 remains undiagnosed. It is known that in their lifetime, 25% of the DM patients develop Diabetic Foot Ulcers (DFU), which may lead to minor and major amputations and consequently death [2]. It is also known that patients that developed DFU have a great probability (40%) of developing them again [3]. Measures are required to early identify the formation of DFU, so health professionals can act promptly and with success.

The DFU are associated with neuropathy and/or peripheral artery disease in the lower extremity of people with diabetes [4], this affects the skin temperature and is object of being monitored with infrared thermal imaging (IRT). IRT in medicine is a non-invasive, non-ionizing, fast, safe and remote imaging method that records the skin surface thermal energy emitted transforming it in temperature maps, providing real-time physiology data [5]. A formation of a DFU is normally associated with a rise in temperature, being this an early sign [6, 7].

The artificial intelligence computational classification methods have been employed in medical IRT since 2002 with several applications, being the k-Nearest Neighbour (k-NN) the technique that provided better results [8].

2. Methodology

A total of 56 DFU early stage patients were examined at the specialized diabetic foot centre, Centro Hospitalar do Porto, EPE. The images were collected after the participants signed the informed consent and the procedure have been explained to them, being the study approved by the hospital ethical committee. Regions of Interest (ROI) were defined in the areas where more often the DFU occur at the plantar foot (Figure 1). The data collection followed the international guidelines [9,10] using a 10 minutes' acclimatization period and the room being acclimatized in a temperature around 22°C with relative humidity of <50%. The Infrared camera used to capture the images was the FLIR A325sc, with a FPA sensor of 320x240, a Non-Equivalent Temperature Difference (NETD) of <50mK at 30°C and a measurement uncertainty of $\pm 2\%$ of the overall reading.

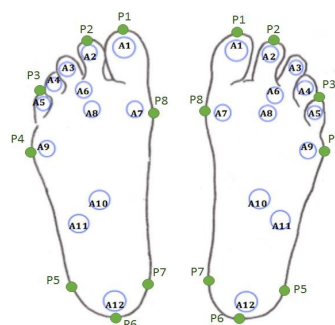


Fig. 1. The regions of interest (ROI) used to analyse the plantar feet thermal images.

A computational tool was developed in C# programming language to read the images, place the ROIs and extract the mean temperature, median temperature and standard deviation per ROI, the affected ROIs were signed, this was then stored in a PostgreSQL database in that was used by another developed tool to classify the data, for quality assurance an open-source suite of machine learning software Weka (<https://www.cs.waikato.ac.nz/ml/weka/>) was used to compare the obtained results. The Figure 2 presents the solution infrastructure.

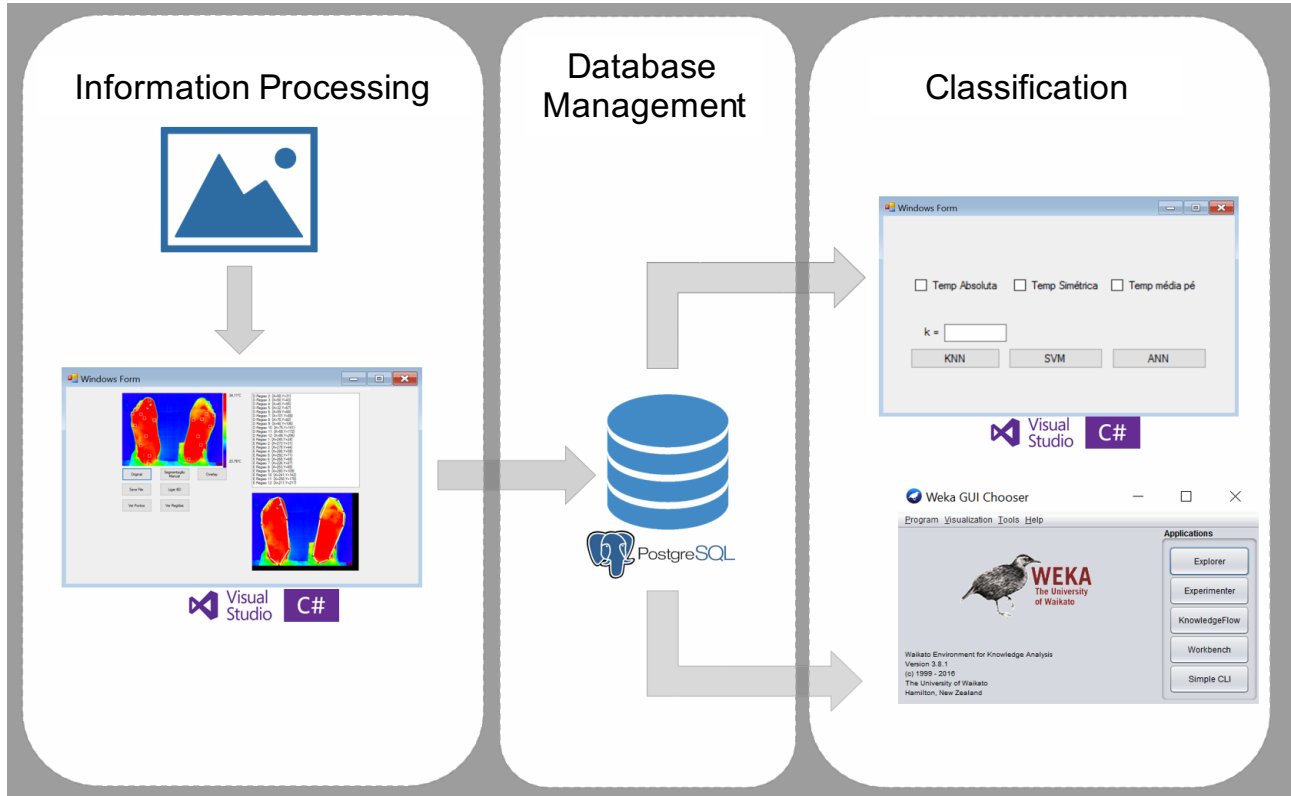


Fig. 2. The infrastructure of the images analysis and data classification.

The temperature in degrees Celsius (T) is obtained from the radiometric value (S) and the Planck constants R1, R2, B, F and O, which are obtained from the proprietary thermal image files. The temperature is calculated by equation 1.

$$T(^{\circ}C) = \frac{B}{\ln\left(\frac{R1}{R2 \cdot (S+O)} + F\right)} - 273.15 \quad (1)$$

The developed system can be divided into five main parts: the localization and extraction of metadata from binary files, image processing, identification of regions of interest (ROI), structuring and populating the database, and finally, the development of a tool to allow automatic classification. In order to assess the quality of the results obtained from the classification process, a similar operation with the same data was performed in parallel using the Weka framework. The determination of the ROIs is presented in the Figure 3, where the image is loaded, an overlay with control points based in the model (Figure 1) is displayed over the thermal image, it can be adjusted with the mouse for adequate placement and based on it, the ROIs are placed automatically and the mean, median and standard deviation is extracted from each ROI to be used as input for classification.

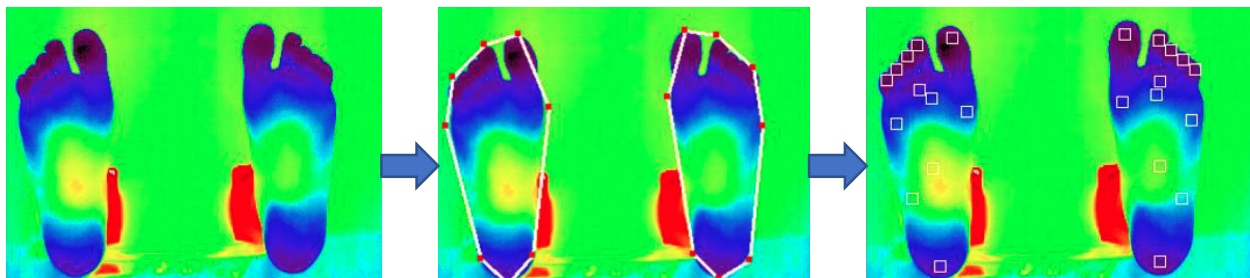


Fig. 3. The ROIs determination process.

3. Results

The thermal parameters (mean, median and standard deviation) per ROI were successfully obtained from each ROI of the processed images, to verify the correct classification it was matched with the clinical classification of the location of DFU at each image. For producing the classification results, based in the distribution of the thermal parameter it was verified that only the k-NN classifier could be used given the low disparity of the data (Figure 4), the positive prediction of ANN and SVM methods was 0% and the negative prediction was 100%. The obtained classifications accuracy from the k-NN operator using the mean and median absolute values of the ROIs is shown at table 1.

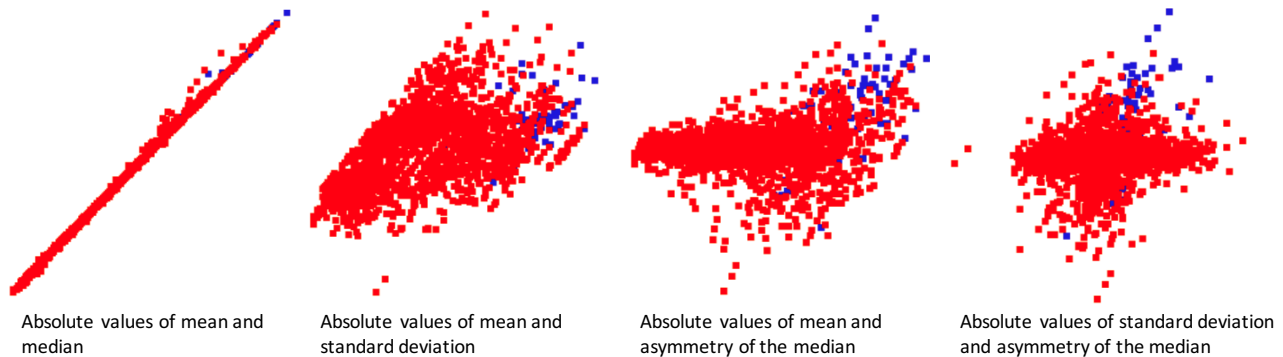


Fig. 4. The dataset distribution of the thermal parameters selected for classification.

Table 1. Results from the data classification accuracy using the k-NN method for the absolute means and medians.

k	Developed program		Weka	
	accuracy	positive prediction	accuracy	positive prediction
1	90.8%	28%	91.2%	6.5%
3	92.1%	14.3%	93.4%	9.7%
5	92.5%	20%	92.3%	6.5%
7	92.5%	20%	92.1%	9.7%

The configuration of the classifier that obtained better classification from the developed program was the 5 number of k-NN classes, with an accuracy of 92.5%. With the same dataset, from the Weka framework the best performance was provided from 3 number of k-NN classes, with an accuracy of 93.4%.

4. Discussion

The developed classification solution has presented higher accuracy for 5 or more classes, 92.5%. Classification through k-NN shows very acceptable results. The accuracy value obtained with the developed program is very close to the value obtained in the Weka program.

However, due to the fact that in the program created more ways of calculating the distances between the various elements were implemented than in the Weka, a higher positive prediction was obtained with the developed program.

Since it was not possible to create a representation of the data where a two-dimensional separation was verified, it was not possible to develop the SVM and ANN classifiers, as initially planned. A test performed in the Weka for these classifiers justified this impossibility, due to the fact that a positive precision of 0% and a negative precision of 100% was obtained.

In either case, the negative accuracy obtained is always greater than the positive precision. This is due to the fact that few images of feet with ulcers have been tested, in the elements for the classification there are more samples of ROIs without ulcer than of ROIs with ulcers.

5. Conclusion

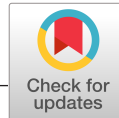
The developed application allowed to classify DFU at ROIs with high accuracy. With a larger number of samples, it is expected that this accuracy rises and it could be implemented at specialized units on daily practice for early DFU identification, which would lead to prompt care and would avoid any further costs and consequences for the patient.

6. Acknowledgments

The authors gratefully acknowledge the partial funding of project NORTE-01-0145-FEDER-000022 - SciTech - Science and Technology for Competitive and Sustainable Industries, co-financed by Programa Operacional Regional do Norte (NORTE2020), through Fundo Europeu de Desenvolvimento Regional (FEDER) and of project LAETA - UID/EMS/50022/2013.

REFERENCES

- [1] International Diabetes Federation. Diabetes Atlas, 8th edition. Retrieved December 30, 2017 and available at: <http://www.diabetesatlas.org/>
- [2] Singh N., Armstrong DG, Lipsky, B.A. Preventing foot ulcers in patients with diabetes. *Jama* 2005; 293:217-228.
- [3] Bus SA., Waaijman R., Arts M., de Haart M., Busch-Westbroek T., van Baal J., Nollet F. Effect of custom-made footwear on foot ulcer recurrence in diabetes: A multicenter randomized controlled trial. *Diabetes Care* 2013; 36:4109-4116.
- [4] Bakker K., Apelqvist J., Lipsky BA., Van Netten JJ., Schaper NC. The 2015 iwgdg guidance documents on prevention and management of foot problems in diabetes: Development of an evidence-based global consensus. Retrieved December 30, 2017 and available at: http://www.iwgdf.org/files/2015/website_development.pdf
- [5] Ring EFJ., Ammer K. Infrared thermal imaging in medicine. *Physiological measurement* 2012; 33(3): R33-R46.
- [6] Armstrong DG., Holtz-Neiderer K., Wendel C., Mohler MJ., Kimbriel HR., Lavery LA. (2007). Skin temperature monitoring reduces the risk for diabetic foot ulceration in high-risk patients. *The American journal of medicine* 2007; 120(12):1042-1046.
- [7] Ring EFJ. Thermal Imaging Today and Its Relevance to Diabetes. *Journal of Diabetes Science and Technology* 2010; 4(4):857-862.
- [8] Vardasca R., Vaz L., Mendes J. Classification and decision making with infrared medical thermal imaging, Classification in BioApps: Automation of Decision Making, Dey N., Ashour AS., Borra S. (Eds.), in *Studies in Lecture Notes in Computational Vision and Biomechanics* book series. Springer 2018; chapter 4:79-104.
- [9] Ammer K. The Glamorgan Protocol for recording and evaluation of thermal images of the human body. *Thermology international* 2008; 18(4):125-144.
- [10] Ring EFJ., Ammer K. The technique of infrared imaging in medicine. *Thermology international* 2000; 10(1):7-14.



ORIGINAL ARTICLE

WILEY

Recent use of medical infrared thermography in skin neoplasms

C. Magalhaes¹ | R. Vardasca² | J. Mendes²¹Faculdade de Engenharia, Universidade do Porto, Porto, Portugal²LABIOMEP, INEGI -LAETA, Faculdade de Engenharia, Universidade do Porto, Porto, Portugal

Correspondence

R. Vardasca, LABIOMEP, INEGI -LAETA, Faculdade de Engenharia, Universidade do Porto, Porto, Portugal.
Email: rvardasca@fe.up.pt

Funding information

NORTE2020, Grant/Award Number: NORTE-01-0145-FEDER-000022; Fundação para a Ciência e a Tecnologia, Grant/Award Number: PEst-OE/EME/LA0022/2013

Abstract

Background: Infrared thermal imaging captures the infrared radiation emitted by the skin surface. The thermograms contain valuable information, since the temperature distribution can be used to characterize physiological anomalies. Thus, the use of infrared thermal imaging (IRT) has been studied as a possible medical tool to aid in the diagnosis of skin oncological lesions. The aim of this review is to assess the current state of the applications of IRT in skin neoplasm identification and characterization.

Methods: A literature survey was conducted using the reference bibliographic databases: Scopus, PubMed and ISI Web of Science. Keywords (thermography, infrared imaging, thermal imaging and skin cancer) were combined and its presence was verified at the title and abstract of the article or as a main topic. Only articles published after 2013 were considered during this search.

Results: In total, 55 articles were encountered, resulting in 14 publications for revision after applying the exclusion criteria. It was denoted that IRT have been used to characterize and distinguish between malignant and benign neoplasms and different skin cancer types. IRT has also been successfully applied in the treatment evaluation of these types of lesions.

Conclusion: Trends and future challenges have been established to improve the application of IRT in this field, disclosing that dynamic thermography is a promising tool for early identification of oncological skin conditions.

KEYWORDS

dynamic thermal imaging, medical diagnostic information, skin cancer, steady-state thermal imaging

1 | INTRODUCTION

Over the last years, skin cancer incidence has risen to a worrying level, as a consequence of risky behaviours that people are subject to, especially excessive exposure to UV radiation. As the mortality rates associated with these tumours decrease with the early detection, a precise diagnosis is imperative to prevent unnecessary complications.^{1,2} Thermoregulation is one of the main functions of the human skin and is primarily controlled by vasculature alterations that occur when the body is subjected to external or internal stimulus, for example, heat exposure and alterations in the carbon dioxide level respectively.³ This particular characteristic has been used for

ages as a diagnosis aid, since skin temperature impairments often indicate health issues. Therefore, methods that take advantage of this feature, such as infrared thermal (IRT) imaging, have been explored for new applications in the medical field. Thermography, or IRT, is a contactless sensing method that uses a thermal camera to record the infrared radiation that is emitted by the skin, involving no health hazard for the patient, due to the absence of ionizing radiation. The temperature distribution of the surface under analysis is displayed in a thermogram, providing physiological information that can be used to detect temperature abnormalities, like the ones encountered between a skin neoplasm and the healthy tissue that surrounds it.⁴⁻⁶ In addition, this tool can be applied dynamically, that is, with a thermal

stimulus prior to the image acquisition process,⁷ with the goal of increasing the temperature differences between the lesion and the surrounding skin, or in a steady-state, without any heat stress. Thus, several researchers have studied the use of dynamic infrared in skin neoplasms, as a complementary tool in the diagnosis process, to improve the accuracy of the procedure, decreasing, simultaneously, the stress and discomfort of the patient.⁸⁻¹⁰ This systematic review aims to ascertain the current state of the applications of medical thermography in skin neoplasms, as well as understand possible challenges that can arise during this process, establishing improvements for future studies conducted in this area.

2 | MATERIAL AND METHODS

2.1 | Search strategy

The literature research was conducted, using the following combination of keywords, in the bibliographic databases: Scopus, PubMed and ISI Web of Science respectively: ((TITLE-ABS-KEY (skin cancer) AND TITLE-ABS-KEY (thermography OR (infrared imaging) OR (thermal imaging)))); ((skin cancer [Title/Abstract]) AND (thermography[Title/Abstract] OR (infrared imaging[Title/Abstract]) OR (thermal imaging[Title/Abstract])); TOPIC: (skin cancer) AND TOPIC: (thermography OR (infrared imaging) OR (thermal imaging)). The terms used for the search were clear and basic, to increase the number of results encountered, and the field selection applied in each reference source was used to guarantee the consistency of the research. The Boolean operator OR was included in the search, since "infrared imaging" and "thermal imaging" are often used as synonyms of "thermography." Only publications with dates from 1 January 2014 to the date of this research, that is, 31 March 2017 were included. A duplicate removal was performed at the end.

2.2 | Screening and eligibility results

The title and abstracts of the encountered publications were, firstly, analysed, including only the articles that referred the use of medical thermography for the evaluation of skin neoplasms.

The first eligibility criterion involved the elimination of articles that reported the use of IRT imaging in skin cancer cells, instead of the neoplasm itself. Additionally, meeting abstracts and revision articles were eliminated, making the second criterion. The third selection parameter consisted of keeping the articles written in English and excluding publications in other languages. Considering that this review is focused in a single imaging modality, that is, thermographic, some articles based on the use of infrared spectral imaging, encountered due to the terms used in the bibliographic research, were removed, making it the fourth eligibility criteria. Finally, publications focused on the description of thermal technology used for the detection of skin cancer, were eliminated from the remaining results.

The final set of articles was then separated into three main classes: clinical studies for diagnosis applications, treatment monitoring in clinical situations and theoretical studies, for a full-text review. The entire process was performed taking into account the PRISMA rules for systematic reviews described in Refs. (11,12). Figure 1 summarizing the phases of this revision process.

3 | RESULTS

The conducted bibliographic search resulted in a total of 51 publications, being 10, 9 and 32 encountered in ISI Web of Knowledge, PubMed and Scopus respectively. Four additional records were identified through Google Scholar, being included in the literature search results. After duplicate removal, 29

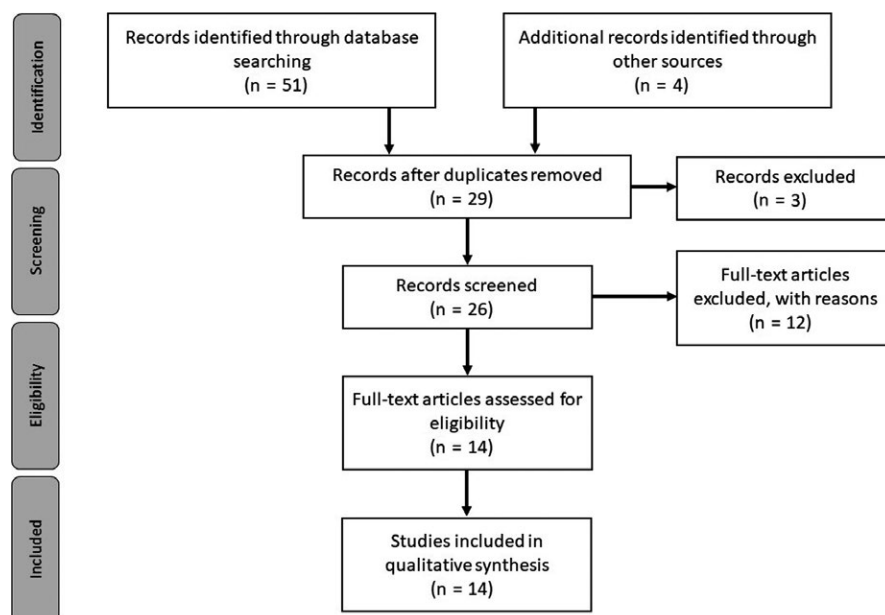


FIGURE 1 PRISMA flow diagram. Adapted from Moher et al¹²

articles were kept. The abstract and title screening resulted in the exclusion of 3 articles, since no application of medical thermography to skin neoplasms was studied in the publication. The eligibility criteria previously mentioned lead to the elimination of 12 articles, being the first, second, third and fourth criterion responsible for the exclusion of 1, 3, 3 and 5 publications respectively. Thus, 14 full-text articles remained for revision, 6 articles describe the use of IRT as a diagnosis support tool in clinical applications, 3 concern the use of thermography for skin neoplasms treatment screening in clinical studies and 5 are included in the theoretical studies category, for diagnosis purposes.

3.1 | Diagnosis support method—clinical studies

Concerning the use of IRT for the detection and identification of skin lesions, consent is verified in all the articles, indicating that thermography, applied with all its variants, has the possibility to be an effective complementary diagnostic support tool. The differences in temperature encountered between lesion areas and the surrounding tissue proved to be useful in the distinction between malignant and benign skin neoplasms.^{13,14} Godoy et al¹³ evidenced these results, using dynamic thermal imaging (DTI), with the recordings of the thermal recovery of skin tumours, after the application of a cold stress, achieving sensitivity and specificity values of 95% and 83% respectively.

The characterization of distinct types of skin lesions using IRT, has also been successfully studied, with the goal of providing more information to the practitioner during the diagnosis process, either by a steady-state¹⁵ or a dynamic¹⁶ process. A common idea is denoted by Di Carlo et al,¹⁶ with respect to the thermal patterns presented by the neoplasms, referring that, in general, malignant lesions are characterized by hyperthermic patterns, while the benign ones, present lower emissivity values. The use of video thermography allowed the complete separation (100%) between basal cell carcinomas (BCC) and actinic keratosis (AK) lesions, having the first type of skin neoplasm displayed a hypothermic halo and the latter a hyperthermic one.¹⁶ The work of Stringasci et al¹⁵ with steady-state thermography, reinforced, by and large, these findings, having BCC showed lower emissivity values and intradermal naevus lower temperatures than the basal type. The distinction between squamous cell carcinoma (SCC), which showed an hyperthermic pattern, and AK, with temperature values similar to the skin, was also successfully carried out.

Infrared thermal imaging proved to be a secure tool to aid in the detection of melanoma^{17,18} with high specificity, even though it presents varying sensitivity values, depending, partly, on the equipment used. Solivetti et al¹⁷ showed that telethermography, associated with thermo-stimulation, allows the detection of melanoma skin cancer without false positives, avoiding discomfort and stress for patients with unnecessary biopsies. Moreover, in a distinct study,¹⁸ DTI was able to detect 60.87% of early melanomas, showing the potential of this tool for precocious diagnosis.

3.2 | Treatment monitoring—clinical studies

Apart from diagnosis, medical thermography has demonstrated its usefulness on the patient follow-up, through the evaluation of skin lesions, such as AK¹⁹ and melanoma,²⁰ after treatment. Laino et al¹⁹ used active telethermography to evaluate the reduction in the hyperthermic halo of AK, after its removal and lesion site treatment with Eryfotona. Eryfotona. IRT also helped in the temperature monitoring of malignant melanoma, during electrical stimulation therapy via liquid metal printed electronics on mice skin, as seen in,²⁰ showing no alterations, in the thermal pattern of the lesion site, during this step.

Additionally, steady-state thermographic measurements have been used to verify the changes that occur, in the skin temperature gradient, of BCC, during treatment with photodynamic therapy,²¹ having Cholewka et al verified that some temperature changes in the place of injury might be caused by the treatment itself and need to be considered in the conclusions drawn.

3.3 | Theoretical studies

Infrared thermal imaging has shown its potential, in theoretical studies, for the detection of melanoma, in distinct phases of development. Bonmarin and Le Gal²² constructed a computational model that emulated different skin cancer stages, and tested the ability of steady-state and transient-state—lock-in thermal imaging (LIT)—thermography in the detection of such tumours. The phase images, retrieved from the demodulation of the transient skin surface temperature signals, seem promising for the detection of such precocious lesions. Another mathematical model, developed by Bhowmik et al²³ studied the use of dynamic infrared imaging, in 4 different melanoma stages, that is, early stage (ES I), Clark II (CL II), III (CL III) and IV (CL IV), for its detection and establishment of criteria for the early diagnosis. Even though it was shown that IRT evaluation of stage I melanoma was achievable, with an accurate analysis of the thermograms, the presented model was not fully efficient in the detection of early stage melanoma. In a more recent study, the same author²⁴ proposed the use of frequency modulated thermal wave imaging, for the detection of the abovementioned stages, in a 3D computational model. The active thermal imaging method proposed, displayed a low efficiency in the detection of ES I and CL II, being its identification only possible, when combined with the phase images acquired from the thermal signals. Steady-state thermography was also successfully used to distinguish between benign lesions and melanomas with no vasculature,²⁵ depending on the metabolic rate and tumour size selected for the theoretical model.

Cheng and Herman²⁶ used DTI, in a 2D skin surface model, to study the most suited cooling method and parameters for the detection of early stages melanoma. The optimal conditions included constant cooling at 20°C for a period of 2 minutes that can be adjusted according to the stage of the lesion under evaluation.

4 | DISCUSSION OF TRENDS AND FUTURE CHALLENGES

For clinical studies, the increase in the patient population number is one of the main trends appointed for future work, by some authors,^{13,16,17,21} in order to confirm the validity of the presented methods and attain extensive statistical analysis. The development of new image acquisition protocols is also of concern, due to the common presence of hair, that affects the thermal measurements, and the need of patient immobility, during the image acquisition process, which can be uncomfortable for the subject under test.¹³

Further research, focusing on the development of new diagnosis algorithms, for the analysis and processing of the thermal images, are needed, to improve the final results.¹⁵ It is of value to exploit, in a more detailed way, the physiology of skin neoplasms, to better understand the differences in temperature, between the lesion site and the surrounding healthy skin, during the thermal recovery.¹³ Additionally, the definition of rates of specificity and sensitivity of the thermal information, retrieved from the studies' results, are also of importance.¹⁵

Concerning theoretical approaches, the construction or refinement of 3D skin lesion computational models is necessary, in order to resemble, as much as possible, with a real biological model.²⁵ Upcoming research, related to the study of different modulation frequencies in LIT is appointed as necessary for the diagnosis of stage I and II melanoma.²² Moreover, the investigation of different tumour sizes, locations and varying blood vessel sizes could also be of interest, for future work.^{23,25}

The use of IRT dynamically appears to be a rising tendency in skin cancer studies,^{13,16-19,22-24,26} as a mean of improving thermal patterns, facilitating the detection and characterization of different skin cancer types.

5 | CONCLUSION

Infrared thermal imaging is a non-invasive, inexpensive imaging modality that is easy to perform, taking advantage of thermal cameras to detect the infrared radiation emitted by the skin, to originate thermal patterns characteristic of a specific body region. It has been used not only as an assistive tool for the diagnosis of skin cancer lesions, such as, melanoma, BCC, SCC and AK but also for skin lesion monitoring after treatment. Even though, its success has been reported in the identification of skin cancer, theoretical studies indicate that early stage melanoma identification is still not achievable. Several improvements for future work have been noted with the goal of developing this technique to its full potential, particularly its dynamic application, increasing the quality of the medical services provided to the patients, in skin cancer-related procedures.

ACKNOWLEDGEMENTS

The authors gratefully acknowledge the partial funding of Project NORTE-01-0145-FEDER-000022—SciTech—Science and

Technology for Competitive and Sustainable Industries, cofinanced by Programa Operacional Regional do Norte (NORTE2020), through Fundo Europeu de Desenvolvimento Regional (FEDER) and the FCT—Foundation for Science and Technology under the project (PEst-OE/EME/LA0022/2013).

CONFLICT OF INTEREST

There is no conflict of Interest.

ORCID

R. Vardasca  <http://orcid.org/0000-0003-4217-2882>

REFERENCES

- Apalla Z, Nashan D, Weller RB, Castellsagué X. Skin cancer: epidemiology, disease burden, pathophysiology, diagnosis, and therapeutic approaches. *Dermatol Ther (Heidelb)*. 2017;7:5-19. <https://doi.org/10.1007/s13555-016-0165-y>.
- Brunssen A, Waldmann A, Eisemann N, Katalinic A. Impact of skin cancer screening and secondary prevention campaigns on skin cancer incidence and mortality: a systematic review. *J Am Acad Dermatol*. 2017;76:129-139.e10. <https://doi.org/10.1016/j.jaad.2016.07.045>.
- Kolarsick PAJ, Kolarsick MA, Goodwin C. Anatomy and physiology of the skin. *J Dermatol Nurses Assoc*. 2011;3:203-213. <https://doi.org/10.1097/JDN.0b013e3182274a98>.
- Pirtini Çetingül M, Herman C. Quantification of the thermal signature of a melanoma lesion. *Int J Therm Sci*. 2011;50:421-431. <https://doi.org/10.1016/j.ijthermalsci.2010.10.019>.
- Ring EFJ, Ammer K. Infrared thermal imaging in medicine. *Physiol Meas*. 2012;33:R33-R46. <https://doi.org/10.1088/0967-3334/33/3/R33>.
- Wilson SB, Spence VA. A tissue heat transfer model for relating dynamic skin temperature changes to physiological parameters. *Phys Med Biol Phys Med Biol*. 1988;33:895-912.
- Kaczmarek M, Nowakowski A. Active dynamic thermography in medical diagnostics. In: Ng EY, Etehadtavakol M, eds. *Application of Infrared to Biomedical Sciences*. Series in BioEngineering. Singapore: Springer Singapore; 2017:291-310. <https://doi.org/10.1007/978-981-10-3147-2>.
- Pirtini Çetingül M, Herman C. The assessment of melanoma risk using the dynamic infrared imaging technique. *J Therm Sci Eng Appl*. 2011;. <https://doi.org/10.1115/1.4004424>.
- Santa Cruz GA, Bertotti J, Marín J, et al. Dynamic infrared imaging of cutaneous melanoma and normal skin in patients treated with BNCT. *Appl Radiat Isot*. 2009;67(7-8 SUPPL.):54-58. <https://doi.org/10.1016/j.apradiso.2009.03.093>.
- Herman C, Pirtini Çetingül M. Quantitative visualization and detection of skin cancer using dynamic thermal imaging. *J Vis Exp*. 2011;51:e2679. <https://doi.org/10.3791/2679>.
- Liberati A, Altman DG, Tetzlaff J, et al. The PRISMA statement for reporting systematic reviews and meta-analyses of studies that evaluate health care interventions: explanation and elaboration. *PLoS Med*. 2009;6:e1000100. <https://doi.org/10.1371/journal.pmed.1000100>.
- Moher D, Liberati A, Tetzlaff J, Altman D; The PRISMA Group. Preferred reporting items for systematic reviews and meta-analyses: the PRISMA statement. *PLoS ONE*. 2009;6:1-6. <https://doi.org/10.1371/journal.pmed.1000097>.

13. Godoy SE, Ramirez DA, Myers SA, et al. Dynamic infrared imaging for skin cancer screening. *Infrared Phys Technol*. 2015;70:147-152. <https://doi.org/10.1016/j.infrared.2014.09.017>.
14. Hashemiyani M, Valipoori Goodarzi F, Haddadnia J. Diagnosis of malignant melanoma based on tissue changes in spatial thermography images. *J Dermatology Cosmet*. 2016;6:221-226.
15. Stringasci MD, Moriyama LT, Salvio AG, Bagnato VS, Kurachi C. Thermographic diagnostics to discriminate skin lesions: a clinical study. In: Kurachi C, Svanberg K, Tromberg BJ, Bagnato VS, eds. *Biophotonics South America Proc. of SPIE Proc. of SPIE*, Vol 9531. 2015. <https://doi.org/10.1117/12.2180967>.
16. Di Carlo A, Elia F, Desiderio F, Catricalà C, Solivetti FM, Laino L. Can video thermography improve differential diagnosis and therapy between basal cell carcinoma and actinic keratosis? *Dermatol Ther*. 2014;27:290-297. <https://doi.org/10.1111/dth.12141>.
17. Solivetti FM, Desiderio F, Guerrisi A, et al. HF ultrasound vs PET-CT and telethermography in the diagnosis of In-transit metastases from melanoma: a prospective study and review of the literature. *J Exp Clin Cancer Res*. 2014;33:96. <https://doi.org/10.1186/s13046-014-0096-3>.
18. Laurino C, Palmieri B. Wide instrumental screening in monitoring early melanoma. *Eur J Oncol*. 2015;20:41-52.
19. Laino L, Elia F, Desiderio F, et al. The efficacy of a photolyase-based device on the cancerization field: a clinical and thermographic study. *J Exp Clin Cancer Res*. 2015;34:84. <https://doi.org/10.1186/s13046-015-0203-0>.
20. Li J, Guo C, Wang Z, Gao K, Shi X, Liu J. Electrical stimulation towards melanoma therapy via liquid metal printed electronics on skin. *Clin Transl Med*. 2016;5:21. <https://doi.org/10.1186/s40169-016-0102-9>.
21. Cholewka A, Stanek A, Kwiatek S, et al. Proposal of thermal imaging application in photodynamic therapy—preliminary report. *Photodiagnosis Photodyn Ther*. 2016;14:34-39. <https://doi.org/10.1016/j.pdpdt.2015.12.003>.
22. Bonmarin M, Le Gal F-A. Lock-in thermal imaging for the early-stage detection of cutaneous melanoma: a feasibility study. *Comput Biol Med*. 2014;47:36-43. <https://doi.org/10.1016/j.combiomed.2014.01.008>.
23. Bhowmik A, Repaka R, Mishra SC. Thermographic evaluation of early melanoma within the vascularized skin using combined non-Newtonian blood flow and bioheat models. *Comput Biol Med*. 2014;53:206-219. <https://doi.org/10.1016/j.combiomed.2014.08.002>.
24. Bhowmik A, Repaka R, Mulaveesala R, Mishra SC. Suitability of frequency modulated thermal wave imaging for skin cancer detection—a theoretical prediction. *J Therm Biol*. 2015;51:65-82. <https://doi.org/10.1016/j.jtherbio.2015.03.007>.
25. Agyingi E, Wiandt T, Maggelakis S. A quantitative model of cutaneous melanoma diagnosis using thermography. In: Bélair J, Frigaard IA, Kunze H, Makarov R, Melnik R, Spiteri RJ, eds. *Mathematical and Computational Approaches in Advancing Modern Science and Engineering*. Cham: Springer International Publishing; 2016:167-175. https://doi.org/10.1007/978-3-319-30379-6_16.
26. Cheng TY, Herman C. Analysis of skin cooling for quantitative dynamic infrared imaging of near-surface lesions. *Int J Therm Sci*. 2014;86:175-188. <https://doi.org/10.1016/j.ijthermalsci.2014.06.033>.

How to cite this article: Magalhaes C, Vardasca R, Mendes J.

Recent use of medical infrared thermography in skin neoplasms. *Skin Res Technol*. 2018;00:1-5.

<https://doi.org/10.1111/srt.12469>

BILATERAL DIFFERENCES IN ASSESSING BODY CORE TEMPERATURE WITH NON/OR MINIMAL CONTACT METHODS IN YOUNG ADULTS

R. Vardasca^{1,5}, R.A. Frade², J. Moreira², D. Marques², C. Magalhaes², A. Seixas^{3,4}, J. Mendes¹, E.F.J. Ring⁵

¹ LABIOMER, LAETA-INEGI, Faculdade de Engenharia, Universidade do Porto, Porto, Portugal

² Faculdade de Engenharia, Universidade do Porto, Porto, Portugal

³ Faculdade de Ciências da Saúde, Universidade Fernando Pessoa, Porto, Portugal

⁴ LABIOMER, LAETA-INEGI, Faculty of Sport, University of Porto, Porto, Portugal

⁵ Medical Imaging Research Unit, Faculty of Computing, University of South Wales, Pontypridd, UK

Introduction

There are several sites in which the human body core temperature can be remotely and minimally invasively assessed, which could be used to identify febrile states in a threat of pandemic situations at high populational traffic places (e.g. airports, ports, universities, schools, public buildings). In those locations, a fast method is required for temperature screening the masses. However, attention is needed for its implementation (1). Standards (2,3) have been released indicating how to act in that situation. The usual non/or minimal invasive sites used to assess core body temperature are the axilla, the tympanic membrane and the inner canthi of the eye. Thus, these sites are bilateral and can be measured in only one side, there is an absence of data in comparing bilateral measurements, however it is expected that they present some variation. The aim of this research is to compare the bilateral differences at human body sites (axilla, inner-canthi and tympanic membrane) when using the available remote and minimally invasive methods.

Methods

198 healthy volunteers (97 males and 101 females) with mean age 23 ± 9 years old, BMI of 22.5 ± 2.9 , underwent temperature screening through axillar and tympanic thermometer and frontal facial thermal imaging using internationally accepted capture protocol (4,5) and screening guidelines (2,3) in an environmental controlled examination room. For the axilla temperature assessment, a Beurer thermometer FT 09/1 (measurement accuracy of $\pm 0.1^\circ\text{C}$ and operational range from 35.5 to 42°C) was used. The tympanic membrane measurements were obtained with a Hartmann Thermoal duo scan thermometer (measurement accuracy of $\pm 0.1^\circ\text{C}$ and operational range from 35 to 42°C). The thermal images were obtained using a thermal camera FLIR E60 (Focal Plane Array sensor size of 320×240 , NETD of 50mK at 30°C and a traceability of $\pm 2\%$ of the overall reading). Mean temperature values were obtained from the different methods. Every time that a bilateral difference higher than 1°C was found in the thermometer methods, the measurement was repeated, and the smaller difference was taken out of three assessments. The IR measurements were assessed by three different operators using the FLIR ThermoCAM Researcher Pro 2.10 software package. The agreement between the 3 operators was assessed calculating the intraclass correlation coefficient (ICC) and using the Bland-Altman method, assessing agreement and limits of agreement (average ± 2 standard deviation of differences). Differences between the three measurement methods were assessed

with the Friedman's two-way analysis of variance by ranks test with factors methods vs. site. A repeated measures ANOVA was used to compare the mean differences between the right and left side in the inner canthi, axillar and tympanic measurement site separately. All statistics were calculated using the IBM SPSS v24 software package.

Results

The table 1 presents the average temperature (\pm standard deviation) values, and maximum and standard deviation of bilateral differences per measurement site. The consistency of data at the inner canthi of the eye was 0.960 and 0.959 per the left and right respectively. Among the three evaluators the ICC was 0.922 and 0.918 for the left and right inner canthi respectively. The agreement between the site measurements of the right and left sides of the body was excellent in the inner canthi ($\text{ICC} = 0.990$), good for the axillar temperature ($\text{ICC} = 0.844$) and moderate for the tympanic temperature ($\text{ICC} = 0.695$).

In terms of bilateral differences between assessment methods, the ICC was 0.99 ($p < 0.05$), 0.844 ($p < 0.01$) and 0.695 per inner canthi of the eyes thermal imaging, axilla thermometer and tympanic membrane thermometer methods correspondingly. The repeated measures ANOVA detected significant differences in the differences between the right and left sides of the body ($F = 7.920$; $p = 0.002$). The agreement between the three methods was poor. In the pairwise analysis, the agreement between the different temperature assessment methods was 0.089 for the inner canthi and axilla, -0.009 for inner canthi and tympanic membrane and 0.225 for axilla and tympanic membrane. Significant differences were found in the temperature measurements for all sites pairs ($p \geq 0.001$).

Discussion

The three studied methods were able to estimate the core body temperature in afebrile participants. The bilateral higher variations were found at the tympanic membrane assessment method and the smaller at the inner canthus thermal imaging approach. The thermal imaging method proved that at the studied areas of interest there was good data consistency and small inter operators' variability. There was statistical difference between left and right sites at the inner canthi and axilla measurements, being higher for the axilla. The bias analysis demonstrated that the smaller bias was found in the inner canthi of the eye measurement.

Table 1

Mean temperature values, and maximum, mean (\pm standard deviation) and limits of agreement of bilateral differences per measurement site.

site	Mean Temperatures		Bilateral differences		
	Right	Left	Maximum	Mean (\pm s.d.)	Limits of agreement
Inner canthi	36.0 ± 0.5	36.0 ± 0.5	0.3	$0.07 (\pm 0.09)$	0.26
Axilla	36.3 ± 0.4	36.2 ± 0.5	1.1	$0.26 (\pm 0.32)$	0.91
Tympanic membrane	36.4 ± 0.6	36.4 ± 0.6	2.0	$0.32 (\pm 0.56)$	1.36

Conclusion

All methods were able to estimate the body core temperature. However, the major bilateral agreement was found at the inner canthi of the eye thermal imaging method. Further research is needed to understand the higher bilateral variability in using the traditional thermometer axilla and tympanic membrane assessments, since these are the methods currently used within a clinical setup.

Acknowledgment

The authors gratefully acknowledge the partial funding of project NORTE-01-0145-FEDER-000022 - SciTech - Science and Technology for Competitive and Sustainable Industries, cofinanced by Programa Operacional Regional do Norte (NORTE2020), through Fundo Europeu de Desenvolvimento Regional (FEDER) and of the project LAETA - UID/EMS/50022/2013.

THE REVISED ISO STANDARD FOR SCREENING THERMOGRAPHS FOR HUMAN FEBRILE TEMPERATURE SCREENING

EFJ Ring¹, R Vardasca^{1,2}, DD Pascoe³

¹ University of South Wales, Pontypridd CF37 1DL UK

² UISPA/LAETA/INEGI, Faculty of Engineering, University of Porto, 4200-465 Portugal

³ Auburn University, Alabama 36849 USA

Introduction

Following the outbreak of the highly infectious SARS in the Far East in 2000 and further pandemic influenza outbreaks around the world, there was an international response to consider fever screening particularly among the international travelling public. This screening was based on the premise that most pandemic diseases are accompanied by an elevated core temperature. The International Standards Organisation called a group of experts together for a series of meetings to create new standard recommendations for the use of infrared imaging to detect passengers with raised body temperature. The initial methodology had been published by the Singapore Standards Authority using facial thermograms. It was recommended that under controlled conditions febrile passengers could be detected by remote sensing. After 5 years the ISO committee was reconvened to update this document.

Areas for revision: The committee was able to draw on experience from the fact that certain areas of the recommendations were not clear enough. There was further need for extending the range of potential pandemic infections where this technology could be usefully deployed. Finally, more studies had become available from which the reference list could be updated.

Definitions

These were expanded. A more precise description of the region of the inner canthus of the eyes was described. Experimental studies confirmed that with strict protocols this site was the optimal area of the face to indicate fever. The use of the colour display was clarified e.g. The SCREENING THERMOGRAPH shall be provided with at least one colour mapping mode where the colours follow the order of the visible spectrum (e.g., rainbow scale) such that blue is cooler and red is hotter. Many examples of the industrial colour scale were found which is far less sensitive to the narrow temperature band in a human face thermogram. The definition of the required correct positioning of the camera and the subject's face was also expanded. Clarifications such as the use of the calibration source were also expanded. The EXTERNAL TEMPERATURE REFERENCE SOURCE should be set at a value near the THRESHOLD TEMPERATURE. The minimum temperature range of the EXTERNAL TEMPERATURE REFERENCE SOURCE was

References

1. Mercer JB, Ring EFJ. Fever screening and infrared thermal imaging: concerns and guidelines. *Thermology International* 2009; 19(3); p. 67-69.
2. Ring EFJ, Ammer K. The technique of infrared imaging in medicine, *Thermology international* 2000; 10(1); p. 7-14.
3. Ammer K. The Glamorgan Protocol for recording and evaluation of thermal images of the human body, *Thermology international* 2008, 18(4); p. 125-144.
4. ISO TC121/SC3-IEC SC62D, Particular requirements for the basic safety and essential performance of screening thermographs for human febrile temperature screening, 2008.
5. ISO/TR 13154:2009 ISO/TR 8-600, Medical Electrical Equipment-Deployment, implementation and operational guidelines for identifying febrile humans using a screening thermograph, 2009.

Received: 29.11.2018, revision accepted 07.03.2018

chosen to be slightly broader than the minimum temperature range of the THRESHOLD TEMPERATURE. The CALIBRATION SOURCE is required to be sufficiently large so that the SCREENING THERMOGRAPH's measurement is not affected by its small size and to allow a clear identification of the display colour within the WORKABLE TARGET PLANE. The CALIBRATION SOURCE should not be larger than 10 % of the FACE, so as to not adversely affect the infrared camera assessment. The target area for measurement has also been expanded: the current evidence indicates that the region medially adjacent to the inner canthi is the preferred site for fever screening due to the stability of that measurement site. This is due to this region being directly over the internal carotid artery.

Relevant Infections: Since the more recent serious problem in Africa caused by the EBOLA outbreak, a list of potential infections that can be usefully screened by thermal imaging and those that do not manifest with an increase in temperature (fever) have been added.

Conclusion

Significant improvements and expansion of the original ISO standard for fever screening with infrared thermal imaging for fever detection have now been achieved and internationally accepted. Evidence that the original recommendations work when properly applied as described has been published. Equally there is evidence that not using the methodology correctly fails to provide the necessary discrimination for separating febrile from non febrile persons. To correctly apply this standard requires investment in both trained personnel and appropriate calibrated technology. The Ebola crisis demonstrated that this is an economic challenge for a number of countries, where local hygiene may be at levels where risk of infection and delays in bringing full medical care when urgently needed.

References

- IEC/FDIS 80601-2-59, Medical electrical equipment - Part 2-59 Particular requirements for the basic safety and essential performance of screening thermographs for human febrile temperature screening.

Received: 06.11.2017 accepted: 25.01.2018



IPOPORTO

INSTITUTO PORTUGUÊS DE ONCOLOGIA DO PORTO FG, EPE

Parecer CES IPO: 285/2017

Assunto: Avaliação do pedido realização de projeto investigação ***“Avaliação térmica dinâmica de neoplasia da pele”***

Investigadora Principal: **Ana Carolina dos Santos Ribeiro Magalhães**

Data: 12 de outubro de 2017

PARECER

É parecer desta CES, não existir impedimento de natureza ética ao desenvolvimento do referido estudo de Investigação.

Dr. Artur Lima Bastos
Presidente da CES – IPO Porto EPE

RUA DR. ANTONIO BERNARDINO DE ALMEIDA
4200-072 PORTO - PORTUGAL

T. (+351) 22 506 40 00 E-MAIL: dr ipo@ipo.porto.min-saude.pt
F. (+351) 22 506 40 01

Capital Social: 39.500.000,00 € Registo na Conservatória do Registo Comercial do Porto com o N.º 57894 - NIPC 501362293

Accredited by



INFORMAÇÃO AOS VOLUNTÁRIOS

Projeto de investigação: **Avaliação térmica dinâmica de neoplasias da pele**

Instituto Português de Oncologia do Porto Francisco Gentil, E.P.E.

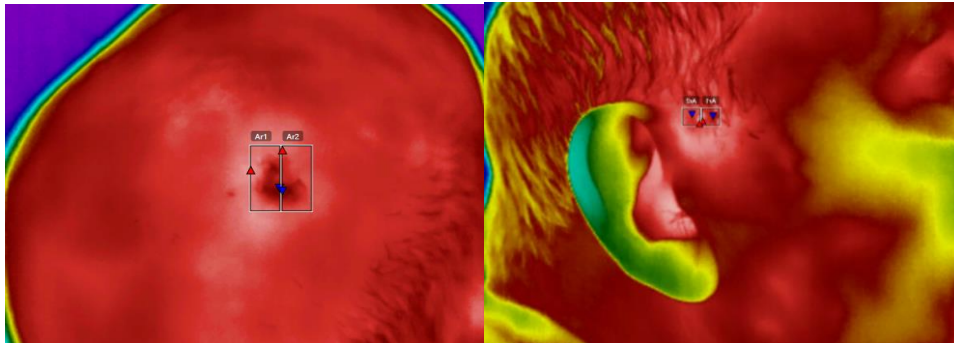
Faculdade de Engenharia da Universidade do Porto

1. O porquê deste projeto de investigação?

Este projeto pretende caracterizar, com termografia médica dinâmica, a assinatura térmica de diferentes tipos de neoplasias da pele. Para tal, serão correlacionados os resultados obtidos, através da avaliação dos termogramas recolhidos da área lesada, com os dados clínicos do paciente, nomeadamente, o resultado da biopsia. Este trabalho de investigação permitirá no futuro disponibilizar mais informação aos profissionais de saúde que poderá ser utilizada como complemento ao diagnóstico de lesões da pele, ou prevenção de recorrências destas mesmas, melhorando, assim, os cuidados prestados aos pacientes.

2. O que é um termograma?

Um termograma é uma imagem que permite visualizar a distribuição da temperatura à superfície da pele. Este pode ser observado nas figuras abaixo, representativas de termogramas infravermelhos de neoplasias da pele.



Estas imagens são obtidas utilizando câmaras termográficas que detetam e capturam perdas de calor naturais que ocorrem à superfície da pele, sendo o processo de aquisição idêntico ao método utilizado em fotografia convencional. Assim, este é um procedimento não-invasivo e não-ionizante, sendo, por isso, inócuo e indolor. Neste projeto de investigação será realizada uma avaliação térmica dinâmica, sendo, por isso, aplicado um estímulo térmico, antes do processo de captura, à zona lesada da pele. As imagens recolhidas serão usadas para fins médicos e académicos, sendo mantida a confidencialidade dos dados de cada paciente, assim como de toda a informação que irá ser gravada de modo seguro. A identificação de qualquer indivíduo é impossível através de uma imagem termográfica sem que a identificação deste mesmo esteja anexada.

3. O que é uma neoplasia da pele?

Uma neoplasia é o resultado de um processo patológico que consiste num crescimento anormal de tecido, havendo uma divisão excessiva e descontrolada de células. Estas podem ser malignas, sendo designadas por cancro, ou benignas.

O número de cancros de pele diagnosticados, e. g., melanomas, tem aumentado nos últimos anos, sendo uma das doenças mais comuns no mundo. A taxa de incidência é semelhante para homens e mulheres, sendo a exposição excessiva à radiação ultravioleta apontada como a principal causa para

esta doença. Em Portugal são detetados, anualmente, mais de 10000 novos casos de cancro da pele, existindo uma taxa de mortalidade de 2,45 em cada 100000 indivíduos, um valor que poderia ser reduzido com a deteção precoce deste tipo de lesões.

Atualmente, o diagnóstico de neoplasias da pele é efetuado por um dermatologista com base na regra ABCDE (Assimetria, Bordo, Cor, Diâmetro, Evolução), dependendo bastante da experiência do médico. Assim, uma lesão minimamente suspeita, conduz à remoção desta mesma e a posterior biópsia, com vista a obter um diagnóstico robusto. De forma a evitar procedimentos desnecessários e dolorosos para o paciente, e a permitir a identificação antecipada deste tipo de neoplasias, outros métodos para auxiliar o processo de diagnóstico de lesões da pele têm sido explorados, como Laser Doppler, Dermoscopia e Termografia infravermelha.

4. O que necessito que faça para participar neste projeto?

Venho por este meio, pedir a sua colaboração num projeto de investigação simples e rápido, onde apenas serão retiradas algumas imagens da zona da pele, onde se localiza a lesão. Este processo envolve várias etapas.

Antes da captura das imagens, o paciente deve permanecer numa sala climatizada, expondo a área de interesse – pele com lesão –, com o intuito de a mesma atingir a temperatura pretendida. Este processo demora cerca de 10 minutos. Enquanto isso, a pessoa deverá preencher e tomar conhecimento de alguns formulários. Entre estes incluem-se, o consentimento informado e o questionário de dados biométricos associado à patologia.

No dia das recolhas algumas precauções deverão ser tomadas antes do período de recolha, tais como:

- Não ingerir uma refeição pesada;
- Não participar em atividades cansativas e desgastantes;
- Não ingerir bebidas alcoólicas ou café e não fumar num período até duas horas antes da recolha das imagens;
- Remover todo o tipo de bijuteria e relógios durante o período de captura;
- Não aplicar à pele da região lesada qualquer tipo de creme corporal;
- Por fim, permanecer estático nas posições solicitadas pelo investigador para o procedimento de captura.

5. Quanto tempo vai durar?

A participação de cada indivíduo neste projeto irá demorar aproximadamente 15 minutos (incluindo o tempo de descanso). As recolhas deverão ser feitas quando for da sua conveniência.

6. Vou ser pago pela minha participação?

Infelizmente, o financiamento é limitado, pelo que não irá receber qualquer pagamento pela sua participação neste estudo. Contudo, irá contribuir significativamente para desenvolvimentos únicos e importantes na área da utilização da termografia médica dinâmica na dermatologia. Após a participação rebaçados serão oferecidos como sinal de gratidão. As imagens recolhidas poderão também ser enviadas via email caso sejam solicitadas pelo voluntário.

7. Contacto

Nome: Ana Carolina dos Santos Ribeiro Magalhães

Instituição: Faculdade de Engenharia da Universidade do Porto

Email: anacmag1@gmail.com

Telemóvel: 918775039

Consentimento Informado

Considerando a "Declaração de Helsínquia", da Associação Médica Mundial

(Helsínquia 1964; Tóquio 1975, Hong Kong 1989; Somerset West 1996; Edimburgo 2000; Washington 2002, Tóquio 2004 e Seoul, 2008)

Designação do projeto de investigação

Avaliação térmica dinâmica de neoplasias da pele

Eu, abaixo-assinado (nome completo do doente adulto ou do voluntário são) _____

Recebi o texto de *Informação ao Participante* relativo ao procedimento que concordei efetuar. Compreendi a explicação que me foi fornecida pelo investigador que assina este documento. Foi-me ainda dada oportunidade de fazer as perguntas que julguei necessárias, e de todas obtive resposta satisfatória.

Tomei conhecimento de que, de acordo com as recomendações da Declaração de Helsínquia, a informação ou explicação que me foi prestada versou os objetivos, os métodos, os benefícios previstos, os riscos potenciais e o eventual desconforto. Além disso, foi-me afirmado que tenho o direito de anular a todo o tempo a minha participação no estudo, sem que isso possa ter como efeito qualquer prejuízo na assistência que me é prestada.

Por isso, consinto que me seja aplicado o método, o tratamento ou o inquérito proposto pelo investigador.

Assinatura do doente ou voluntário são: _____ Data: 28/11/2017

Nome do Investigador responsável: Gabriela Regalado _____ Data: 28/11/2017

Assinatura do Investigador responsável: _____ Data: 28/11/2017

Anulação do Consentimento Informado

Declaro que recebi a *Informação ao Participante* relativo ao projeto de investigação em questão, que me foi proposto pelo investigador que assina este documento e **pretendo anular** o consentimento dado na data ____/____/201__.

Assinatura do doente ou voluntário são: _____ Data: ____/____/201__

Assinatura do Investigador responsável: _____ Data: ____/____/201__

Nota: Fornecimento obrigatório de cópia ao participante.

Biometric data associated with the pathology

T = 22,0 °C
H = 37,9 %

U. PORTO
FEUP FACULDADE DE ENGENHARIA
UNIVERSIDADE DO PORTO

IPO PORTO

Avaliação térmica dinâmica de neoplasias da pele – Questionário de participação

Participante nº 123
IPO: 17643622

Tipo de Neoplasia: Espinocelular

Idade: 81

Sexo: ☒ Feminino

Altura: 1,55

☐ Masculino

Peso: 54

Cor de olhos: ☐ Azul

☒ Verde

☐ Castanho

☐ Outra

Escala Fitzpatrick: ☐ Tipo I

☒ Tipo II

☐ Tipo III

☐ Tipo IV

☐ Tipo V

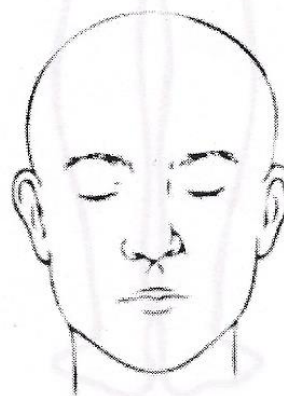
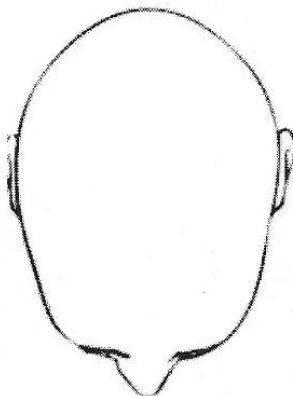
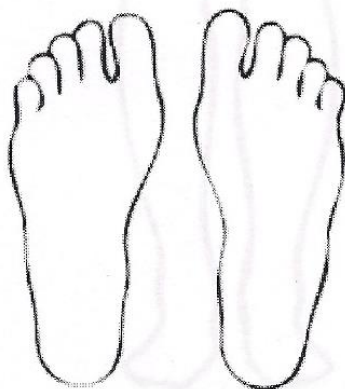
☐ Tipo VI

Sinais: ☐ Sim

☒ Não

Direita

Esquerda



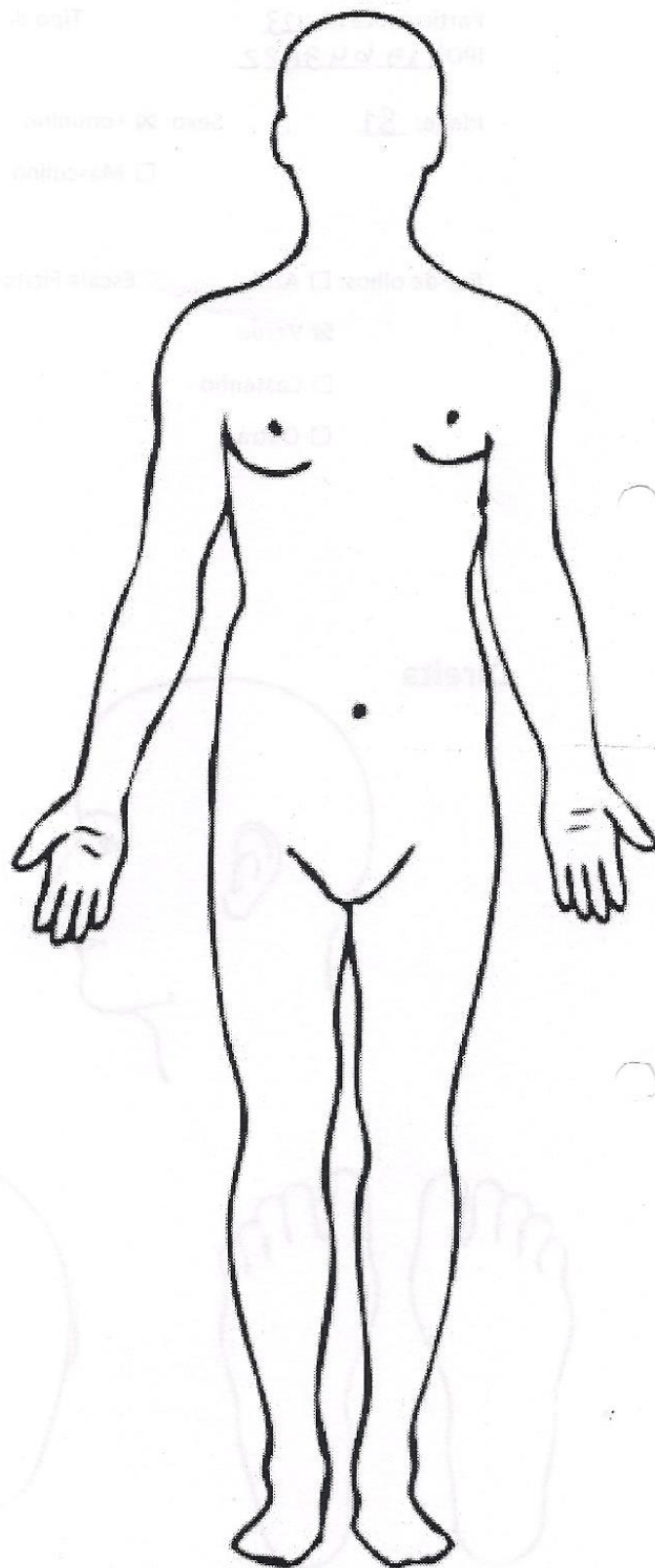
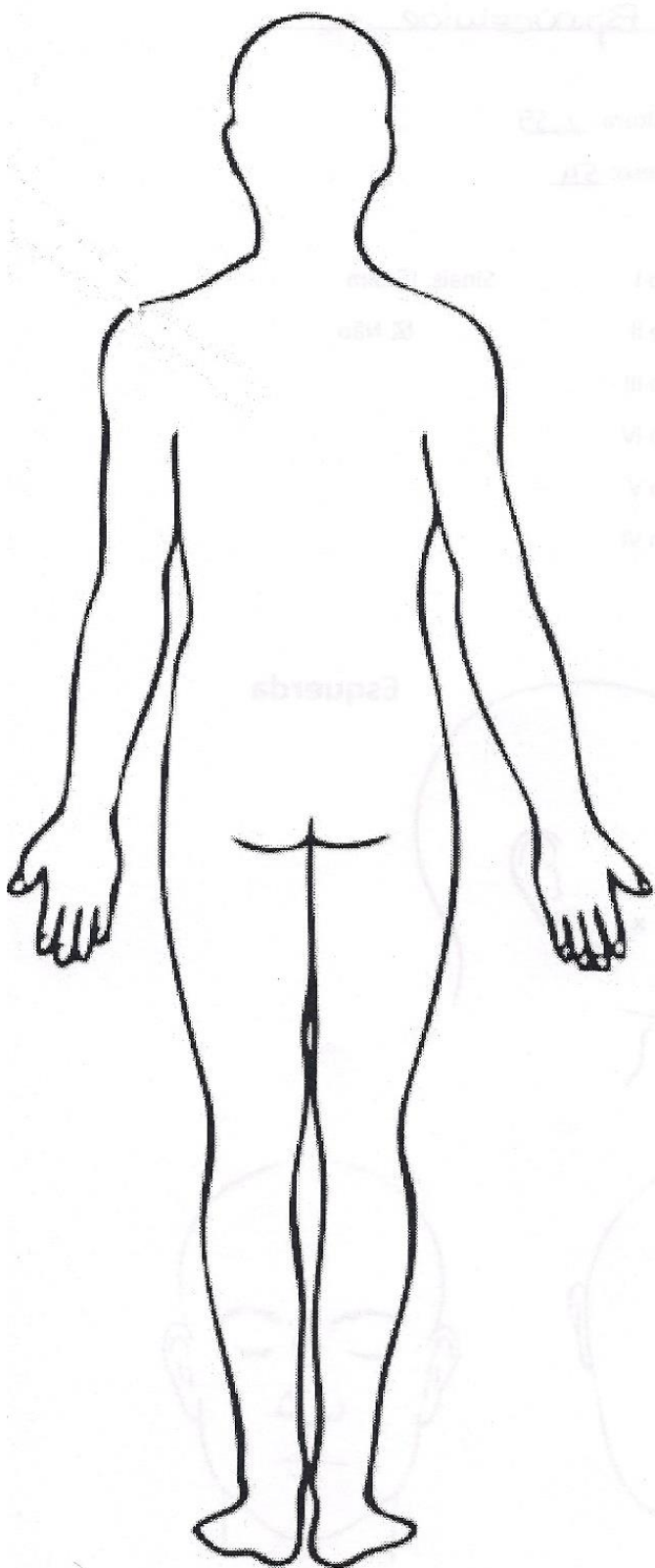
☐ Superior

☐ Inferior

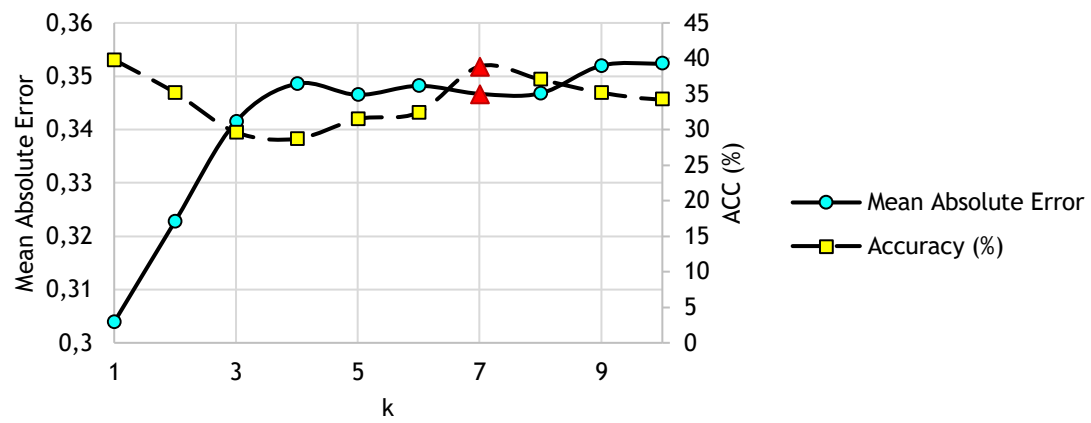
Inicial: 11915

Contralateral: 11920

Recuperação: 11921; 11922-11926



Mean absolute error and accuracy values as the number of neighbours (k) varies.
(classification tests with 10-fold cross-validation for steady-state parameters).



Frequency table, concerning patients' characteristics.

	Label	Frequency (n)	Frequency (%)
Skin Neoplasm Type	0	51	15.9
	1	118	36.9
	2	16	5.0
	3	29	9.1
	4	30	9.4
	5	14	4.4
	6	11	3.4
	7	29	9.1
	8	22	6.9

	Label	Frequency (n)	Frequency (%)
Age group	0	2	0.6
	1	9	2.8
	2	22	6.9
	3	42	13.1
	4	57	17.8
	5	84	26.3
	6	104	32.5

	Label	Frequency (n)	Frequency (%)
Sex	0	192	60.0
	1	128	40.0

	Label	Frequency (n)	Frequency (%)
Height	0	20	6.2
	1	128	39.6
	2	119	36.8
	3	44	13.6
	4	9	2.8

	Label	Frequency (n)	Frequency (%)
Weight	0	51	15.9
	1	118	36.9
	2	16	5.0
	3	29	9.1
	4	30	9.4
	5	14	4.4

	Label	Frequency (n)	Frequency (%)
BMI	0	5	1.6
	1	125	39.1
	2	131	40.9
	3	56	17.5
	4	2	0.6
	5	1	0.3

	Label	Frequency (n)	Frequency (%)
Eye colour	0	71	22.2
	1	91	28.4
	2	158	49.4

	Label	Frequency (n)	Frequency (%)
Fitzpatrick scale	0	0	0.0
	1	15	4.7
	2	123	38.4
	3	156	48.8
	4	26	8.1

	Label	Frequency (n)	Frequency (%)
Skin mar	0	193	60.3
	1	127	39.7

True Positive (TP), True Negative (TN), False Positive (FP) and False Negative (FN) values obtained for the classification tasks Melanoma vs Nevi, SCC vs AK and Ben vs Mal., according to the features selected for input vector

Steady-state: S1, S2, ..., S40 and SM feature vector

	Classifier	TP	FP	TN	FN
Melanoma vs Nevi	SMO - Poly	6	0	10	3
	SMO - RBF	0	0	10	9
	iBk (k=1)	3	2	8	6
	iBk (k=6)	0	0	10	9
	iBk (k=7)	0	0	10	9
	Multilayer Perceptron	5	0	10	4

	Classifier	TP	FP	TN	FN
SCC vs AK	SMO - Poly	21	8	1	2
	SMO - RBF	23	9	0	9
	iBk (k=1)	9	4	5	14
	iBk (k=6)	21	7	2	2
	iBk (k=7)	14	7	2	9
	Multilayer Perceptron	12	3	6	11

	Classifier	TP	FP	TN	FN
Ben vs Mal	SMO - Poly	61	38	12	9
	SMO - RBF	70	50	0	0
	iBk (k=1)	51	34	16	19
	iBk (k=6)	58	40	10	12
	iBk (k=7)	50	34	16	20
	Multilayer Perceptron	69	48	2	1

Steady-state: S1, S2, ..., S40 and SSTD feature vector

	Classifier	TP	FP	TN	FN
Melanoma vs Nevi	SMO - Poly	5	0	10	4
	SMO - RBF	0	0	10	9
	iBk (k=1)	4	3	7	5
	iBk (k=6)	1	0	10	8
	iBk (k=7)	0	0	10	9
	Multilayer Perceptron	7	1	9	2

	Classifier	TP	FP	TN	FN
SCC vs AK	SMO - Poly	21	6	3	2
	SMO - RBF	23	9	0	0
	iBk (k=1)	14	4	5	9
	iBk (k=6)	21	7	2	2
	iBk (k=7)	15	6	3	8
	Multilayer Perceptron	11	3	6	12

	Classifier	TP	FP	TN	FN
Ben vs Mal	SMO - Poly	70	49	1	0
	SMO - RBF	70	50	0	0
	iBk (k=1)	51	33	17	19
	iBk (k=6)	59	44	6	11
	iBk (k=7)	53	39	11	17
	Multilayer Perceptron	69	47	3	1

Dynamic: DX, DO, ..., D5 and MX, M0, ..., M5 feature vector

	Classifier	TP	FP	TN	FN
Melanoma vs Nevi	SMO - Poly	0	2	9	6
	SMO - RBF	0	0	11	6
	iBk (k=1)	2	1	10	4
	iBk (k=6)	0	0	11	6
	iBk (k=7)	0	0	11	6
	Multilayer Perceptron	1	0	11	5

	Classifier	TP	FP	TN	FN
SCC vs AK	SMO - Poly	7	1	10	5
	SMO - RBF	12	11	0	0
	iBk (k=1)	8	7	4	4
	iBk (k=6)	3	2	9	3
	iBk (k=7)	10	5	6	2
	Multilayer Perceptron	8	3	8	4

	Classifier	TP	FP	TN	FN
Ben vs Mal	SMO - Poly	49	32	8	13
	SMO - RBF	62	40	0	0
	iBk (k=1)	39	28	12	23
	iBk (k=6)	52	34	6	10
	iBk (k=7)	42	28	12	20
	Multilayer Perceptron	45	27	13	17

Dynamic: DX, DO, ..., D5 and STD_X, STD₀, ..., STD₅ feature vector

	Classifier	TP	FP	TN	FN
Melanoma vs Nevi	SMO - Poly	10	11	0	2
	SMO - RBF	0	0	11	6
	iBk (k=1)	0	1	10	6
	iBk (k=6)	0	1	10	6
	iBk (k=7)	0	0	11	6
	Multilayer Perceptron	1	4	7	5

	Classifier	TP	FP	TN	FN
SCC vs AK	SMO - Poly	1	0	11	5
	SMO - RBF	12	11	0	0
	iBk (k=1)	6	5	6	6
	iBk (k=6)	3	5	6	9
	iBk (k=7)	6	9	2	6
	Multilayer Perceptron	5	5	6	7

	Classifier	TP	FP	TN	FN
Ben vs Mal	SMO - Poly	61	39	1	1
	SMO - RBF	62	40	0	0
	iBk (k=1)	31	24	16	31
	iBk (k=6)	43	30	10	19
	iBk (k=7)	37	27	13	25
	Multilayer Perceptron	55	35	5	7